



DEPARTAMENTO DE FÍSICA TEÓRICA I
UNIVERSIDAD COMPLUTENSE DE MADRID

DOCTORAL THESIS

Bipartite entanglement of localized separated systems

Author:
Carlos SABÍN LESTAYO

Supervisor:
Dr. Juan LEÓN GARCÍA

INSTITUTO DE FÍSICA FUNDAMENTAL
CONSEJO SUPERIOR DE INVESTIGACIONES CIENTÍFICAS



November 2011. Committee: M. A. Martín-Delgado, A. Luis, I. Cirac, E. Solano, A. Cabello.

Para Mencha.
Para Nicolás.

Agradecimientos

“People are afraid to face how great a part of life is dependent on luck” (Woody Allen, *Match Point*)

Déjenme que les cuente una historia sobre el azar.

El azar llevó a un estudiante sin ambiciones investigadoras de los últimos cursos de Física a una conferencia divulgativa de Guillermo García Alcaine sobre Mecánica Cuántica, dirigida a los alumnos. Al final de la charla, Guillermo hizo publicidad sobre un Trabajo Académicamente Dirigido que le gustaría dirigir, con un tema relacionado con el entrelazamiento. Puesto que mis compañeros estaban en clase (donde sin duda debería estar yo también), prácticamente nadie de los últimos cursos recibió esa propaganda, y fue la única que se hizo. Así que no tuve ninguna competencia cuando al día siguiente aparecí por su despacho. Ése fue el comienzo de más de dos años de investigación, que dieron lugar, además del mencionado trabajo, a una Tesis de Máster y un artículo sobre clasificación y medida del entrelazamiento. El recuerdo de Guillermo y su sentido del humor me acompaña siempre, con su ejemplo de rigor, honestidad y perfeccionismo, cualidades que en mí se dan en tan pequeñas dosis que son sólo torpes remedos de las suyas. Sólo tengo para él admiración y gratitud.

Por motivos que no vienen al caso, Guillermo ya no dirigía Tesis Doctorales. Por el camino yo me había ido creyendo que podía dedicarme a eso de la investigación, pero el tiempo iba pasando sin que se me abriera ninguna puerta. El día que hice el último examen de la carrera, mi costumbre de leer los carteles de las paredes (que tanto solía exasperar a mis acompañantes) me llevó a leer un anuncio de Tesis Doctoral de un tal Juan León del Instituto de bla, bla, bla sobre...¡teoría del entrelazamiento! ¿Ven lo que les decía sobre el azar?

La expresión “padre científico” se usa muchas veces con cierta alegría para designar la relación de cierto investigador con su director de Tesis. Pocas veces es tan cierta como en mi caso. Juan confió en mí sin tener demasiados motivos para hacerlo y decidió hacer frente, por pura bondad, a todas las dificultades que desde el principio se vio que yo le procuraría. Tuvo varias ocasiones para deshacerse elegantemente de mí, pero no lo hizo. En lugar de eso se desvivió por ayudarme. Me enseñó rigor, disciplina intelectual, ambición investigadora, y después comprendió que podía, que debía dejarme volar con libertad. Hoy yo le hablo ya como los hijos adolescentes hablan a sus padres, mezclando la indiferencia con el sarcasmo. Es pura máscara: jamás olvidaré todo lo que Juan

ha hecho por mí.

Guillermo, Juan... a hombros de gigantes tales, ¿quién no acertaría a ver con claridad? Pero recuerden que yo quería hablarles del azar. Yo ya llevaba un tiempo en el Consejo, aguantando cada mañana la mirada entre irónica (“¿a dónde va éste?”) y admonitoria (“¡haz algo, idiota!”) de D. Santiago Ramón y Cajal y D. Severo Ochoa, (cuyas estatuas se erigieron a los pocos días de llegar yo en sustitución del busto de algún olvidado político de la dictadura), cuando Juanjo García Ripoll sacó plaza en nuestro grupo. Un día que comimos los dos juntos en el comedor, surgió la idea de intentar ver qué aplicaciones podrían tener los resultados que habíamos ido obteniendo Juan y yo en el campo emergente de los circuitos superconductores. Ahí empezó nuestra colaboración con Juanjo. Su asombrosa intuición, cimentada sobre un abrumador conocimiento de toda la Física experimental y teórica de los siglos XX y XXI, permitieron dar a esta Tesis otro salto de calidad. Gracias a él además pude entrar en contacto con Kike (así quiere él que lo escribamos) Solano, cuyo entusiasmo y atrevimiento, su visión poética y romántica del oficio, son un estímulo para todos los investigadores que nos cruzamos en su camino, quienes secretamente aspiramos a ser, cuando seamos jóvenes, como él.

Pero basta ya de hacer la pelota a los maestros. Durante la elaboración de esta Tesis, como es natural, conocí a muchas personas. La mejor de todas ellas es mi buen amigo Borja Peropadre. Su bondad, sensatez, perspicacia y sabiduría me hacen seguir confiando en la condición humana y tratar de ser mejor. ¡Quién le iba a decir a un sociópata como yo que iba a disfrutar tanto compartiendo un despacho! También son buenos amigos el inimitable Marco del Rey, cuya exigencia intelectual y espíritu crítico elevaron considerablemente la calidad del capítulo 5 de esta Tesis, el Dr. Edu Martín Martínez, el SúperManager Emilio Alba, Andrea Cadarso y el resto de gente de QUINFOG, así como Alejandro Bermúdez, Juan Manuel Pérez Pardo, Fernando Lledó, Luis Garay, Lucas Lamata, Pol Forn, Jorge Casanova y quién sabe cuánta gente que olvido, pero con la que habré compartido al menos el café aguado de algún congreso. Diré también que sin Paco y sin David, y el resto del Centro de Estudios Cuzco, no habría podido terminar esta Tesis.

Muchos padres intentan educar a sus hijos a su imagen y semejanza, confiando en que repitan sus doctrinas y consignas. Mis padres no me enseñaron otra ideología que el amor y los buenos sentimientos, y les estoy muy agradecido por ello. Si hubiera heredado la mitad de la originalidad y libertad de pensamiento de mi padre José Ramón, de su inquietud y su curiosidad, de su insobornable integridad e individualidad, de su amor por la lectura y el conocimiento, de su profundidad para entender lo esencial, me daría por satisfecho. Si algo hubiera aprendido del amor incondicional de mi madre Rosalía, de su entrega desinteresada por la familia, de su capacidad para seguir adelante por amargo que sea lo que le ofrezca la vida, para tirar de recursos y mantenerlo todo en pie y en orden con originalidad y creatividad, ya sería mucho. Espero que cuando tengan esta Tesis en sus manos sientan, aunque sea por un instante, que en el fondo mereció la pena.

Todo lo que soy, para bien o para mal, tiene que ver con mi hermano Mon,

poeta, profesor, ingeniero y filólogo (si mencionamos sólo lo más evidente). El me enseñó, entre otras muchas cosas, a ser libre, a amar la cultura, a no tener miedo a pensar y a seguir tu propio camino, y aunque él no se acuerde, me convenció sin pretenderlo para que estudiara Física en lugar de Filosofía. Su influencia sobre mí ha sido tan grande que lo he tenido que asesinar en sentido Freudiano muchas veces, para resucitarlo inmediatamente. Y mi hermana María, a la que llamaba cuando lloraba desconsolado de niño, completó mi formación como hombre, con su profundo sentido de la generosidad y la justicia. No puedo evitar acordarme ahora de mi tía Carolita, que ya no podrá felicitarme desde el cielo.

Durante la elaboración de esta Tesis me casé, mi mujer tuvo dos embarazos, nació un hijo al que he visto crecer, aprender a andar y a construir sus primeras frases. Esta Tesis es para ellos. Para Menchita, que ha confiado en mi capacidad y en mis posibilidades mucho más que yo mismo, que ha sacrificado tanto para que llegara este día, que con su sola presencia da sentido a la extraña comedia de estar vivo, de poner un pie delante de otro y caminar, uno, dos, inspirar, espirar, para Menchita que es el único motivo por el que he seguido en pie tras esa noches en las que despertaba de pronto y sentía tanto miedo. Sin ella, “las estrellas, a pesar de su lámpara encendida perderían el camino/ ¿qué sería del Universo?” Para Nicolás, que pronto cumplirá dos años, a quien deseo que no entienda jamás ni una palabra de lo que dice esta Tesis, que encuentre la felicidad más fácilmente que su viejo, su pobre viejo que no podrá enseñarle más que algún poema y aquello que dice esa vieja canción de los 60, la misma que escuchaba Desmond Hume en el búnker:

“You have to make your own kind of music/ sing your own special
song/ make your own kind of music/ even if nobody else sings along”

Madrid, Septiembre del 2011.

List of publications

Chapter 3

* (In this chapter, authors in alphabetical order)

- “Entanglement swapping between spacelike separated atoms” , Juan León, Carlos Sabín, Phys. Rev. A **78**, 052314 (2008).
- “Photon exchange and correlation transfer in atom-atom entanglement dynamics”, Juan León, Carlos Sabín, Phys. Rev. A **79**, 012301 (2009).
- “Generation of atom-atom correlations inside and outside the mutual light cone” , Juan León, Carlos Sabín, Phys. Rev. A **79**, 012304 (2009).
- “A case of entanglement generation between causally disconnected atoms” , Juan León, Carlos Sabín, Int. J. Quant. Inf. **7**, 187-193 (2009).
- “Atom-atom entanglement generated at early times by two photon emission”, Juan León, Carlos Sabín, Phys. Scr. T**135** 014034 (2009).

Chapter 4

- “Dynamics of entanglement via propagating microwave photons”, Carlos Sabín, Juan José García-Ripoll, Enrique Solano, Juan León, Phys. Rev. B **81**, 184501 (2010).
- “Detecting ground-state qubit self-excitations in circuit QED: A slow quantum anti-Zeno effect”, Carlos Sabín, Juan León, Juan José García-Ripoll, Phys. Rev B **84**, 024516 (2011).

Chapter 5

- “The Fermi problem with artificial atoms in circuit QED”, Carlos Sabín, Marco del Rey, Juan José García-Ripoll, Juan León. Phys. Rev. Lett. **107**, 150402 (2011).

- “Short-time quantum detection: probing quantum fluctuations”, Marco del Rey, Carlos Sabín, Juan León. Submitted to Phys. Rev. Lett. arXiv:1108.0672.

Chapter 6

- “Quantum simulation of the Majorana equation and unphysical operations”, Jorge Casanova, Carlos Sabín, Juan León, Iñigo L. Egusquiza, Rene Gerritsma, Christian F. Roos, Juan José García-Ripoll, Enrique Solano. Accepted to Phys. Rev. X. arXiv:1102.1651.
- **To be submitted** “On Majorana Hamiltonians”, Carlos Sabín, Jorge Casanova, Juan José García-Ripoll, Juan León, Enrique Solano, Iñigo L. Egusquiza.
- **To be submitted** “Quantum simulation of relativistic potentials without potentials”, Carlos Sabín, Jorge Casanova, Juan José García-Ripoll, Lucas Lamata, Enrique Solano, Juan León.

Other publications not included in this Thesis

- “A classification of entanglement in three-qubit systems”, Carlos Sabín, Guillermo García-Alcaine, European Physical Journal D, **48**, 435-442 (2008).

Contents

Agradecimientos	i
List of publications	v
1 Introduction	1
2 Preliminaries	8
2.1 Matter-radiation interaction. Hamiltonian	8
2.1.1 Introduction	8
2.1.2 Two level-atoms. Interaction picture	11
2.1.3 Rotating wave approximation and beyond	11
2.1.4 Rabi and Jaynes-Cummings models	12
2.2 Circuit QED	12
2.3 Entanglement measures in two-qubit systems	13
3 Dynamics of entanglement in matter-radiation interaction	16
3.1 Generation of entanglement inside and outside the mutual light cone	16
3.1.1 Introduction	16
3.1.2 The model	18
3.1.3 The case with $n = 0$	20
3.1.4 Photon emission	21
3.1.5 Tracing over the field	24
3.1.6 Different initial states	25
3.1.7 Conclusions	30
3.2 Entanglement swapping between spacelike separated atoms	31
3.2.1 Introduction	31
3.2.2 Entanglement swapping between spacelike separated atoms	32
3.2.3 Conclusions	37
3.3 Entanglement Sudden Death and Sudden Birth. Photon ex- change and correlations transfer in atom-atom entanglement dy- namics	38
3.3.1 Introduction	38
3.3.2 Hamiltonian and state evolution	40

3.3.3	Sudden death and revival of atom-atom entanglement . . .	41
3.3.4	Atom-field entanglement	44
3.3.5	Tripartite entanglement	48
3.3.6	Conclusions	50
4	Circuit QED as a quantum simulation of matter-radiation interaction beyond RWA	51
4.1	Detecting ground state qubit self-excitations in circuit QED: slow quantum anti-Zeno effect	52
4.1.1	Introduction	52
4.1.2	Detecting ground state qubit self-excitations	53
4.1.2.1	The Rabi model	53
4.1.2.2	Detecting excitations with one measurement	55
4.1.2.3	Repeated measurements: survival probability	57
4.1.2.4	Numerical experiments	58
4.1.2.5	Weak measurements	62
4.1.2.6	Relaxation and dephasing	62
4.1.3	Conclusions	64
4.2	Entanglement dynamics via propagating microwave photons	65
4.2.1	Introduction	65
4.2.2	Superconducting qubits coupled to a quantum field	67
4.2.3	Entanglement dynamics and single photons	70
4.2.4	Experimental implementation	71
4.2.5	Conclusions	73
5	Causality in matter-radiation interactions	74
5.1	The Fermi problem with artificial atoms in circuit QED	74
5.1.1	Introduction	74
5.1.2	There are no causality problem in Fermi's two-qubit system	75
5.1.3	Experimental proposal	79
5.1.4	Conclusions	82
5.2	Quantum fluctuations and short-time quantum detection	83
5.2.1	Introduction	83
5.2.2	What does a detector's click mean?	83
6	Quantum simulations of relativistic dynamics. Majorana physics	87
6.1	On Majorana Hamiltonians	88
6.1.1	Introduction	88
6.1.2	Majorana Hamiltonians.	88
6.1.3	Hamiltonization.	90
6.1.4	Examples	92
6.1.5	Conclusions and outlook.	94
6.2	Quantum simulation of Majorana equation and unphysical operations	95
6.2.1	Introduction	95
6.2.2	Quantum simulation of antiunitary operations	96

6.2.3	Simulating antiunitary operations	96
6.2.4	Conclusions	100
6.3	Quantum simulation of relativistic potentials without potentials .	101
6.3.1	Introduction	101
6.3.2	One particle systems	101
6.3.3	Examples	103
6.3.4	Bipartite systems	106
6.3.5	Conclusions	106
A		107
B		111
C		113
D	Majorana equation in 1+1 dimensions	117
E	Implementation of the quantum simulation of the Majorana equation in trapped ions	120
	Conclusions	122
	Bibliography	126

Chapter 1

Introduction

In their famous paper of 1935, Einstein, Podolsky and Rosen (EPR) tried to show that Quantum Mechanics couldn't be a complete theory due to the prediction of strange correlations appearing among the parties in some states of composite systems [1]. Later that year, in a letter to Einstein, Schrödinger referred to the phenomenon with the German word “verschränkung”, that was translated by himself to “entanglement” in [2]. Considered unphysical and paradoxical by EPR - “no reasonable definition of reality could be expected to permit this”-, Bohr [3] and Schrödinger [2] immediately acknowledged entanglement as an essential feature of the theory. Today, after the series of experiments based on Bell inequalities [4] ruling out local hidden variable theories [5], Quantum Mechanics and its relativistic field version Quantum Field Theory are not considered just as mere mathematical models that fit with outstanding precision a huge bulk of experimental data, but also a complete theory of Nature at the atomic and subatomic level. Being at the very heart of the theoretical building of Quantum Mechanics, entanglement is thus an essential feature of Nature. Besides its importance from this foundational viewpoint, entanglement is also a key resource for Quantum Information and Quantum Computation tasks.

In the early days after its discovery entanglement was considered as a consequence of the interaction. For instance, Schrödinger wrote [2]:

“When two systems,[...] enter into temporary physical interaction due to known forces between them, and when after a time of mutual influence the systems separate again, then they can no longer be described in the same way as before.[...] By the interaction, the two representatives (or Ψ -functions) have become entangled”

Therefore, the “magic” of entanglement relies completely on the quantum state, which is generated by a direct interaction between the parties. Today, we know that this is not a complete picture. For instance, in the “entanglement swapping” protocol [6] the parties that get finally entangled do not interact directly with each other. Instead if we want to entangle A and B with this protocol, A has to share an entangled state with some third party C and also B indepen-

dently with the same C. Then, a measurement of the state of C leaves A and B in an entangled state. But in this case the origin of the A-B entanglement can be traced back to the origin of the A-C and B-C entanglements which, following Schrödinger would be again the interaction.

In some sense, the entangling interaction can be regarded as a “black box” that generates the desired initial entangled state. In typical experiments involving entanglement, the black box may be a nonlinear crystal exhibiting Spontaneous Parametric Down-Conversion [7]. A “pump” laser beam is directed to the crystal and some of the photons split into entangled pairs, which are then used in the experiment. But what it is inside the box? Where it is exactly the magic? Can we have a deeper look onto the origin and the generation of entanglement? These are some questions that we will try to analyze in this Thesis.

Actually, the above is deeply connected with modern investigations on the intriguing notion of “vacuum entanglement”. That the vacuum of the field is an entangled state was discovered by Summers and Werner in the 1980’s [8], but it was considered as a mere formal theoretical result until it attracted some attention from a different perspective [9]. In [9], vacuum entanglement is exploited to generate entanglement between two spacelike separated detectors. After a finite time of interaction with a scalar field initially in the vacuum state, the two-level detectors state is shown to evolve from an initial separable state to an entangled one, even if the detectors remain spacelike separated. The standard interpretation of this effect is that the entanglement initially contained in the vacuum state of the field is transferred to the detectors, like in the standard entanglement swapping described above but replacing C by two spacelike separated regions of the field and without measurements. An alternate view was given in [10], where the entanglement between spacelike separated detectors is attributed to the exchange of virtual photons between them. Whatever the point of view, the mathematical structure underlying the phenomenon is the same, namely the Feynman propagator of the field. The fact that this object is not restricted to the lightcone was noticed by Feynman himself [11].

An important part of this Thesis is devoted to going a step further the previous results on entanglement generation between spacelike separated objects [10, 9, 12] by moving to the physical framework of matter-radiation interaction and performing a thorough analysis of the phenomenon, keeping also in mind possible applications in realistic Quantum Information protocols. In a nutshell, one of the main goals was to propose the first realistic experimental proposal to test these effects in the lab. Unfortunately, as we will explain with more detail in the main text, a lot of experimental difficulties arise when dealing with real atoms and photons. This is the main reason to come to the different but related framework of circuit QED.

In circuit QED, superconducting qubits can play the role of artificial two-level atoms that can be coupled to transmission lines along which photons propagate. Thus, these systems mimic the standard matter-radiation interaction with the advantage of experimental amenability. Although they are interesting by themselves, circuit QED setups can be regarded as 1D Quantum Simulations of Quantum Optics setups. In this thesis, we will exploit the analogy to propose

the desired experimental test of “outside the lightcone” entanglement . Besides, we will explore some features of the novel physics showing up in this emerging field, as a consequence of the possibility of achieve very large values of the qubit-field coupling strength and the breakdown of the standard Rotating Wave Approximation.

A natural question showing up when dealing with effects as those described above is: What about causality? Is it violated? Indeed the relationship between entanglement and causality has been present since the EPR paper. At first sight it may seem that the perfect correlations appearing for instance in the paradigmatic singlet state represent by themselves an instantaneous transmission of information. This seems to be also the viewpoint of Einstein himself when he write to Born the famous “spukhafte Fernwirkung”-commonly translated as “spooky action at a distance”. Today, we know that Quantum Mechanics is actually a nonsignaling theory [13, 14], that is, the statistics of the measurements performed by B is completely independent of the measurements realized by A if A and B are spacelike separated. This entails that information between A and B cannot be transmitted at superluminal rates. In the singlet state, B can only get information on the state of A if both parties share some previous information on the shared entangled state and on the choice of the observable measured by A. In general, is well known in Quantum Information that quantum correlations have to be assisted with Classical Communication -which is of course subluminal- in order to transmit information. Therefore, the fact that a separable state can evolve to an entangled one “faster than light” does not represent a violation of Einsteinian causality, since cannot be used by itself to transmit information.

Although this general principle is clear, the translation to the particular setup consisting of a pair of neutral atoms interacting with the electromagnetic field -the one that we extensively deal with in this Thesis- has been an open theoretical problem -the so-called Fermi problem- since the 1930's. In particular, in 1932 Fermi [15] proposed a “gedanken” experiment to check that the probability of excitation of one of the atoms behaves in a causal fashion (see Chapter 5 for more details). Although Fermi's conclusions were conceptually right about the causal nature of the model, a mathematical flaw of his computations opened a Pandora box that couldn't be closed neither by a theoretical consensus nor by an experimental test [16, 17]. An important part of this Thesis is devoted to show that there are no causality problems in Fermi two-atom's system and to propose a feasible experimental test, taking advantage again of the possibilities offered by circuit QED. The results of such experiment could close an eight-decade old controversy on the foundations of Quantum Mechanics and Quantum Field Theory.

As we have explained above, circuit QED setups play a central role in this Thesis, as 1D Quantum Simulators of matter-radiation interaction. In a nutshell, a Quantum Simulator, as Feynman envisioned [18] is an experimentally amenable quantum device that mimics the dynamics of an inaccessible quantum model. The emerging field of Quantum Simulations is developing very fast a number of such devices in several branches of Physics. In particular, in

this Thesis we pay attention to Quantum Simulations with trapped ions of Relativistic Quantum Mechanics systems. [19]. Relativistic Quantum Mechanics can be understood as a Quantum Field Theory with a fixed number of particles, thus it amounts to Quantum Field Theory below the energy threshold of pair creation. In this low-energy regime is the right model for relativistic particles. Surprisingly, its equations -such as Klein-Gordon or Dirac ones- come with a wealth of striking predictions, like “Zitterbewegung” or Klein paradox, which are very far from a direct detection in the lab [20, 21]. In this sense, recent experiments with trapped ions simulators of the Dirac equation [22] have shed light on the nature and experimental implications of the mentioned phenomena. An important goal for the future would be to simulate the fully relativistic version of the two-atom model used in most part of this Thesis where the atoms would be replaced by relativistic particles following the Dirac equation. Steps in this direction are given at the end of this Thesis, where bipartite systems of relativistic interacting particles are considered. In the meanwhile, we take a little diversion from the main course and propose the quantum simulation of a crucially different but related one- particle relativistic dynamics, namely the Majorana equation- see details in chapter 6-. The very interesting properties of this equation -which takes its roots in the prematurely lost overwhelming genius of Ettore Majorana [23] but was actually introduced in [24, 25]- lead us to the introduction of a new class of mathematical objects with physical content, that we refer to in this Thesis as “Majorana Hamiltonians”.

Besides the Majorana equation, this new class of generalized Hamiltonians is connected with a wider range of applications, going from the implementation of operations like time reversal and charge conjugation to the partial transpose- a crucial formal operation in Quantum Information due to its relationship with entanglement measures-. These operations are “unphysical”, in the sense that they are not associated to operations that can be implemented directly in the laboratory. Instead, they entail a mathematical formal computation that has to be performed for instance in a classical computer and require the knowledge of the quantum state. With the techniques developed in this Thesis these operations can now be simulated with real physical operations, without stopping an ongoing experiment. From a fundamental viewpoint the similarities and differences between Majorana Hamiltonians and standard textbook Hamiltonians allows us to explore important questions lying at the foundations of Quantum Mechanics and Quantum Field Theory.

Structure of the Thesis. Brief summary of objectives and results.

The structure of this thesis is the following.

- In chapter 2 we will just provide the reader with some theoretical background on the formalism used in the main text.

- In chapter 3 we will analyze different aspects of the entanglement dynamics in a system consisting of a pair of two-level neutral atoms with an electric dipole coupling to the electromagnetic field. We mainly focus in the relationship of entanglement with the existence or lack of a causal connection between the atoms.
 - * In section 3.1 we analyze whether a pair of neutral two level atoms can become entangled in a finite time while they remain causally disconnected. The interaction with the electromagnetic field is treated perturbatively in the electric dipole approximation. First, we start from an initial state in which the field is in the vacuum and only one atom is excited. We obtain the final atomic correlations for the cases where $n = 0, 1$, or 2 photons are produced in a time t , and also when the final field state is unknown. Our results show that correlations are sizable inside and outside the mutual light cone for $n = 1$ and 2, and also that quantum correlations become classical by tracing over the field state. For $n = 0$ we obtain entanglement generation by photon propagation between the atoms, the correlations come from the indistinguishability of the source for $n = 1$, and may give rise to entanglement swapping for $n = 2$. Finally, we consider a similar scenario but starting with both atoms excited as initial state.
 - * In section 3.2 we show a mechanism that projects a pair of neutral two-level atoms from an initially uncorrelated state to a maximally entangled state while they remain spacelike separated. The atoms begin both excited in a common electromagnetic vacuum, and the radiation is collected with a partial Bell-state analyzer. If the interaction time is short enough and a certain two-photon Bell state is detected after the interaction, a high degree of entanglement, even maximal, can be generated while one atom is outside the light cone of the other, for arbitrary large interatomic distances.
 - * In section 3.3 we analyze the entanglement dynamics of a system composed by a pair of neutral two-level atoms that are initially entangled, and the electromagnetic field, initially in the vacuum state, within the formalism of perturbative quantum field theory up to the second order. We show that entanglement sudden death and revival can occur while the atoms remain spacelike-separated and therefore cannot be related with photon exchange between the atoms. We interpret these phenomena as the consequence of a transfer of atom-atom entanglement to atom-field entanglement and viceversa. We also consider the different bi-partitions of the system, finding similar relationships between their entanglement evolutions.
- In chapter 4 we move to the framework of circuit QED with artificial atoms, considering these setups as Quantum Simulators of a 1D version of matter-radiation interaction.

- * In section 4.1 we explore a consequence of the breakdown of the Rotating Wave Approximation in the ultrastrong coupling regime of circuit QED. In particular, we study an ultrastrong coupled qubit-cavity system subjected to slow repeated measurements. We demonstrate that even under a few imperfect measurements it is possible to detect transitions of the qubit from its free ground state to the excited state. The excitation probability grows exponentially fast in analogy with the quantum anti-Zeno effect. The dynamics and physics described in this section is accessible to current superconducting circuit technology.
- * In section 4.2 we propose a simple circuit QED experiment to test the generation of entanglement between two superconducting qubits that are initially in a separable state. Instead of the usual cavity QED picture, we study qubits which are coupled to an open transmission line and get entangled by the exchange of propagating photons. We compute their dynamics using a full quantum field theory beyond the rotating-wave approximation and explore a variety of regimes which go from a weak coupling to the recently introduced ultrastrong coupling regime. Due to the existence of single photons traveling along the line with finite speed, our theory shows a light cone dividing the spacetime in two different regions. In one region, entanglement may only arise due to correlated vacuum fluctuations, while in the other the contribution from exchanged photons shows up.
- In chapter 5 we show that the nonlocal quantum correlations phenomena considered in previous chapters are perfectly compatible with Einsteinian causality by showing explicitly that Fermi's two-atom system behaves in a causal way, and explore the theoretical consequences of going beyond RWA in a quantum detection.
 - * In particular, in section 5.1 we propose a feasible experimental test of a 1-D version of the Fermi problem using superconducting qubits. We give an explicit non-perturbative proof of strict causality in this model, showing that the probability of excitation of a two-level artificial atom with a dipolar coupling to a quantum field is completely independent of the other qubit until signals from it may arrive. We explain why this is in perfect agreement with the existence of nonlocal correlations and previous results which were used to claim apparent causality problems for Fermi's two-atom system.
 - * In section 5.2 we study the information provided by a detector click on the state of an initially excited two level system. By computing the time evolution of the corresponding conditioned probability beyond the rotating wave approximation, we show that a click in the detector is related with the decay of the source only for long times of interaction. For short times, non-rotating wave approximation effects like self-excitations of the detector, forbid a naïve interpretation

of the detector readings. These effects might appear in circuit QED experiments.

- Finally, in chapter 6 we consider different quantum simulations, namely of relativistic quantum mechanics setups.

- * In section 6.1, we introduce the notion of Majorana Hamiltonians, objects that are in general neither linear nor antilinear but with an associated dynamics which conserves the norm. The Majorana equation, that is, the relativistic quantum mechanical equation of a fermion with Majorana mass term, is the archetypal example of this family. We analyze some amazing properties like the relevance of initial global phases in the dynamics that makes them detectable and, as a consequence, the inadequacy of the notion of mixed states. We provide an alternative description in terms of standard Hamiltonians, showing that a Majorana Hamiltonian can be mapped to a Hamiltonian in a real Hilbert space. In this way, Majorana Hamiltonians and antiunitary operators can be experimentally demonstrated.

- * In section 6.2 we show how to design a quantum simulator for the Majorana equation, a pseudohamiltonian - Majorana-hamiltonian-relativistic wave equation that might describe neutrinos and other exotic particles beyond the standard model. The simulation demands the implementation of charge conjugation, an unphysical operation that opens a new front in quantum simulations, including the discrete symmetries associated with complex conjugation and time reversal. Finally, we show how to implement this general method in trapped ions.

- * Finally, in section 6.3 we show that a potential can be simulated with a free Dirac or Majorana Hamiltonian since there is a local phase transformation between solutions of the equation with a potential and solutions of the free equation. The transformation depends on the potential, which is codified in the phase. In some cases, the probability density is unchanged, entailing that the particle behaves under the potential as if it were free. It is valid for a large class of potentials for the Majorana equation and a different class in the Dirac case, which explains why Dirac and Majorana particles exhibit different behavior under the same potentials. We extend the results to two-body equations with interaction potentials.

This thesis concludes with five appendices. The first three develop with more detail some involved computations related with chapters 3, 4 and 5. Finally, appendix D is devoted to a theoretical explanation on the 1-D Majorana equation and appendix E sheds light onto the implementation of the quantum simulation of the Majorana equation with trapped ions.

Chapter 2

Preliminaries

2.1 Matter-radiation interaction. Hamiltonian

2.1.1 Introduction

Throughout this work we will deal with a system consisting of one or more two-level systems (qubits in the language of Quantum Information) interacting with the electromagnetic quantum field. This section is devoted to provide a brief summary of the theoretical grounds of the employed model, with no pretension of completeness. Wider textbook treatments on these topics can be found in [26], [27], [28], [29].

We will start with the well known minimal-coupling Hamiltonian of an atom interacting with a quantum field:

$$H = \sum_i \frac{1}{2m_i} (\mathbf{p}_i - q_i \mathbf{A}(\mathbf{x}_i))^2 + V(|\mathbf{x} - \mathbf{x}_i|) + \sum_{\lambda} \int d^3\mathbf{k} \hbar \omega_{\mathbf{k}} (a_{\mathbf{k}\lambda}^\dagger a_{\mathbf{k}\lambda} + \frac{1}{2}), \quad (2.1)$$

\mathbf{p}_i , \mathbf{x}_i , being the momentum and position, respectively of each particle of mass m_i and charge q_i bound by a potential V to a force center (nucleus) located at \mathbf{x} . The quantum electromagnetic field can be written down in terms of the creation and annihilation operators for each mode \mathbf{k} (with frequency $\omega_k = c|\mathbf{k}|$) and polarization λ : $a_{\mathbf{k}\lambda}^\dagger$, $a_{\mathbf{k}\lambda}$ as:

$$\mathbf{A}(\mathbf{x}_i) = \sqrt{\frac{\hbar}{2c\epsilon_0(2\pi)^3}} \sum_{\lambda} \int \frac{d^3k}{\sqrt{k}} (e^{i\mathbf{k}\cdot\mathbf{x}_i} \epsilon(\mathbf{k}, \lambda) a_{k\lambda} + e^{-i\mathbf{k}\cdot\mathbf{x}_i} \epsilon^*(\mathbf{k}, \lambda) a_{k\lambda}^\dagger) \quad (2.2)$$

$\epsilon(\mathbf{k}, \lambda)$ being the polarization vectors for each λ and assuming the commutation relationships

$$[a_{\mathbf{k}\lambda}, a_{\mathbf{k}'\lambda'}^\dagger] = \delta^3(\mathbf{k} - \mathbf{k}') \delta_{\lambda\lambda'}. \quad (2.3)$$

(2.1) would be the quantized version of the classical minimal-coupling Hamiltonian, which can be derived from a Lagrangian whose Euler-Lagrange equations give rise to the correct equations of motion of the system, namely the Maxwell equations for the field and the Lorentz equations for the particles. Notice that we can split (2.1) into a “free” part H_0 and an interaction part H_I :

$$H = H_0 + H_I \quad (2.4)$$

with

$$H_0 = \sum_i \frac{\mathbf{p}_i^2}{2m_i} + \frac{q_i^2 \mathbf{A}^2(x_i)}{2m} + V(|\mathbf{x} - \mathbf{x}_i|) + \sum_\lambda \int d^3\mathbf{k} \hbar \omega_{\mathbf{k}} (a_{\mathbf{k}\lambda}^\dagger a_{\mathbf{k}\lambda} + \frac{1}{2}), \quad (2.5)$$

and

$$H_I = - \sum_i \frac{q_i \mathbf{p}_i \cdot \mathbf{A}(x_i)}{m}. \quad (2.6)$$

But then:

$$H_0 \neq H_{0R} + H_{0P}, \quad (2.7)$$

that is, the “free” part of the Hamiltonian cannot be decomposed into the free Hamiltonian of the radiation,

$$H_{0R} = \sum_\lambda \int d^3\mathbf{k} \hbar \omega_{\mathbf{k}} (a_{\mathbf{k}\lambda}^\dagger a_{\mathbf{k}\lambda} + \frac{1}{2}) \quad (2.8)$$

and the Hamiltonian of the particles without field:

$$H_{0P} = \sum_i \frac{\mathbf{p}_i^2}{2m_i} + V(|\mathbf{x} - \mathbf{x}_i|). \quad (2.9)$$

There is an extra, “self-interaction” term: $\frac{q_i^2 \mathbf{A}^2(x_i)}{2m_i}$. Thus the eigenstates of H_0 (2.5) are not product states of eigenstates of H_{0R} and H_{0P} . To avoid this, instead of using the Hamiltonian in (2.1) we will move to a different equivalent description of the system.

To this end we start by assuming the so-called “long wavelength approximation”, which amounts to replacing $\mathbf{A}(\mathbf{x}_i)$ (2.2) by $\mathbf{A}(\mathbf{x})$ in the Hamiltonian (2.1). This approximation is only valid for those modes verifying $\mathbf{k} \cdot |\mathbf{x} - \mathbf{x}_i| \ll 1$, that is, for wavelengths much larger than the atomic size. Then, we can apply the following unitary transformation:

$$U = e^{\frac{-i}{\hbar} \mathbf{d}(\mathbf{x}) \cdot \mathbf{A}(\mathbf{x})} \quad (2.10)$$

where we have introduced the electric dipole moment \mathbf{d} :

$$\mathbf{d}(\mathbf{x}) = \sum_i q_i (\mathbf{x}_i - \mathbf{x}). \quad (2.11)$$

This unitary transformation is an example of displacement operator, whose properties are well known in the framework of coherent states of the electromagnetic field. Using these properties and with a little algebra it is possible to arrive to the transformed Hamiltonian:

$$H' = U H U^{-1}, \quad (2.12)$$

and assuming that we are dealing with a globally neutral atom,

$$\sum_i q_i = 0, \quad (2.13)$$

H' takes the form:

$$H' = H_{0R} + H_{0P} + V' + H'_I. \quad (2.14)$$

The first two terms are the free Hamiltonians of the particles and the field respectively (2.8)-(2.9). The third term V' is:

$$V' = \sum_{\lambda} \int d^3\mathbf{k} \frac{1}{2\epsilon_0 (2\pi)^3} (\boldsymbol{\epsilon} \cdot \mathbf{d}(\mathbf{x}))^2, \quad (2.15)$$

a divergent contribution which cancels out with one of the terms coming from the energy shift caused by emission and reabsorption of photons, as we will see in the next chapter. Thus, we can let this term drop. The last term is an interaction Hamiltonian:

$$H'_I = -\mathbf{d}(\mathbf{x}) \cdot \mathbf{E}(\mathbf{x}) \quad (2.16)$$

where $\mathbf{E}(x)$ is the electric field vector operator:

$$\mathbf{E}(\mathbf{x}) = i \sqrt{\frac{\hbar c}{2\epsilon_0 (2\pi)^3}} \sum_{\lambda} \int d^3k \sqrt{k} (e^{i\mathbf{k}\cdot\mathbf{x}} \boldsymbol{\epsilon}(\mathbf{k}, \lambda) a_{k\lambda} - e^{-i\mathbf{k}\cdot\mathbf{x}} \boldsymbol{\epsilon}^*(\mathbf{k}, \lambda) a_{k\lambda}^{\dagger}). \quad (2.17)$$

So, finally we can split the new Hamiltonian H' (2.14) into:

$$H' = H'_0 + H'_I \quad (2.18)$$

but now

$$H'_0 = H_{0R} + H_{0P}, \quad (2.19)$$

in contrast with (2.7). Obviously, H and H' are equivalent descriptions of the system since they are related through a unitary transformation (2.10), (2.12), but states have to transform also according to the unitary. Throughout this work, we will use the Hamiltonian given by (2.16), (2.18), (2.19), whose ‘bare’ eigenstates are product states of eigenstates of the free Hamiltonians for the particles and the field. Equivalent results would be obtained with the Hamiltonian in (2.1), provided that the states are correctly transformed through (2.10).

2.1.2 Two level-atoms. Interaction picture

Now we will particularize to the case of two-level atoms and move to the interaction picture. We consider that we have an atom with a ground state $|g\rangle$ and an excited state $|e\rangle$ such that:

$$H_0 |g\rangle = E_g |g\rangle, H_0 |e\rangle = E_e |e\rangle \quad (2.20)$$

and

$$E_e - E_g = \hbar\Omega. \quad (2.21)$$

Under that conditions, we can use the completeness relation

$$\mathbf{1} = |g\rangle \langle g| + |e\rangle \langle e|, \quad (2.22)$$

in order to write the electric dipole moment operator in a simple form. That is:

$$\begin{aligned} \mathbf{d}(t) &= (|g\rangle \langle g| + |e\rangle \langle e|) e^{\frac{iH_0 t}{\hbar}} \mathbf{d} e^{-\frac{iH_0 t}{\hbar}} (|g\rangle \langle g| + |e\rangle \langle e|) \\ &= e^{-\frac{i\Omega t}{\hbar}} \mathbf{d}_{ge} \sigma^- + e^{\frac{i\Omega t}{\hbar}} \mathbf{d}_{eg} \sigma^+, \end{aligned} \quad (2.23)$$

with

$$\mathbf{d}_{ge} = \mathbf{d}_{eg}^* = \langle g| \mathbf{d} |e\rangle \quad (2.24)$$

and

$$\sigma^- = |g\rangle \langle e|, \sigma^+ = |e\rangle \langle g|. \quad (2.25)$$

Thus the interaction Hamiltonian (2.16) in the interaction picture takes the form:

$$H'_I(t) = -\mathbf{d}(\mathbf{x}, t) \cdot \mathbf{E}(\mathbf{x}, t), \quad (2.26)$$

with $\mathbf{d}(\mathbf{x}, t)$ given by (2.23) and the standard expression for the electric field vector operator in the interaction picture:

$$\begin{aligned} \mathbf{E}(\mathbf{x}, t) = i \sqrt{\frac{\hbar c}{2\varepsilon_0 (2\pi)^3}} \sum_{\lambda} \int d^3k \sqrt{k} & (e^{i(\mathbf{k}\mathbf{x} - \omega_k t)} \boldsymbol{\epsilon}(\mathbf{k}, \lambda) a_{k\lambda} - \\ & e^{-i(\mathbf{k}\mathbf{x} - \omega_k t)} \boldsymbol{\epsilon}^*(\mathbf{k}, \lambda) a_{k\lambda}^\dagger). \end{aligned} \quad (2.27)$$

In the next chapter, we will extensively use the Hamiltonian (2.26), and a 1-D version of it will be considered in chapters 4 and 5.

2.1.3 Rotating wave approximation and beyond

The Hamiltonian in (2.26) can be written as a sum of four terms using (2.23) and (2.27), each of them containing two operators: an atomic ladder operator σ^\pm and a creation or annihilation Fock operator $a_{k\lambda}, a_{k\lambda}^\dagger$. Thus we have two terms $\sigma^- a_{k\lambda}^\dagger, \sigma^+ a_{k\lambda}$ associated to the frequency $\Omega - \omega$ and two terms $\sigma^- a_{k\lambda}, \sigma^+ a_{k\lambda}^\dagger$ associated to the frequency $\Omega + \omega$. The rotating wave approximation (RWA) let the latter so-called counter-rotating terms drop, retaining only the

first two ones. The usual argument is that the counter-rotating terms oscillate very quickly and average to zero in observable time scales. This is generally true in the Quantum Optics realm, due to the weak atom-field coupling. As we will see in this thesis (chapters 4 and 5), the argument fails for stronger couplings, as those appearing in circuit QED, where counter-rotating terms can be relevant at experimental times. Even for weak couplings, a theoretical analysis of the short-time behavior like the one in chapter 3 must take the non-RWA terms into account. Therefore, throughout this thesis the RWA will not be assumed.

2.1.4 Rabi and Jaynes-Cummings models

When the boundary conditions of the system are such that the electromagnetic field is restricted to a given region of space, engineered in such a way that the fundamental frequency of the field ω_0 approximately matches with the frequency Ω of the qubit transition, then the multimode expansion of the electric field in the Hamiltonian (2.16) (or (2.26) in the interaction picture) can be restricted to only one mode ω_0 . In that case, the Rabi model is obtained. If the RWA is applied to the Rabi model, the resulting hamiltonian is the celebrated Jaynes-Cummings model, describing a two-level system in an optical cavity. We will deal with the Rabi model in circuit QED in chapter 4.

2.2 Circuit QED

Although the oscillations in electrical circuits are usually described by classical mechanical laws, at micro and nano scales and ultra-low temperatures, the thermal noise can be negligible compared to the spacing and width of the energy levels, unveiling the quantum nature of the system. Moreover, non-linear elements such as Josephson junctions do not obey the principle of correspondence, that is, the averages of the momentum and position operators do not follow the classical equations of motion, making apparent the necessity of a fully quantum-mechanical description of such elements. Thus non-trivial quantum effects can be observed in systems that can be considered as macroscopic, in the sense that they contain a huge number of elementary particles -the quantum numbers being collective degrees of freedom such as flux or charge-. Among all the possibilities opened up by this novel approach to Quantum Mechanics, in this thesis we are concerned with just one: circuit Quantum Electrodynamics.

A systematic quantization procedure of the usual elements of a circuit, such as inductances, capacitances and resistances is given in [30, 31] within the approach of lumped-element circuits, valid when the relevant wavelengths are much larger than the element's size. This can also be extended to waveguides -also called transmission lines- which can be regarded as a chain of infinitesimally small LC lumped-element circuits, obtaining a quantized Hamiltonian which is the 1-D version of 2.8. With this lumped-element approach is also possible to obtain a quantum description of several types of superconducting qubits, using different combinations of superconductors and Josephson junctions [32, 33].

Engineering the length of the transmission line to match the fundamental wavelength of the qubit transition, a cavity QED system like the ones described in section 2.1.4 is obtained [34, 35]. Without this restriction the full hamiltonian of the matter-radiation interaction emerges [36, 37], but in a range of experimental parameters different from the typical one in Quantum Optics. In this artificial 1D version of atomic QED, the frequency of the qubit transition is in the order of Ghz, and thus the relevant wavelengths of the field are in the microwave regime.

In chapters 4 and 5 of this Thesis, we will exploit the possibilities of circuit QED as a quantum simulator of matter-radiation interaction, taking advantage of its experimental amenability, which includes the possibility of achieve very strong qubit-field couplings, entering into a regime in which non-RWA effects can be observed in the lab.

2.3 Entanglement measures in two-qubit systems

In this thesis, we will analyze the dynamics of the entanglement between qubits, like the two-level atoms described in the previous sections. In this section we give a brief description of the notion of entanglement and discuss different ways of quantify it.

Let us start with pure states of two-qubit systems, which take the following general form:

$$|\Psi\rangle = \sum_{i,j} \alpha_{ij} |ij\rangle, \quad (2.28)$$

$|ij\rangle$, ($i, j = e, g$) being a basis of the Hilbert space $\mathcal{H}_A \otimes \mathcal{H}_B$ for qubits A and B. These pure two-qubit states are called separable if it can be written as:

$$|\Psi\rangle = |\Psi\rangle_A |\Psi\rangle_B, \quad (2.29)$$

$|\Psi\rangle_A, |\Psi\rangle_B$ being states of the Hilbert spaces $\mathcal{H}_A, \mathcal{H}_B$, respectively. Otherwise, the state is referred to as entangled, and exhibit correlations between the parties that cannot be achieved classically. For the non-pure case, a state ρ is separable if they can be written as

$$\rho = \sum_i p_i \rho_i^A \otimes \rho_i^B, \quad (2.30)$$

where ρ_i^A and ρ_i^B are state operators of subsystems A and B respectively, $p_i \geq 0 \forall i$, $\sum_i p_i = 1$. Otherwise ρ is entangled.

In general, an entanglement measure is some function of the state that is zero for separable states and non-zero for entangled ones. Besides, some technical properties must be fulfilled, the most standard one being the so-called monotonicity under Local Operations and Classical Communication (LOCC): these operations cannot create entanglement, thus any entanglement measure must non-increase under them. There are several measures of the entanglement of pure bipartite states; we shall cite only three of them: von Neumann's entropy of reduced states, concurrence [38], and negativity. [39].

The Von Neumann's entropy of a state ρ is defined in Information Theory as

$$S(\rho) = - \sum_j p_j \log_2 p_j, \quad (2.31)$$

being p_j the eigenvalues of ρ . Reduced states ρ_A, ρ^B are the result of tracing ρ over qubits B and A respectively:

$$\rho_A = Tr_B \rho, \rho_B = Tr_A \rho. \quad (2.32)$$

Von Neumann's entropy of reduced states is the simplest measure of bipartite entanglement for pure states, but its extension to non-pure states does not correctly discriminate between separable and entangled states. Therefore, it is not a good measure of entanglement for general mixed states.

Concurrence is the more usual measure of entanglement for non-pure two-qubit states. It is defined as

$$\mathcal{C}(\rho) = \max\{0, \sqrt{\lambda_1} - \sqrt{\lambda_2} - \sqrt{\lambda_3} - \sqrt{\lambda_4}\}, \quad (2.33)$$

where $\{\lambda_i\}$, ($i = 1...4$) are the eigenvalues of

$$R = \rho \tilde{\rho} \quad (2.34)$$

in decreasing order, with

$$\tilde{\rho} = (\sigma_y \otimes \sigma_y) \rho^* (\sigma_y \otimes \sigma_y), \quad (2.35)$$

and ρ^* being the complex conjugate of the state operator ρ . In arbitrary dimensions, operational generalizations of concurrence are known only for pure states. Therefore, it is a good measure of entanglement for general two-qubit states (pure or not) and for pure states in any dimension, but not for mixed bipartite states of arbitrary dimensions.

Finally, the negativity of a bipartite state ρ , defined in [40] as:

$$N(\rho) = -2 \sum_i \sigma_i(\rho^{TA}), \quad (2.36)$$

where $\{\sigma_i(\rho^{TA})\}$ are the negative eigenvalues of the partial transpose ρ^{TA} of the total state ρ respect to the subsystem A, defined as

$$\langle i_A, j_B | \rho^{TA} | k_A, l_B \rangle = \langle k_A, j_B | \rho | i_A, l_B \rangle, \quad (2.37)$$

A and B denoting the two subsystems: this is twice the value of the original definition of the negativity in [39]. It can be proved that for pure bipartite states of arbitrary dimensions the negativity (2.37) is equal to the concurrence [40]. The main advantage of the negativity is that it can be evaluated in the same way for pure and non-pure states in arbitrary dimensions, although there are entangled mixed states with zero negativity in every dimensions except 2×2 (two qubits) and 2×3 (a qubit and a qutrit) [41], [42]. Thus, negativity is

not in general an ideal measure of bipartite entanglement of non-pure states: no measure discriminating separable from entangled states in the general non-pure case is known. However, non-zero negativity is a sufficient condition for entanglement and for *distillability* [41] (a state is said to be distillable if a maximally entangled state can be obtained from it through (LOCC)), a very important property for Quantum Information tasks.

Chapter 3

Dynamics of entanglement in matter-radiation interaction

“A devil with merely local powers like a parish vestry would be too inconceivable a thing” (Sir Arthur Conan Doyle, *The hound of the Baskervilles*)

In this chapter we will analyze exhaustively the entanglement dynamics in a system consisting of a pair of two-level atoms interacting through a quantum electromagnetic field. In Section 3.1 we start from different initial separable states and consider different projections onto final states of the field. In Section 3.2 a protocol for generating highly entangled states between spacelike separated atoms is considered. Finally, in section 3.3 we start from an initial entangled state and study the phenomena of entanglement sudden death and entanglement sudden birth. Throughout all the chapter, entanglement measures are used to compute the evolution of entanglement and relate its behavior to the spacetime region in which the atoms are placed.

3.1 Generation of entanglement inside and outside the mutual light cone

3.1.1 Introduction

Quantum superposition and entanglement are the cornerstones lying at the foundations of quantum information and the principal support of the new quantum technologies which are at different stages of conception and development at present. Putting entanglement to work, enabling its use as a resource, is the key to the success of these technologies. Therefore, a complete understanding

of entanglement, necessary at the fundamental level, is also important for these developments to occur.

As we have explained in Chapter 1, entanglement can be envisaged in very different forms; it originally appeared in quantum mechanics [1] as a direct connection between distant particles, a residue of past direct interaction between them [2]. In quantum field theory entanglement can be traced back to the non-locality of the vacuum state [8, 43] or, simply, to field propagation. Similar arguments operate for a lattice of coupled oscillators [44].

In this section we analyze some features of entanglement generation closely related to the microscopic causality of quantum field theory. Put in simple words, this work attempts to ascertain whether a pair of spatially separated parties (say, a pair of neutral two-level atoms A and B) can get entangled in a finite time while they remain causally disconnected [15, 45, 46]. Each party interacts locally with the electromagnetic field, the carrier of the interaction. We stress here that, as shown in [46], perturbation theory produces non-signalling [14] results for this system and that the apparent causality violations come from the nonlocal specification of some final states. At first sight, the question can be answered in the negative; if the parties remain causally separated from each other, they can not entangle. However, the propagator $D(x, y)$ is finite even when $c(x - y)^0 < |\mathbf{x} - \mathbf{y}|$, and perhaps some correlations could be exchanged between both parties [10]. Alternatively, the correlations could be blamed on the preexisting entanglement between different parts of the vacuum [9, 12], which could be transferred to the atoms. Whatever the point of view, correlations are exchanged through (time ordered) products, while only commutators are restricted to be causal [47]. Our analysis can not sidestep that the role of the field goes beyond that of a mere carrier, quanta could be absorbed from the field or escape in the form of photons [48, 49]. How does the entanglement between A and B depend on the state of the field? This question shapes our discussion below.

We will include in the final state all the perturbatively accessible field states, analyzing for each of them the correlations in the reduced atomic state. We compute the entanglement measures for different values of $(x - y)^0$ and $|\mathbf{x} - \mathbf{y}|$, that lie inside the atoms mutual light cone and beyond. The atomic state that results after tracing over the states of the field is separable, which means, in the scheme of [9], that there is no transference of vacuum entanglement, only classical correlations. In [9], these correlations become entanglement when a suitable time dependent coupling with the scalar field is introduced. As pointed out in [12], this would require an unrealistic control of the atom-field interaction in the electromagnetic case that we are dealing with here. As an alternative way to achieve entanglement between the atoms we consider a post-selection process of the field states with $n = 0, 1, 2$ photons. This is a nonlocal operation and therefore entanglement generation is allowed. In [10], only the vacuum case when $|\mathbf{x} - \mathbf{y}| \gg c(x - y)^0$ was analyzed, and no entanglement measures were considered. We get quantum correlations for all the different field states. We also get useful hints on the nature of the correlations, whether they come from photon exchange, source indistinguishability, etc.

3.1.2 The model

We will consider the field initially in the vacuum state, including the cases with 0, 1 and 2 final photons to analyze perturbatively the amplitudes and density matrices to order α . We assume that the wavelengths relevant in the interaction with the atoms, and the separation between them, are much longer than the atomic dimensions. As seen in the previous chapter, under these conditions the Hamiltonian can be split into two parts

$$H = H_0 + H_I \quad (3.1)$$

that are separately gauge invariant. The first part is the Hamiltonian in the absence of interactions other than the potentials that keep A and B stable,

$$H_0 = H_{0PA} + H_{0PB} + H_{0R}. \quad (3.2)$$

H_{0PA} , H_{0PB} being the corresponding “free” Hamiltonians (2.9) of particles A and B , respectively, and H_{0R} is given by (2.8). The second contains all the interaction of the atoms with the field

$$H_I = - \sum_{n=A,B} \mathbf{d}_n(t) \mathbf{E}(\mathbf{x}_n, t), \quad (3.3)$$

where \mathbf{E} is the electric field (2.27), and

$$\mathbf{d}_n = \sum_i q_i (\mathbf{x}_i - \mathbf{x}_n) \quad (3.4)$$

is the electric dipole moment (2.11) of atom n , whose matrix elements (2.24) we will take as real and of equal magnitude for both atoms

$$\begin{aligned} \mathbf{d}_A &= \mathbf{d}_{Age} = \mathbf{d}_{Aeg} \\ \mathbf{d}_B &= \mathbf{d}_{Bge} = \mathbf{d}_{Beg} \\ |\mathbf{d}_A| &= |\mathbf{d}_B| \end{aligned} \quad (3.5)$$

$|e\rangle$ and $|g\rangle$ being the excited and ground states of the atoms, respectively.

In what follows we choose a system given initially by the product state,

$$|\psi(0)\rangle = |eg0\rangle \quad (3.6)$$

in which atom A is in the excited state $|e\rangle$, atom B in the ground state $|g\rangle$, and the field in the vacuum state $|0\rangle$. The system then evolves under the effect of the interaction during a lapse of time t into a state:

$$|\psi(t)\rangle = T[e^{-i \int_0^t dt' H_I(t')/\hbar}] |\psi\rangle_0, \quad (3.7)$$

(T being the time ordering operator) that, to order α , can be given in the interaction picture as

$$\begin{aligned} |\text{atom}_1, \text{atom}_2, \text{field}\rangle_t &= ((1 + A) |eg\rangle + X |ge\rangle) |0\rangle \\ &+ (U_A |gg\rangle + V_B |ee\rangle) |1\rangle + (F |eg\rangle + G |ge\rangle) |2\rangle \end{aligned} \quad (3.8)$$

where

$$\begin{aligned}
A &= \frac{1}{2} \langle 0 | T(\mathcal{S}_A^+ \mathcal{S}_A^- + \mathcal{S}_B^- \mathcal{S}_B^+) | 0 \rangle, \quad X = \langle 0 | T(\mathcal{S}_B^+ \mathcal{S}_A^-) | 0 \rangle \\
U_A &= \langle 1 | \mathcal{S}_A^- | 0 \rangle, \quad V_B = \langle 1 | \mathcal{S}_B^+ | 0 \rangle \\
F &= \frac{1}{2} \langle 2 | T(\mathcal{S}_A^+ \mathcal{S}_A^- + \mathcal{S}_B^- \mathcal{S}_B^+) | 0 \rangle, \quad G = \langle 2 | T(\mathcal{S}_B^+ \mathcal{S}_A^-) | 0 \rangle,
\end{aligned} \tag{3.9}$$

being

$$\begin{aligned}
\mathcal{S}_n &= -\frac{i}{\hbar} \int_0^t dt' H_I(t') = \mathcal{S}_n^+ + \mathcal{S}_n^- \\
\mathcal{S}_n^\pm &= -\frac{i}{\hbar} \int_0^t dt' e^{\mp \frac{i\Omega t'}{\hbar}} \sigma^\pm \mathbf{d}_n \mathbf{E}(\mathbf{x}, t),
\end{aligned} \tag{3.10}$$

(the sign of the superscript in 3.10 is associated to the energy difference between the initial and final atomic states of each emission) and $|n\rangle$, $n = 0, 1, 2$ is a shorthand for the state of n photons with arbitrary momenta and polarizations, i.e.

$$|1\rangle \langle 1| = \sum_\lambda \int d^3 \mathbf{k} |\mathbf{k}, \epsilon(\mathbf{k}, \lambda)\rangle \langle \mathbf{k}, \epsilon(\mathbf{k}, \lambda)|, \tag{3.11}$$

etc. Ω is the frequency of the atomic transition, as defined in (2.21).

Among all the terms that contribute to the final state (3.8) only X corresponds to interaction between both atoms, which is “real” interaction only if $ct > r$ (r being the interatomic distance). This would change at higher order in α . Here, A describes intra-atomic radiative corrections, U_A and V_B single photon emission by one atom, and G by both atoms, while F corresponds to two photon emission by a single atom. Details on the computations of these quantities would be given in Appendix A.

In Quantum Optics terms like V_B , F and G are usually neglected by the introduction of a RWA. But here we are interested in the short time behavior, and therefore all the terms must be included, as in [46, 50, 51]. Actually, only when all the non-RWA effects are considered, it could be said properly that the probability of excitation of atom B is completely independent of atom A when $r > ct$ [50, 51] (r being the distance between the atoms).

Note that the actions in (3.10) depends on the atomic properties Ω and \mathbf{d}_n , and on the interaction time t . In our calculations we will take $(\Omega |\mathbf{d}_n| / ec) = 5 \cdot 10^{-3}$, which is of the same order as the $1s \rightarrow 2p$ transition in the hydrogen atom, consider $\Omega t \gtrsim 1$, and analyze the cases $(r/ct) \simeq 1$ near the mutual light cone, inside and outside.

Given a definite field state $|n\rangle$ the pair of atoms is in a pure two qubits state as shown in (3.8). We will denote these states by $|AB\rangle_n$, then

$$\rho_{AB}^{(n)} = |AB\rangle_{nn} \langle AB|, \tag{3.12}$$

and the corresponding reduced states by

$$\rho_A^{(n)} = Tr_B \rho_{AB}^{(n)}, \quad \rho_B^{(n)} = Tr_A \rho_{AB}^{(n)}, \tag{3.13}$$

in the following, and will compute the entropy of entanglement $\mathbb{S}^{(n)}$ [52]:

$$\mathbb{S}^{(n)} = \text{Tr} \rho_A^{(n)} \log \rho_A^{(n)} \quad (3.14)$$

and the concurrence $\mathbb{C}^{(n)}$ [38]:

$$\mathbb{C}^{(n)} = \max\{0, \sqrt{\lambda_i} - \sum_{j \neq i} \sqrt{\lambda_j}\} \quad (3.15)$$

λ_i being the largest of the eigenvalues λ_j ($j = 1, \dots, 4$) of

$$R_{AB} = [(\sigma_y \otimes \sigma_y) \rho_{AB} * (\sigma_y \otimes \sigma_y)] \rho_{AB} \quad (3.16)$$

for them.

3.1.3 The case with $n = 0$

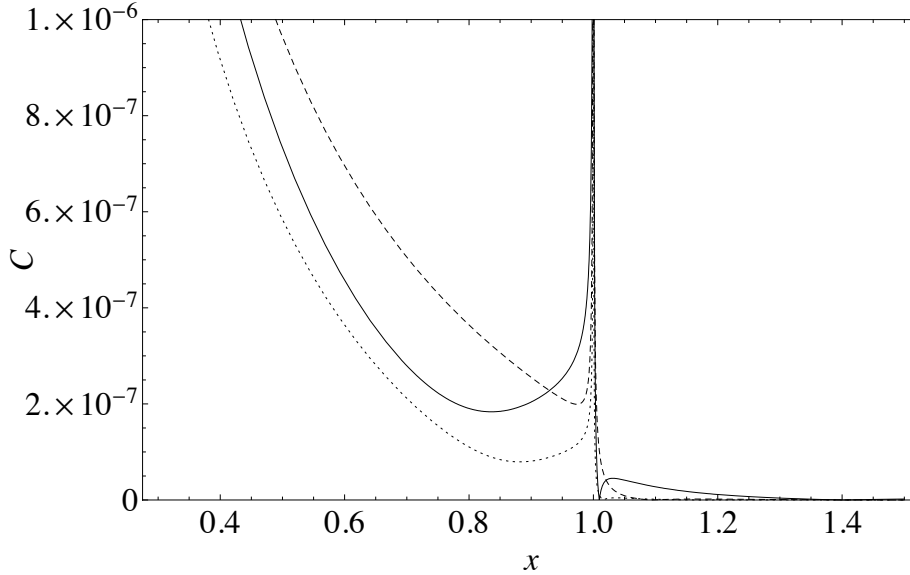


Figure 3.1: Concurrence of the atomic state in the e.m. vacuum $\rho_{AB}^{(0)}$ as a function of $x = (r/ct)$ for three values of $z = (\Omega r/c) = 5$ (solid line), 10 (dashed line) and 15 (dotted line). The height of the peak is $\mathbb{C}^{(0)} = 1$.

We first consider the case $n = 0$, where the field is in the vacuum state and, after (3.8), the atoms are in the pure state

$$|AB\rangle_0 = ((1 + A) |EG\rangle + X |GE\rangle) / c_0, \quad (3.17)$$

where $c_0 = \sqrt{|1 + A|^2 + |X|^2}$ is the normalization, giving a concurrence

$$\mathbb{C}^{(0)} = 2|X| |1 + A| / c_0^2. \quad (3.18)$$

It is interesting to note that at lowest order the concurrence arises as an effect of the mutual interaction terms X mediated by photon exchange or, in a different language, by the vacuum fluctuations. As expected, at higher orders the radiative corrections described by A dress up these correlations. Analytic lowest order calculations ([53]) showed that they can persist beyond the mutual light cone, vanishing for $x = (r/ct) \rightarrow \infty$. We sketched in Fig. 3.1 the concurrence $\mathbb{C}^{(0)}$ for x around 1. Our computations were done for the illustrative case where both dipoles are parallel and orthogonal to the line joining A and B . We will adhere to this geometrical configuration for the rest in the following. It would correspond to an experimental set up in which the dipoles are induced by suitable external fields. $\mathbb{C}^{(0)}$ shows a strong peak (of height 1) inside a tiny neighborhood of $x = 1$. The features outside the mutual light cone are $\vartheta(|\mathbf{d}|/er)^2 \simeq 10^{-6}$ here, and could be larger if $\Omega t < 1$ entering into the Zeno region (incidentally, $|X| \propto t^4$ for very small t [53]). Notice the change of behavior between the region where the atoms are spacelike separated ($x < 1$) and the region where one atom is inside the light cone of the other ($x > 1$). This quantitative treatment complements the qualitative one given in [10].

The entropy of entanglement written in terms of the small quantity

$$\eta_0 = (|X|/c_0)^2 \in (0, 1) \quad (3.19)$$

is

$$\mathbb{S}^{(0)} = -(1 - \eta_0) \log(1 - \eta_0) - \eta_0 \log \eta_0, \quad (3.20)$$

this is a positive quantity in $(0, 1)$, which attains its maximum possible value $\mathbb{S}^{(0)} = 1$ when the state is maximally entangled at $\eta_0 = 0.5$. This is well within the small neighborhood of $x = 1$ mentioned above. Radiative corrections would shift the maximum to $|X| = |1 + A|$, so the entropy is sensitive to the Lamb shift when this contributes to the dipole radiative corrections.

3.1.4 Photon emission

We now come to the case $n = 1$, where the atoms excite one photon from the vacuum, jumping to the state

$$|AB\rangle_1 = (U_A |gg\rangle + V_B |ee\rangle)/c_1, \quad (3.21)$$

(with $c_1 = \sqrt{|U_A|^2 + |V_B|^2}$), during the time interval t . The density matrix for this case contains the term

$$l = V_B U_A^* = Tr_1 \langle 1 | \mathcal{S}_B^+ | 0 \rangle \langle 1 | \mathcal{S}_A^- | 0 \rangle^* = \langle 0 | \mathcal{S}_A^+ \mathcal{S}_B^+ | 0 \rangle, \quad (3.22)$$

producing a concurrence

$$\mathbb{C}^{(1)} = 2|l|/c_1^2, \quad (3.23)$$

so, even if this case only describes independent local phenomena attached to the emission of one photon by either atom A or B , the concurrence comes from the tangling between the amplitudes u and v which have different loci. The

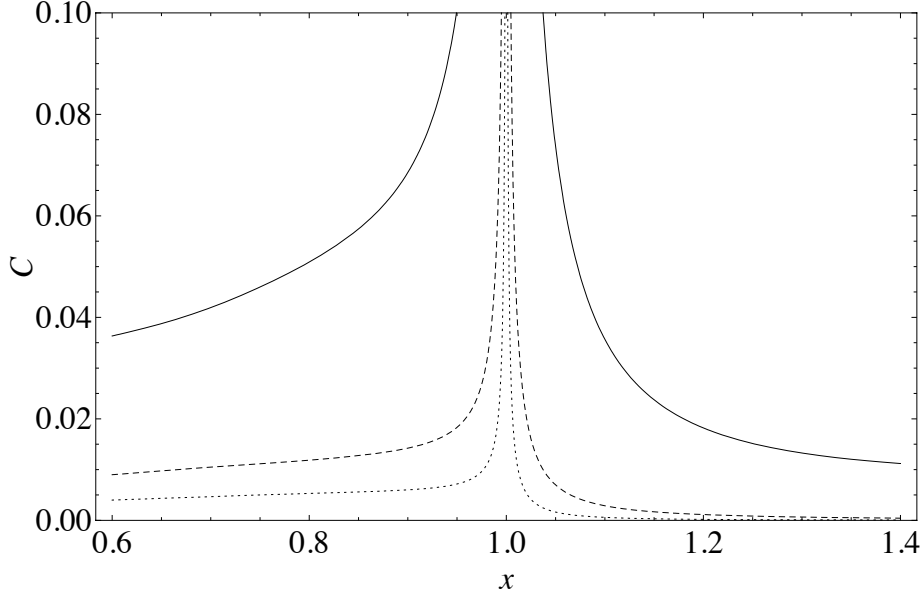


Figure 3.2: Concurrence for one photon final state (3.23) as a function of $x = r/ct$ for three values of $z = \Omega r/c = 5$ (solid line), 10 (dashed line) and 15 (dotted line). Entanglement vanishes as $t \rightarrow \infty$ ($x \rightarrow 0$ for a given r) and is sizeable for $x > 1$.

state of the photon emitted by A and the state of A are correlated in the same way as the state of the photon emitted by B with the state of B are. These independent field-atom correlations are transferred to atom-atom correlations when we trace out a photon line with different ends, A and B , when computing $V U^*$. In fact, while $|U|^2$ and $|V|^2$ are independent of the distance r between the atoms,

$$l = -\frac{cd_A^i d_B^j}{\hbar\epsilon_0} \{(\delta_{ij} - \hat{r}_i \hat{r}_j) M''(r) + (\delta_{ij} + \hat{r}_i \hat{r}_j) \frac{M'(r)}{r}\} \quad (3.24)$$

where

$$M(r) = \int_0^\infty dk \frac{\sin kr}{r} \delta^t(\Omega + ck) \delta^t(\Omega - ck) \quad (3.25)$$

which depends explicitly on r . Above we used $\delta^t(\omega) = \sin(\omega t/2)/(\pi\omega)$, which becomes $\delta(\omega)$ in the limit $t \rightarrow \infty$. In Fig. 3.2 we represent $\mathbb{C}^{(1)}$ in front of $x = r/ct$ for some values of $z = \Omega r/c$. As the Figure shows, there may be a significant amount of concurrence for all x , indicating that $\rho^{(1)}$ is an entangled state inside and outside the mutual light cone. The peak at $x = 1$ comes from the term with phase $k(r-ct)$ that can be singled out from the linear combination of phasors in the integrand of (3.25).

Here we have a lone photon whose source we cannot tell. It might be A or B , with the values of l and $\mathbb{C}^{(1)}$ depending on their indistinguishability. Eventually, RWA will forbid the process $g \rightarrow e + \gamma$ for large interaction times. Therefore, V_B , l and $\mathbb{C}^{(1)}$ will vanish as t grows to infinity ($x \rightarrow 0$ for each value of z in Fig. 2), as can be deduced from the vanishing of $\delta^t(\Omega + ck)$ for $t \rightarrow \infty$.

The entropy of entanglement gives an alternative description of the situation. Its computation requires tracing over one of the parts A or B , so no information is left in $\mathbb{S}^{(1)}$ about r , but it still gives information about the relative contribution of both participating states $|ee\rangle$ and $|gg\rangle$ to the final state. In terms of

$$\eta_1 = |V|^2/c_1^2 \in (0, 1), \quad (3.26)$$

we have

$$\mathbb{S}^{(1)} = -(1 - \eta_1) \log(1 - \eta_1) - \eta_1 \log \eta_1 \quad (3.27)$$

Would not be for the difference between $\Omega + ck$ and $\Omega - ck$, V_B should be equal to U_A , $\eta_1 = 0.5$, and $\mathbb{S}^{(1)}$ would attain its maximum value. Not only this is not the case but, as said above, V_B will vanish with time and only $|gg\rangle$ will be in the final asymptotic state. Notice the result, indistinguishability was swept away because for large t we know which atom (A) emitted the photon. Therefore, the entropy will eventually vanish for large interaction times.

There are two possibilities with $n = 2$; one (with amplitude F) when both photons are emitted by the same atom, the other (with amplitude G) when each atom emits a single photon. The final atomic state

$$|AB\rangle_2 = (F|eg\rangle + G|ge\rangle)/c_2, \quad (3.28)$$

with $c_2 = \sqrt{|F|^2 + |G|^2}$, is in the same subspace as for $n = 0$. The normalization c_2 is $\mathcal{O}(\alpha)$ like the expectation values F , G , so that all the coefficients in $\rho_{AB}^{(2)}$ may be large. The concurrence is

$$\mathbb{C}^{(2)} = 2|FG^*|/c_2^2. \quad (3.29)$$

Due to the tracing over photon quantum numbers, FG^* is a sum of products containing not only factors U_A and V_B , but also r dependent factors like l . The entropy $\mathbb{S}^{(2)}$ is now given in terms of a parameter

$$\eta_2 = |G|^2/c_2^2. \quad (3.30)$$

Notice that

$$|G|^2 = |U_A|^2|V_B|^2 + |l|^2. \quad (3.31)$$

Hence, both $\mathbb{C}^{(2)}$ and $\mathbb{S}^{(2)}$, depend on r . This is different from the single photon case, where the only r dependence was in the coherences of $\rho_{AB}^{(1)}$, which did not feed into $\rho_A^{(1)}$. The correlations came in that case from the indistinguishability of the photon source. The case $n = 2$ resembles that of the entanglement swapping paradigm [6], where there are two independent pairs of down converted photons. Here we have two independent atom - photon pairs. The swapping would arise

in both cases from detecting one photon of each pair. But with the initial state we are considering here, both F and G eventually vanish. More interesting would be the case with the initial atomic state $|ee\rangle$, that will be considered in section 3.1.5.

3.1.5 Tracing over the field

We have seen that if the state of the field is defined, the atomic state is entangled inside and outside the light cone. But what happens if the field state is ignored, that is, if we trace over the field degrees of freedom? Then the atomic state is represented by the following density matrix (in the basis $\{|ee\rangle, |eg\rangle, |ge\rangle, |gg\rangle\}$):

$$\rho_{AB} = \begin{pmatrix} |V_B|^2 & 0 & 0 & l \\ 0 & |1+A|^2 + |F|^2 & (1+X)^* + FG^* & 0 \\ 0 & X(1+A)^* + F^*G & |X|^2 + |G|^2 & 0 \\ l^* & 0 & 0 & |U_A|^2 \end{pmatrix} N^{-1} \quad (3.32)$$

where $l = \langle 0 | \mathcal{S}_A^+ \mathcal{S}_B^+ | 0 \rangle$ was used again, and $N = |1+A|^2 + |X|^2 + |U|^2 + |V|^2 + |F|^2 + |G|^2$.

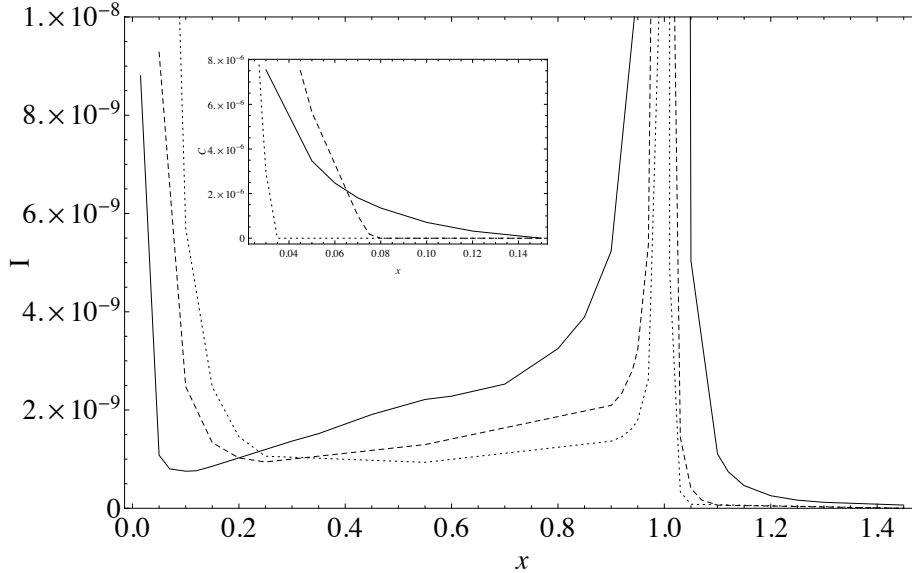


Figure 3.3: Mutual information of ρ_{AB} as a function of $x = r/ct$ for $z = \Omega r/c = 5$ (solid line), 10 (dashed line), 15 (dotted line). The inset shows the finite concurrences that are possible only for small values of x .

The state in (3.32) is an example of the so-called X-states, and the concurrence of such a state is given by:

$$C(\rho_{AB}) = \frac{2}{c} \max \{ |\rho_{23}| - \sqrt{\rho_{11}\rho_{44}}, |\rho_{14}| - \sqrt{\rho_{22}\rho_{33}}, 0 \}. \quad (3.33)$$

Numerical computations show that the concurrence associated to this density matrix always vanishes except for a bounded range of small values of x . Beyond this range ρ_{AB} is a separable state with no quantum correlations, either inside or outside the light cone. But the atoms A and B are mutually dependent even for zero concurrence. Their mutual information

$$\mathbb{I}(\rho_{AB}) = \mathbb{S}(\rho_A) + \mathbb{S}(\rho_B) - \mathbb{S}(\rho_{AB}), \quad (3.34)$$

which measures the total correlations between both parties, is completely classical in this case, but may be finite. We show this quantity in Fig. 3.3 for different values of z with an inset with the concurrence for small values of x .

3.1.6 Different initial states

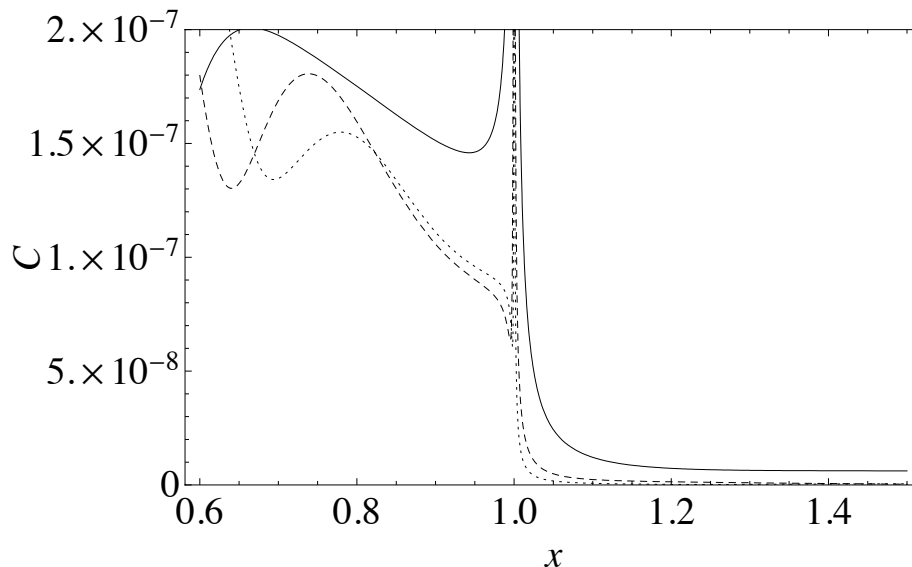


Figure 3.4: Concurrence $\mathcal{C}^{(0)}$ of the atomic state in the e.m. vacuum $\rho_{AB}^{(0)}$ as a function of $x = (r/ct)$ for $z = (\Omega r/c) = 5$ (solid line), 10 (dashed line) and 15 (dotted line). The height of the peak is $\mathcal{C}^{(0)} = 1$. $x \rightarrow 0$ ($t \rightarrow \infty$) is the region usually considered in Quantum Optics.

In what follows we choose a system given initially by the product state,

$$|\psi(0)\rangle = |ee0\rangle \quad (3.35)$$

in which atoms A and B are in the excited state $|e\rangle$ and the field in the vacuum state $|0\rangle$. The system then evolves under the effect of the interaction during a lapse of time t into a state:

$$|\psi(t)\rangle = e^{-i \int_0^t dt' H_I(t')/\hbar} |\psi\rangle_0 \quad (3.36)$$

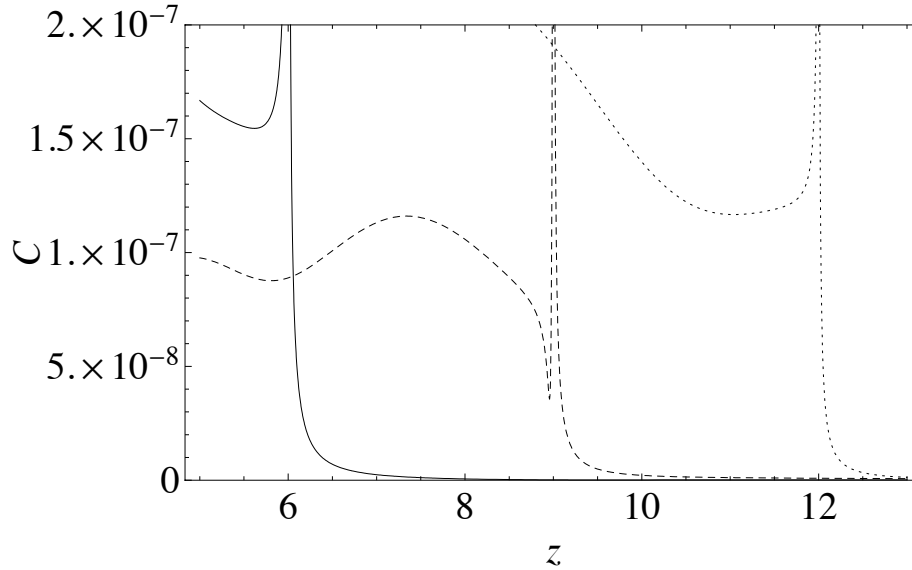


Figure 3.5: Concurrence $\mathcal{C}^{(0)}$ of the atomic state in the e.m. vacuum $\rho_{AB}^{(0)}$ if $|ee\rangle$ is the initial state as a function of $z = (\Omega r/c)$ for $z/x = \Omega t = 6$ (solid line), 9 (dashed line) and 12 (dotted line). $x > 1$ amounts to $z > \Omega t$ in each case.

that, to order α , can be given in the interaction picture as

$$\begin{aligned} |\text{atom}_1, \text{atom}_2, \text{field}\rangle_t &= ((1 + A') |ee\rangle + X' |gg\rangle) |0\rangle \\ &+ (U_A |ge\rangle + U_B |eg\rangle) |1\rangle + (F' |ee\rangle + G' |gg\rangle) |2\rangle \end{aligned} \quad (3.37)$$

where

$$\begin{aligned} A' &= \frac{1}{2} \langle 0 | T(\mathcal{S}_A^+ \mathcal{S}_A^- + \mathcal{S}_B^+ \mathcal{S}_B^-) | 0 \rangle, \quad X' = \langle 0 | T(\mathcal{S}_B^- \mathcal{S}_A^-) | 0 \rangle \\ U_A &= \langle 1 | \mathcal{S}_A^- | 0 \rangle, \quad U_B = \langle 1 | \mathcal{S}_B^- | 0 \rangle \\ F' &= \frac{1}{2} \langle 2 | T(\mathcal{S}_A^+ \mathcal{S}_A^- + \mathcal{S}_B^+ \mathcal{S}_B^-) | 0 \rangle, \quad G' = \langle 2 | T(\mathcal{S}_B^- \mathcal{S}_A^-) | 0 \rangle. \end{aligned} \quad (3.38)$$

The objects \mathcal{S}_n^\pm has been defined in (3.10). As in the previously analyzed case, in (3.37) only X' corresponds to interaction between both atoms, and now is a completely non-RWA term. A' describes intra-atomic radiative corrections, U_A and U_B single photon emission by one atom, and G' by both atoms, while F' corresponds to two photon emission by a single atom.

We begin with the case $n = 0$, where the field is in the vacuum state and, following (3.37), the atoms are in the projected pure state

$$|AB\rangle_0 = ((1 + A') |ee\rangle + X' |GG\rangle) / c_0, \quad (3.39)$$

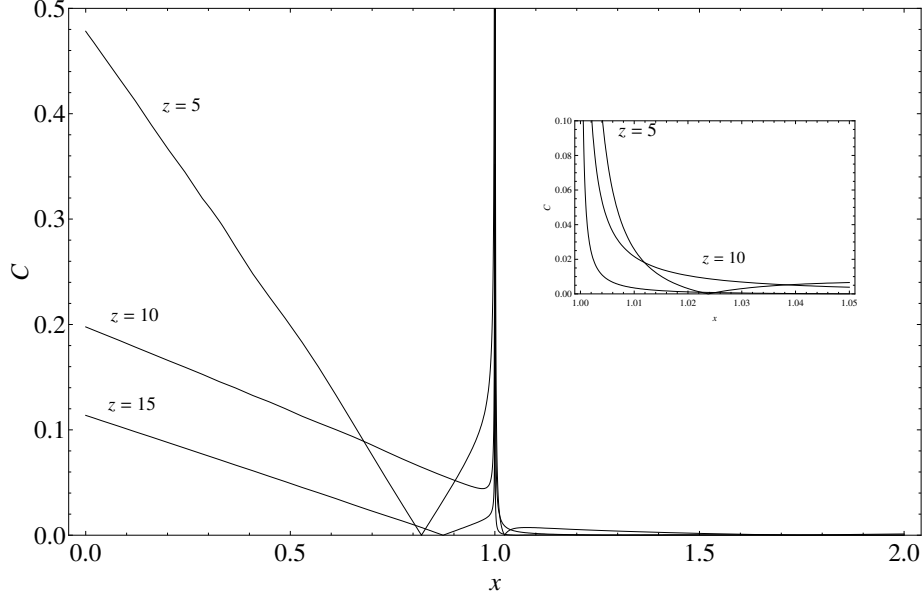


Figure 3.6: Concurrence $\mathcal{C}^{(1)}$ for one photon final state if $|ee\rangle$ is the initial state as a function of $x = r/ct$ for three values of $z = \Omega r/c$. The values of \mathbb{C} for $x > 1$ are of the same order as those displayed in Fig. .

where $c_0 = \sqrt{|1 + A'|^2 + |X'|^2}$ is the normalization, giving a concurrence

$$\mathcal{C}^{(0)} = 2|X'| |1 + A'| / c_0^2. \quad (3.40)$$

The computation of A' and X' can be performed following the lines given in Appendix A where they were computed for the case of a initial atomic state $|eg\rangle$. We will consider that the dipoles are parallel along the z axis, while the atoms remain along the y axis. Under that conditions, using the dimensionless variables $x = r/ct$ and $z = \Omega r/c$:

$$\begin{aligned} A' &= \frac{4iKz^3}{3x} (\ln|1 - \frac{z_{max}}{z}| + 2i\pi), \\ X' &= \frac{\alpha d_i d_j}{\pi e^2} (-\nabla^2 \delta_{ij} + \nabla_i \nabla_j) I, \end{aligned} \quad (3.41)$$

with $K = \alpha |\mathbf{d}|^2 / (e^2 r^2)$ and $I = I_+ + I_-$, where:

$$\begin{aligned} I_{\pm} &= \frac{-i e^{-i \frac{z}{x}}}{2z} [\pm 2 \cos(\frac{z}{x}) e^{\pm iz} Ei(\mp iz) + e^{-iz(1 \pm \frac{1}{x})} \\ &\quad Ei(iz(1 \pm \frac{1}{x})) - e^{iz(1 \pm \frac{1}{x})} Ei(-iz(1 \pm \frac{1}{x}))] \end{aligned} \quad (3.42)$$

for $x > 1$ with the additional term $-2\pi i e^{iz(1-1/x)}$ for $x < 1$. We use the conventions and tables of [54].

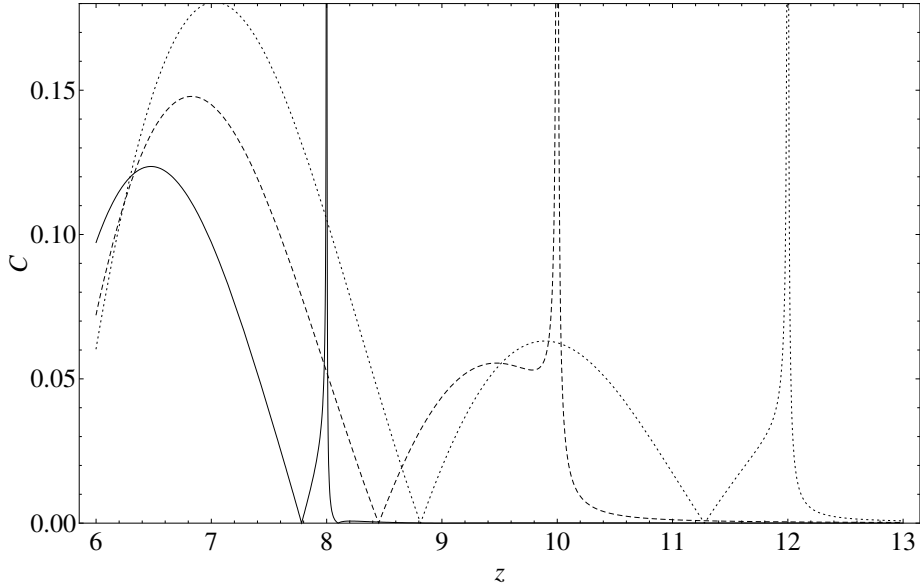


Figure 3.7: Concurrence $\mathcal{C}^{(1)}$ for one photon final state if $|ee\rangle$ is the initial state as a function of $z = \Omega r/c$ for three representative values of the time $\Omega t = 8, 10, 12$ with peaks at $z = 8, 10$ and 12 respectively.

We show in Fig. 3.4 the concurrence $\mathcal{C}^{(0)}$ (3.40) for x near 1 for given values of z . Like the case where $|eg\rangle$ is the initial atomic state, $\mathcal{C}^{(0)}$ jumps at $x = 1$ and has different behaviors at both sides. In Fig. 3.5 the concurrence is sketched as a function of z for given values of $\Omega t = z/x$. The tiny values of the concurrence for the region $z > \Omega t$ (which corresponds to $x > 1$), diminish as t grows and will eventually vanish, since X' is a non-RWA term.

In the case $n = 1$ the final one photon atomic state would be

$$|AB\rangle_1 = (U_A |ge\rangle + U_B |eg\rangle)/c'_1, \quad (3.43)$$

where U_A is the same function of \mathbf{x}_A as U_B is of \mathbf{x}_B , and $c'_1 = \sqrt{2|U_A|^2}$. Now, the indistinguishability of the photon source commented in Section 3.1.3 persists for large t and so does entropy and concurrence. In particular, the r -dependent concurrence is

$$\mathbb{C}^{(1)} = 2|l'|/(c'_1)^2, \quad (3.44)$$

where

$$l' = \langle 0 | \mathcal{S}_A^+ \mathcal{S}_B^- | 0 \rangle. \quad (3.45)$$

We represent it in Fig. 3.6. In Fig. 3.7 we have represented the concurrence for the case where the initial atomic state was $|ee\rangle$ in terms of the inter-atomic distance for three fixed values of time. What we obtain is a shift of the concurrence features to longer r as t grows (so that they appear at the same (r/ct)), in

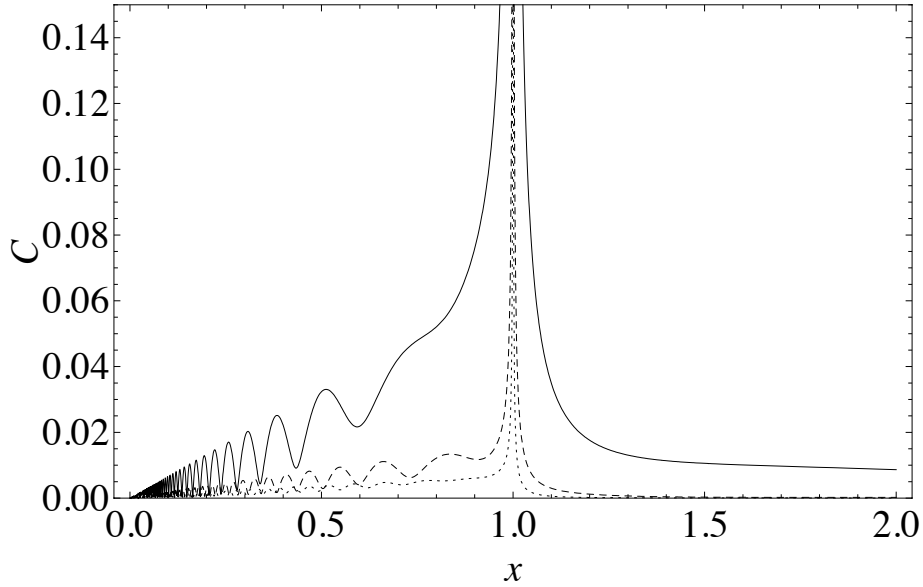


Figure 3.8: Concurrence $\mathcal{C}^{(2)}$ of the atomic state with $n = 2$ photons $\rho_{AB}^{(2)}$ in front of $x = r/(ct)$ for $z = \Omega r/c = 5$ (solid line), 10 (dashed line) and 15 (dotted line).

such a way that, even if t is just the duration of the interaction, it plays the role of propagation time for the generated correlations. They are negligible small for large r , peak at the “light cone” but, on the other hand grow, as we would expect, for larger interaction times.

Now we will focus on the two photon case. The final atomic state

$$|AB\rangle_2 = (F'|eg\rangle + G'|ge\rangle)/c_2, \quad (3.46)$$

with $c_2 = \sqrt{|F'|^2 + |G'|^2}$, is in the same subspace as for $n = 0$. The normalization c_2 is $\mathcal{O}(\alpha)$ like F' , G' , so that all the coefficients in $\rho^{(2)}$ may be large. Therefore, although the probability of attaining this state is small, the correlations are not. The concurrence is

$$\mathcal{C}^{(2)} = 2|F'G'^*|/c_2^2. \quad (3.47)$$

We find that:

$$\begin{aligned} F' &= \theta(t_1 - t_2)(V_A(t_1)U'_A(t_2) + U_A(t_1)V'_A(t_2) \\ &\quad + V_B(t_1)U'_B(t_2) + U_B(t_1)V'_B(t_2)) \\ G' &= U_B U'_A + U_A U'_B \end{aligned} \quad (3.48)$$

with $V_A = \langle 1|\mathcal{S}_A^+|0\rangle$ and $V_B = \langle 1|\mathcal{S}_B^+|0\rangle$. The primes account for the two single photons, i.e.

$$|2\rangle = |\mathbf{k}\epsilon_\lambda, \mathbf{k}'\epsilon_{\lambda'}\rangle. \quad (3.49)$$

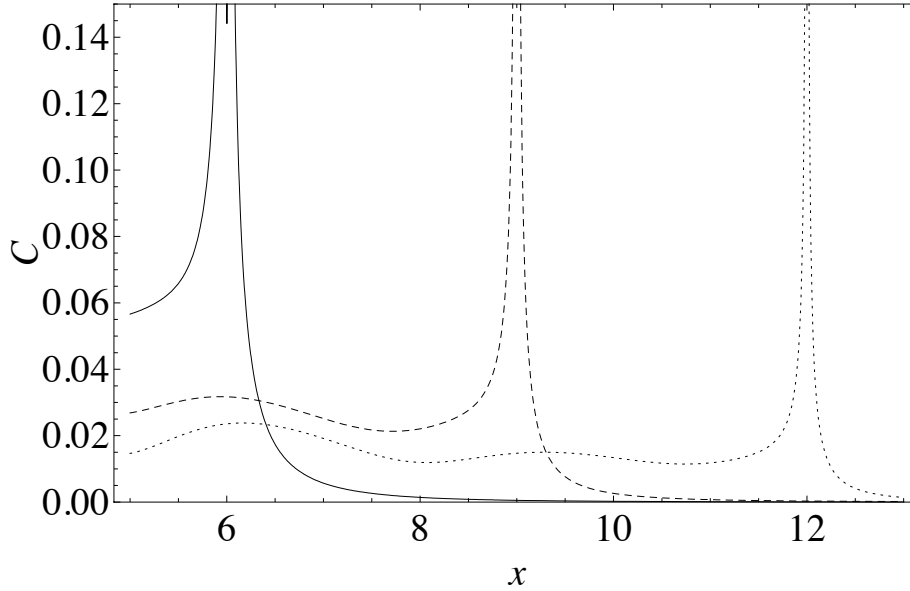


Figure 3.9: Concurrence $\mathcal{C}^{(2)}$ of the atomic state with $n = 2$ photons $\rho_{AB}^{(2)}$ in front of $z = \Omega r/c$ for $\Omega t = z/x = 6$ (solid line), 9 (dashed line) and 12 (dotted line).

The quantities $|U_A|^2 = |U_B|^2 = |U|^2$, $|V_A|^2 = |V_B|^2 = |V|^2$, $l = U_A V_B^* = U_B V_A^*$, $UV^* = U_A^* V_A^* = U_B V_B^*$, $U_B U_A^*$ and $V_A V_B^*$ can be computed following the lines in Appendix A.

In Fig. 3.8 we show $\mathcal{C}^{(2)}$ in front of x for given values of z . When $x \rightarrow 0$ ($t \rightarrow \infty$, i.e. the Quantum Optics regime), F^l vanishes and the final atomic state would be the separable state $|gg\rangle$, with zero concurrence. Entanglement is sizable for $x > 1$, and could be maximized if a particular two photon state was detected, as we will explain in the next section.

In Fig. 3.9, $\mathcal{C}^{(2)}$ is sketched as a function of z for given values of $\Omega t = z/x$. Again, the concurrence for the region $z > \Omega t$ ($x > 1$), diminish as t grows and will eventually vanish, since it is due to f , which is a non-RWA term. Interestingly, as we noted for the single photon emission, $x = 1$ is a singular point that divides the spacetime into two different regions. This occurs even if t is not the propagation time of any physical signal between the atoms. This effect comes from the appearance of effective interaction terms like l , that would be missing if we could discriminate the source of emission of each photon.

3.1.7 Conclusions

In this section we have studied the correlations between a pair of initially separable neutral two-level atoms that are allowed to interact with the electromagnetic

field, initially in the vacuum state. We have computed the concurrences that arise when the final state contains $n = 0, 1$, or 2 photons. They may be sizable for x small ($t \rightarrow \infty$ for a given r) and also around $x = 1$. Only in the case $n = 0$ there are interactions between both atoms, generating an entanglement that may persist asymptotically in the case that $|eg\rangle$ is the initial atomic state. We have carefully taken into account all the terms contributing to the amplitude for finite time (they are $\propto t^4$, not $\propto t^2$ as is sometimes assumed). A small amount of entanglement can be generated between spacelike separated parties due to the finiteness of X when $x > 1$, but a change of behavior appears for $x < 1$. For $n = 2$ the final atoms are in the same subspace than for $n = 0$. There are similar correlations that in this case can give rise to entanglement swapping, by measuring both photons in a definite state for instance. Naturally, in this case entanglement may be sizable for spacelike separated parties, as here this is not related to any kind of propagation. Entanglement in the case with only a final photon ($n = 1$) comes from the indistinguishability of the photon source. It will vanish asymptotically in the case that the initial states is $|eg\rangle$ when eventually only one atom (A in the present case) may emit the photon, and it is also sizable when $x > 1$. It is interesting how these correlations become classical (except for small x) when the states of the field are traced over. We have shown through the mutual information the residues of what were quantum correlations in the individual cases analyzed before.

3.2 Entanglement swapping between spacelike separated atoms

3.2.1 Introduction

There are mainly two different known ways of generate entanglement: by interaction between the atoms (for instance, [55]) or by detection of the emitted photons [48, 56, 57, 58, 49]. Some of these proposals have been realized experimentally (for instance, [59]). For the latter cases, in principle, there is no reason to expect that the swapping [6] of atom-photon to atom-atom entanglement can only begin to occur when one atom enter into the light cone of the other.

The possibility of entanglement generation between spacelike separated atoms is of both theoretical and practical interest, and was addressed from different points of view in [10, 9, 12] and in the previous section of this Thesis. In section 3.1, we analyze this issue perturbatively in a simple model of a pair of two-level atoms interacting locally with the electromagnetic field, initially in the vacuum state. Tracing over the field states, the atoms are only classically correlated, but applying $|n\rangle\langle n|$ ($n = 0, 1, 2$ being the number of photons up to second order in perturbation theory), the atoms get entangled. For $n = 0$ the entanglement is generated by the interaction term and therefore is only relevant when one atom enter into the light cone of the other, despite of the finiteness of the Feynman propagator beyond that region. But for $n = 1, 2$ entanglement may be sizeable, although small, if the interatomic distance is short enough. In [9], the trace

over the field states was considered in a model with a pair of two-level detectors coupled to a scalar field. The detectors may get entangled if a suitable time dependent coupling is introduced, and this was applied to a linear ion trap in [12]. In [10], only the vacuum case when $t \rightarrow 0$ was analyzed, and no entanglement measures were considered.

As commented in chapter 1, there are two possible interpretations for these effects: as a transfer of preexisting entanglement of the vacuum [9, 12] or as a consequence of the propagation of virtual quanta outside the light cone [10]. Both are compared and discussed in [10].

In this section we will go one step further and consider that the photons are detected with definite momenta and polarizations. We show that, in principle, a high degree of entanglement, even maximal, can be generated between spacelike separated atoms if a Bell state of the emitted photons is detected. We will consider a pair of neutral two-level atoms separated by a fixed and arbitrary distance and study the evolution of an initially uncorrelated state under local interaction with the electromagnetic field. We focus on the two-photon emission which, although has a smaller probability of success, shows a larger fidelity of the projected state with the desired state and has a entanglement robust to atomic recoil [60]. The photons pass through a partial Bell-state analyzer [61], and we use entanglement measures to study the evolution of entanglement in the projected atomic states after detection of the different photonic Bell states. The results show that interaction times must be short, but interatomic distances can be as large as desired. The interaction time is independent of the photodetection time, which is only related with the distance from the atoms to the detectors. That distance can be such that the photodetection can occur while the atoms remain spacelike separated.

The results can be interpreted as a transfer of part of the vacuum entanglement after a post-selection process. If no measurement were performed the atoms would have classical correlations transferred by the vacuum. In [9] the classical correlations may become entanglement with a suitable time dependent coupling. The post-selection process can be seen as an alternative way to achieve the entanglement transference. While the results in [10, 9] are mainly theoretical, these could be probed experimentally, and would show for the first time the possibility of transfer entanglement from the vacuum state of the quantum field to spacelike separated atoms.

3.2.2 Entanglement swapping between spacelike separated atoms

In what follows we choose a system given initially by the product state,

$$|\psi(0)\rangle = |ee0\rangle \quad (3.50)$$

in which atoms A and B are in the excited state $|e\rangle$ and the field in the vacuum state $|0\rangle$. As in the previous section, the system then evolves under the effect

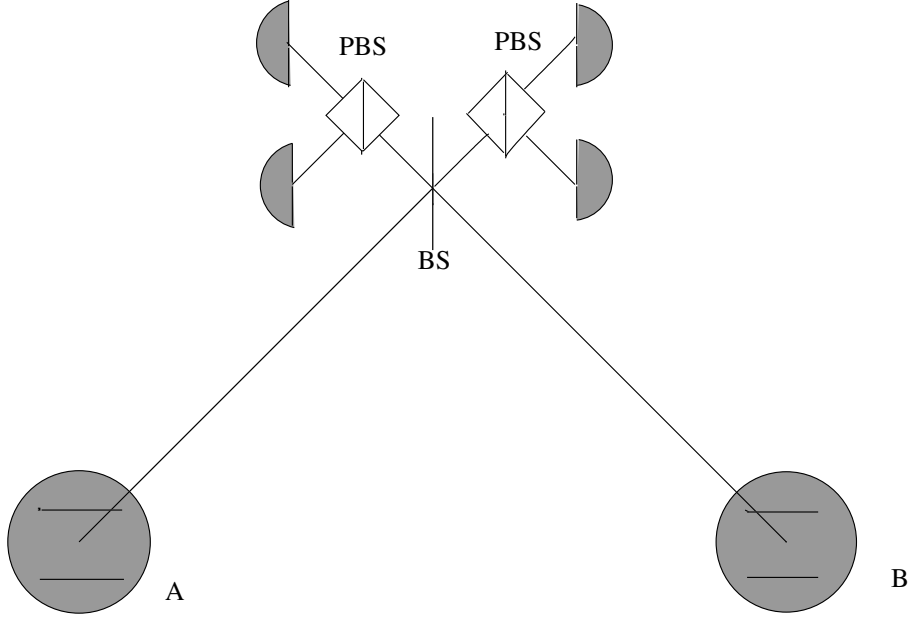


Figure 3.10: Schematic setup for the entanglement swapping described in the text. The atoms A and B are at $(y, z) = (\mp r/2, 0)$. The emitted photons pass through a 50 : 50 BS at $(0, r/2)$ and two PBS at $(\pm d/2\sqrt{2}, L/2 + d/2\sqrt{2})$, and there are four single photon detectors at the output ports of the two PBS, at $(\pm d/\sqrt{2}, r/2 + d/\sqrt{2})$ and $(\pm d/\sqrt{2}, r/2)$. Taking into account that $|\Psi^- \rangle$ and $|\Phi^- \rangle$ are forbidden in our model, a $|\Psi^+ \rangle$ is detected when there are coincidence clicks in two detectors and $|\Phi^+ \rangle$ when there is a double click in one detector. Then the atoms are projected onto the atomic part of the state (3.52).

of the interaction (3.3) during a lapse of time t , and, up to order e^2 , 0, 1 or 2 photons may be emitted. If after that a two-photon state is detected,

$$|\Psi\rangle = |\text{photon}_1, \text{photon}_2\rangle = \sum_{\vec{k}, \vec{k}', \lambda, \lambda'} c_{\vec{k} \vec{k}', \lambda, \lambda'} |\vec{k} \lambda, \vec{k}' \lambda'\rangle \quad (3.51)$$

(being $\hbar \vec{k}$, $\hbar \vec{k}'$ momenta and λ, λ' polarizations), the projected state, up to order e^2 , can be given in the interaction picture as

$$|\text{photons, atom}_1, \text{atom}_2\rangle_t = |\Psi\rangle \left(\frac{F_\Psi |ee\rangle + G_\Psi |gg\rangle}{N} \right) \quad (3.52)$$

where

$$F_\Psi = \frac{1}{2} \langle \Psi | T(\mathcal{S}_A^+ \mathcal{S}_A^- + \mathcal{S}_B^+ \mathcal{S}_B^-) | 0 \rangle, \quad G_\Psi = \langle \Psi | T(\mathcal{S}_B^- \mathcal{S}_A^-) | 0 \rangle \quad (3.53)$$

and $N = \sqrt{|F_\Psi|^2 + |G_\Psi|^2}$. The objects \mathcal{S}_n^\pm were defined in (3.10).

Here, G_Ψ describes single photon emission by both atoms, while F_Ψ corresponds to two photon emission by a single atom. In Quantum Optics, F_Ψ is usually neglected by the introduction of a rotating wave approximation (RWA), but as we will see later, for very short interaction times F_Ψ and G_Ψ may be of similar magnitude. Actually, a proper analysis of this model can be performed only beyond the RWA, as we have commented in the previous section. Without RWA vacuum entanglement cannot be transferred to the atoms with this particular post-selection process. In that case, a one photon post-selection process would entangle the atoms.

(3.53) can be written as:

$$\begin{aligned} F_\Psi &= \frac{1}{2}\theta(t_1 - t_2)\langle\Psi|\mathcal{S}_A^+(t_1)\mathcal{S}_A^-(t_2) + \mathcal{S}_B^+(t_1)\mathcal{S}_B^-(t_2)|0\rangle, \\ G_\Psi &= \langle\Psi|\mathcal{S}_B^-(t_1)\mathcal{S}_A^-(t_2)|0\rangle \end{aligned} \quad (3.54)$$

The photons pass through a partial Bell-state analyzer [61] consisting in a beam splitter (BS) and two polarization beam splitters (PBS) with four single photon detectors at their output ports. If two detectors, one at one output port of one PBS and one at an output port of the other, click at the same time, a state $|\Psi^-\rangle$ is detected, while if the two clicks are in the two output ports of only one PBS, the state is $|\Psi^+\rangle$. If one of the four detectors emits a double click, the state can be $|\Phi^+\rangle$ or $|\Phi^-\rangle$. Taking into account momenta and symmetrization, the Bell states can be written as

$$\begin{aligned} |\Psi^\pm\rangle &= \frac{1}{\sqrt{2}}[|\vec{k}\downarrow, \vec{k}'\uparrow\rangle + |\vec{k}'\uparrow, \vec{k}\downarrow\rangle \\ &\pm (|\vec{k}\uparrow, \vec{k}'\downarrow\rangle + |\vec{k}'\downarrow, \vec{k}\uparrow\rangle)] \\ |\Phi^\pm\rangle &= \frac{1}{\sqrt{2}}[|\vec{k}\downarrow, \vec{k}'\downarrow\rangle + |\vec{k}'\downarrow, \vec{k}\downarrow\rangle \\ &\pm (|\vec{k}\uparrow, \vec{k}'\uparrow\rangle + |\vec{k}'\uparrow, \vec{k}\uparrow\rangle)] \end{aligned} \quad (3.55)$$

where \uparrow and \downarrow are the photon polarizations, with polarization vectors

$$\epsilon(\vec{k}, \uparrow) = \frac{-1}{\sqrt{2}}(\epsilon(\vec{k}, 1) + \epsilon(\vec{k}, 2)) \quad (3.56)$$

and

$$\epsilon(\vec{k}, \downarrow) = \frac{1}{\sqrt{2}}(\epsilon(\vec{k}, 1) - \epsilon(\vec{k}, 2)), \quad (3.57)$$

where

$$\epsilon(\vec{k}, 1) = (\cos\theta_k \cos\phi_k, \cos\theta_k \sin\phi_k, -\sin\theta_k) \quad (3.58)$$

and

$$\epsilon(\vec{k}, 2) = (-\sin\phi_k, \cos\phi_k, 0). \quad (3.59)$$

Here

$$|\vec{k}\lambda, \vec{k}'\lambda'\rangle = a_{\vec{k}\lambda}^\dagger a_{\vec{k}'\lambda'}^\dagger |0\rangle. \quad (3.60)$$

We will use the concurrence (2.33) \mathbb{C} to compute the entanglement of the atomic states when the different Bell states are detected. The concurrence of the atomic part of a state like (3.52) is just given by

$$\mathbb{C} = \frac{2|F_{\Psi}G_{\Psi}^*|}{N^2} \quad (3.61)$$

We assume that the atoms A, B are along the y axis, at $y = \mp L/2$ respectively, and the dipoles are parallel along the z axis, corresponding to an experimental set up in which the dipoles are induced by suitable external fields [10]. We also take

$$|\vec{k}| = |\vec{k}'| = \Omega/c. \quad (3.62)$$

Under that conditions, the first remarkable thing is that for $|\Psi^- \rangle$ and $|\Phi^- \rangle$, we have $F_{\Psi} = G_{\Psi} = 0$. Therefore, at least while only E1 transitions are considered, in this model the Bell-state analyzer is complete: if two different detectors click the state is $|\Psi^+ \rangle$, while if one detector clicks twice the state is $|\Phi^+ \rangle$. First, we focus on $|\Psi^+ \rangle$. Considering (3.54) and (3.55), with the mode expansion for the electric field and the commutation relation for the creation and annihilation operators, a standard computation leads to:

$$\begin{aligned} F_{\Psi} &= \frac{K(\Omega, t, \theta)}{2} j(\Omega t) \cos\left(\frac{z}{2} h_+(\theta, \phi)\right) \\ G_{\Psi} &= K(\Omega, t, \theta) \cos\left(\frac{z}{2} h_-(\theta, \phi)\right), \end{aligned} \quad (3.63)$$

with

$$K(\Omega, t, \theta) = \frac{c\alpha|\mathbf{d}|^2\Omega t^2}{2\pi^2 e^2} \sin\theta_k \sin\theta_{k'}, \quad (3.64)$$

(α being the fine structure constant),

$$j(\Omega t) = \frac{|-1 + e^{2i\Omega t}(1 - 2i\Omega t)|}{(\Omega t)^2}, \quad (3.65)$$

and

$$h_{\pm}(\theta, \phi) = (\sin\theta_k \sin\phi_k \pm \sin\theta_{k'} \sin\phi_{k'}), \quad (3.66)$$

θ_k, ϕ_k corresponding to \hat{k} and $\theta_{k'}, \phi_{k'}$ to \hat{k}' , and $z = \Omega r/c$. Notice that $j(\Omega t)$ decreases as t grows, and eventually vanish as $t \rightarrow \infty$ as required by energy conservation. The r dependence is a result of the individual dependence on the position of each atom, not on the relative distance between them.

Taking into account (3.61) and (3.63) the concurrence is given by:

$$\mathbb{C} = \frac{4|\cos(\frac{z}{2} h_+(\theta, \phi)) \cos(\frac{z}{2} h_-(\theta, \phi))|}{\cos^2(\frac{z}{2} h_+(\theta, \phi)) j(\Omega t) + \cos^2(\frac{z}{2} h_-(\theta, \phi)) \frac{4}{j(\Omega t)}}, \quad (3.67)$$

Now, we assume that the 50:50 BS is at $(y, z) = (0, r/2)$, the two PBS at $(\pm d/2\sqrt{2}, r/2 + d/2\sqrt{2})$ and the four detectors at $(\pm d/\sqrt{2}, r/2 + d/\sqrt{2})$ and $(\pm r/\sqrt{2}, /2)$ (see Fig. 3.10). (3.63) will not depend on the value of d , which is

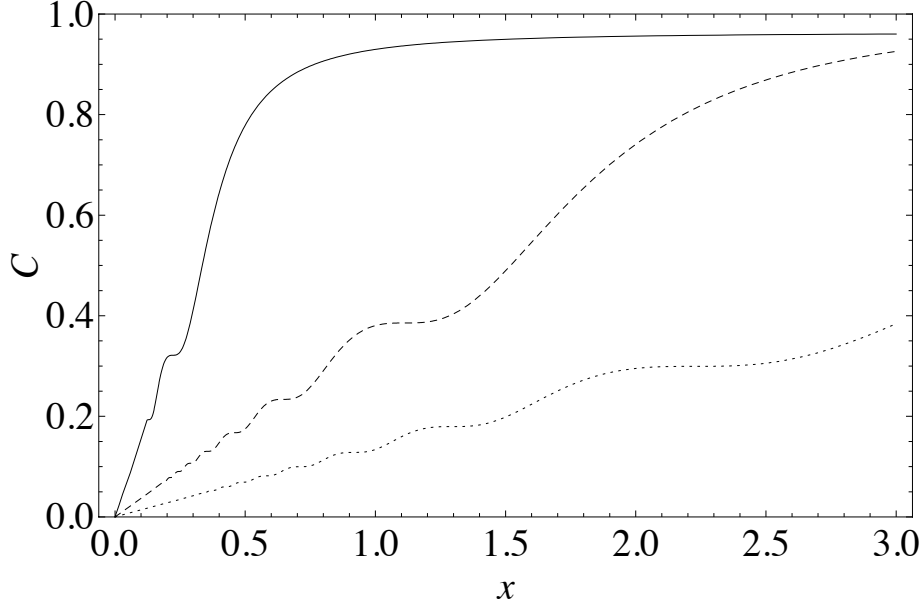


Figure 3.11: Concurrence for the atomic state when a Bell state $|\Psi^+\rangle$ or $|\Phi^+\rangle$ of the photons is detected, as a function of $x = r/ct$ for $z = \Omega r/c = 1$ (solid), 5 (dashed), 10 (dotted). The light cone is at $x < 1$. For $x > 1$ the interaction time is short enough to have a significant amount of entanglement.

the distance traveled by the photon to any detector after leaving the BS. Notice that, with this setup, $h_- = 0$ and $h_+ = \sqrt{2}$. In Fig. 3.11 we represent (3.20) under that conditions as a function of $x = r/ct$ for three different values of z (different values of r). Notice that a high degree of entanglement, maximal for x large enough (short enough interaction times t), can be achieved in all cases when one atom is beyond the light cone of the other ($x > 1$). As $t \rightarrow \infty$ ($x \rightarrow 0$), the concurrence eventually vanishes, in agreement with the fact that the only atomic state allowed by energy conservation is just the separable state $|g, g\rangle$.

In Fig. 3.12 we represent (3.67) as a function of z for three different values of $z/x = \Omega t$, to give an alternative description. The mutual light cone corresponds to the region $z < \Omega t$ in each case. The concurrence oscillates with the position of the atoms, and eventually vanishes at $z = \sqrt{2}(n + 1/2)\pi$ ($n = 0, 1, 2, \dots$), as a consequence of the vanishing of $\cos(z/\sqrt{2})$. For a given interaction time t , the maximum of the concurrence can be achieved for interatomic distances as large as desired. In particular, a maximally entangled state is generated for $\Omega t = 1$, which corresponds to $t \simeq 10^{-15}$ s. In Fig. 3.13 we sketch (3.67) as a function of $\phi = \phi_k = \phi_{k'}$ for given values of x and z . Notice that the maximum values for the entanglement are around $\phi = n\pi/2$ ($n = 0, 1, 2, \dots$), $\pi/2$ corresponding to the setup of Fig. 3.10.

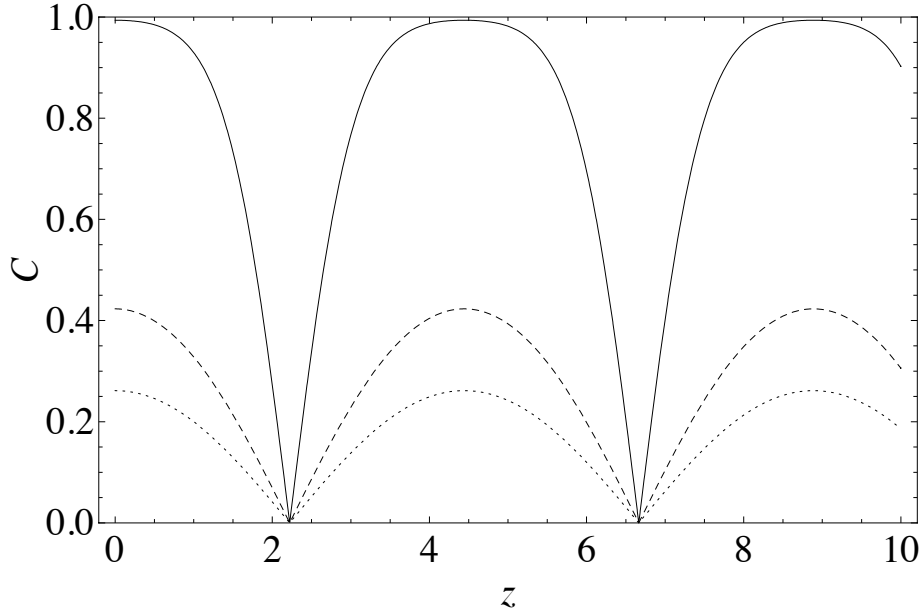


Figure 3.12: Concurrence for the atomic state when a Bell state $|\Psi^+\rangle$ of the photons is detected, as a function of $z = \Omega r/c$ for $\Omega t = 1$ (solid), 4 (dashed), 7 (dotted). The light cone for each curve is at $z < \Omega t$.

So far, we have focused on $|\Psi_+\rangle$, but, in principle, $|\Phi_+\rangle$ could be detected as well. The coefficients F_Ψ and G_Ψ would have opposite sign to those of $|\Psi_+\rangle$ and therefore the concurrence would be the same. But, due to the interaction times considered here, the relaxation time of a single detector must be extremely short in order to emit a double click.

3.2.3 Conclusions

In this section, we have shown that, in principle, two neutral two-level atoms can evolve from an initially uncorrelated state to a highly entangled state in a time shorter than the time required for the light to travel between them. At the initial time, both atoms are excited in a common electromagnetic vacuum. They are allowed to interact with the field due to an induced dipole during a time t and, up to second order in perturbation theory, $n = 0, 1, 2$ photons may be emitted. After that, the emitted radiation pass through a partial Bell-state analyzer. For interaction times $t \simeq 10^{-15} s$ and if a two-photon Bell state $|\Psi^+\rangle$ or $|\Phi^+\rangle$ (the other two are forbidden in this model) is detected after that, the atoms are projected into an entangled state, which may be maximally entangled for short enough t . For a given t , the degree of entanglement oscillates periodically with the distance and the maximum degree available can be achieved for interatomic distances r as large as desired. Notice that the interaction time t , which must be

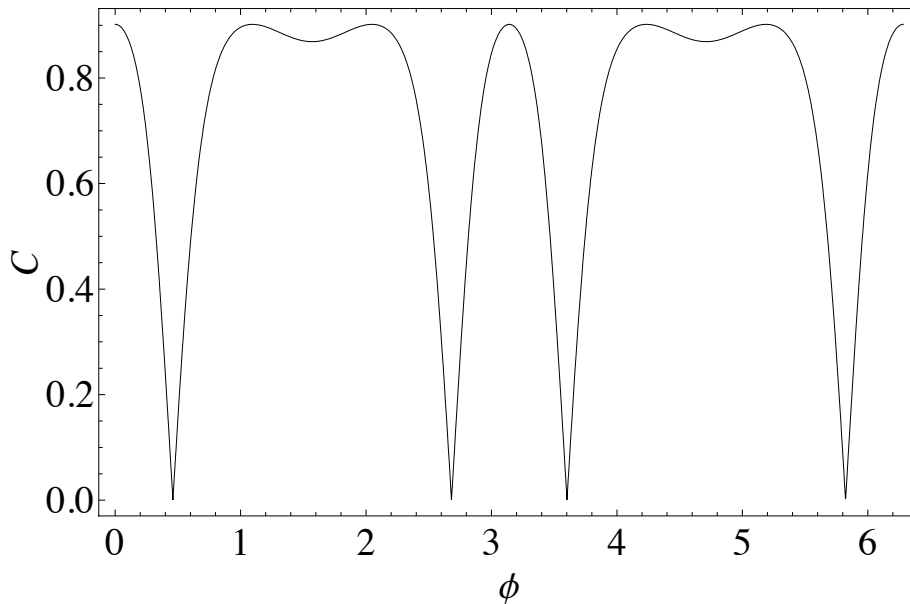


Figure 3.13: Concurrence for the atomic state when a Bell state $|\Psi^+\rangle$ of the photons is detected, as a function of ϕ for $z = \Omega r/c = 5$ and $x = r c/t = 2.5$.

$t \simeq 10^{-15}$ s, is absolutely independent of the time t' at which the photodetection takes place. Since the distance traveled by the photons from the atoms to the detector is $r/\sqrt{2}+d$, d being arbitrary, the photodetection can occur after a time $t' \leq r/c$. A suitable choice of d is necessary in order to ensure that the atoms may remain spacelike separated. The degree of entanglement is independent of d .

3.3 Entanglement Sudden Death and Sudden Birth. Photon exchange and correlations transfer in atom-atom entanglement dynamics

3.3.1 Introduction

Entanglement between qubits may disappear in a finite time when the qubits interact with a reservoir. This is commonly known as “entanglement sudden death” (ESD). After its discovery [62, 63, 64], the phenomenon has attracted great attention (for instance, [65, 66, 67, 68, 69, 70, 71, 72, 73]) and has been observed experimentally [74].

ESD shows up in a variety of systems that can be roughly divided in two sets: those in which the qubits interact individually with different reservoirs and those in which they interact with a common environment. In particular, in [67, 68, 75]

a system of a pair of two-level atoms interacting with a common electromagnetic vacuum is considered. The dynamics of the system is given in all the cases by the Lehmborg-Agarwal master equation [76, 77] which is derived with the rotating wave approximation (RWA) and the Born-Markov approximation. Recently, non-Markovian [69] and non-RWA [78] effects have been considered in systems of qubits coupled individually to different reservoirs. There are good reasons for going beyond the Markovian and RWA scenario in the case of a pair of two-level atoms in the electromagnetic vacuum. For short enough times non-RWA contributions are relevant (see Chapter 3) and a proper analysis of causality issues can only be performed if they are taken into account [46, 50, 51]. Besides, as we shall show in this section the death of the entanglement between the atoms is related with the birth of entanglement between the atoms and the field, and therefore the field is actually a non-Markovian reservoir. This was also the case in [66, 71, 72] with different reservoirs.

In the previous sections, we have applied the formalism of perturbative quantum electrodynamics (QED) to the system of a pair of neutral two-level atoms interacting locally with the electromagnetic field, and for initially separable states analyzed the generation of entanglement. This is a non-Markovian, non-RWA approach. The use of the Lehmborg-Agarwal master equation can be seen as a coarse-grained in time approximation to the perturbative treatment [79]. The first goal of this section is to apply also the QED formalism to analyze the ESD in these systems for initially entangled atomic states, comparing the results with the previously obtained [67, 68] with master equations. We will focus mainly on the range $r/(ct) \approx 1$, r being the interatomic distance and t the interaction time, in order to investigate the role of locality. We will also consider for the first time in these systems the rest of pairwise concurrences, namely the entanglement of each atom with the field, and multipartite entanglement, following the spirit of [66, 71, 72, 73]. While the mentioned papers deal with a four qubit model, our model here consists in two qubits (the atoms) and a qutrit (the electromagnetic field, which may have 0, 1 or 2 photons). We shall show that the phenomenon of revival of entanglement after the ESD [68] can occur for $r > ct$, and therefore is not related with photon exchange as is usually believed. We will see that atom-atom disentanglement is connected with the growth of atom-field entanglement and viceversa. Similar relationship will be obtained among the “atom-(atom+field)” and “field-(atom+atom)” entanglements.

The remainder of this section is organized as follows. In subsection 3.3.2 we will describe the Hamiltonian and the time evolution from the initial state of the system. In section 3.3.3 we will obtain the reduced state of the atoms and analyze the behavior of its entanglement. In section 3.3.4 the same will be performed with the reduced state of each atom and the field, comparing the entanglement cycle with the one obtained in the previous section. Tripartite entanglement will be considered in section 3.3.5 in terms of the entanglement of all the different bi-partitions of the system, and we conclude in section 3.3.6 with a summary of our results.

3.3.2 Hamiltonian and state evolution

In what follows we choose a system given initially by an atomic entangled state, with the field in the vacuum state $|0\rangle$:

$$|\psi(0)\rangle = (\alpha|ee\rangle + \beta|gg\rangle)|0\rangle. \quad (3.68)$$

The system then evolves under the effect of the interaction (3.3) during a lapse of time t into a state:

$$|\psi(t)\rangle = T(e^{-i \int_0^t dt' H_I(t')/\hbar})|\psi\rangle_0, \quad (3.69)$$

Up to second order in perturbation theory, (3.69) can be given in the interaction picture as

$$|\text{atom1, atom2, field}(t)\rangle = \alpha|ee0(t)\rangle + \beta|gg0(t)\rangle \quad (3.70)$$

where

$$\begin{aligned} |ee0(t)\rangle = & ((1 + A')|ee\rangle + X'|gg\rangle)|0\rangle + (U_A|ge\rangle + U_B|eg\rangle)|1\rangle + \\ & (F'|ee\rangle + G'|gg\rangle)|2\rangle \end{aligned} \quad (3.71)$$

and

$$\begin{aligned} |gg0(t)\rangle = & ((1 + A'')|gg\rangle + X''|ee\rangle)|0\rangle + (V_A|eg\rangle + V_B|ge\rangle)|1\rangle + \\ & (F''|gg\rangle + G''|ee\rangle)|2\rangle \end{aligned} \quad (3.72)$$

where

$$\begin{aligned} A' &= \frac{1}{2}\theta(t_1 - t_2)\langle 0|\mathcal{S}_A^+(t_1)\mathcal{S}_A^-(t_2) + \mathcal{S}_B^+(t_1)\mathcal{S}_B^-(t_2)|0\rangle \\ A'' &= \frac{1}{2}\theta(t_1 - t_2)\langle 0|\mathcal{S}_A^-(t_1)\mathcal{S}_A^+(t_2) + \mathcal{S}_B^-(t_1)\mathcal{S}_B^+(t_2)|0\rangle \\ X' &= \langle 0|T(\mathcal{S}_B^-\mathcal{S}_A^-)|0\rangle, X'' = \langle 0|T(\mathcal{S}_B^+\mathcal{S}_A^+)|0\rangle, \\ U_A &= \langle 1|\mathcal{S}_A^-|0\rangle, V_A = \langle 1|\mathcal{S}_A^+|0\rangle \\ U_B &= \langle 1|\mathcal{S}_B^-|0\rangle, V_B = \langle 1|\mathcal{S}_B^+|0\rangle \\ F' &= \frac{1}{2}\theta(t_1 - t_2)\langle 2|\mathcal{S}_A^+(t_1)\mathcal{S}_A^-(t_2) + \mathcal{S}_B^+(t_1)\mathcal{S}_B^-(t_2)|0\rangle \\ F'' &= \frac{1}{2}\theta(t_1 - t_2)\langle 2|\mathcal{S}_A^-(t_1)\mathcal{S}_A^+(t_2) + \mathcal{S}_B^-(t_1)\mathcal{S}_B^+(t_2)|0\rangle, \\ G' &= \langle 2|T(\mathcal{S}_B^-\mathcal{S}_A^-)|0\rangle, G'' = \langle 2|T(\mathcal{S}_B^+\mathcal{S}_A^+)|0\rangle \end{aligned} \quad (3.73)$$

with the definitions and conventions of Section 3.1. Here, A' and A'' describe intra-atomic radiative corrections, U_A (U_B) and V_A (V_B) single photon emission by atom A (B), and G' and G'' by both atoms, while F' and F'' correspond to two photon emission by a single atom. Only X' and X'' correspond to interaction between both atoms. A' , X' , X'' , V_A , V_B , F' , F'' and G' are non-RWA terms. As in the previous sections of this chapter, in our calculations

we will take $(\Omega|\mathbf{d}|/ec) = 5 \cdot 10^{-3}$, which is of the same order as the $1s \rightarrow 2p$ transition in the hydrogen atom, consider $\Omega t \gtrsim 1$, and focus mainly on the cases $(r/ct) \simeq 1$. In this case, we will take into account $|e\rangle$ is actually a triply degenerate state $|e, m\rangle$ with $m = 0, \pm 1$ and we will average over two different independent possibilities for dipole orientations: $\mathbf{d}_A = \mathbf{d}_B = \mathbf{d} = d\mathbf{u}_z$ for transitions with $\Delta m = 0$ [80] and $\mathbf{d} = d(\mathbf{u}_x \pm i\mathbf{u}_y)/\sqrt{2}$ [80] for transitions with $\Delta m = \pm 1$.

3.3.3 Sudden death and revival of atom-atom entanglement

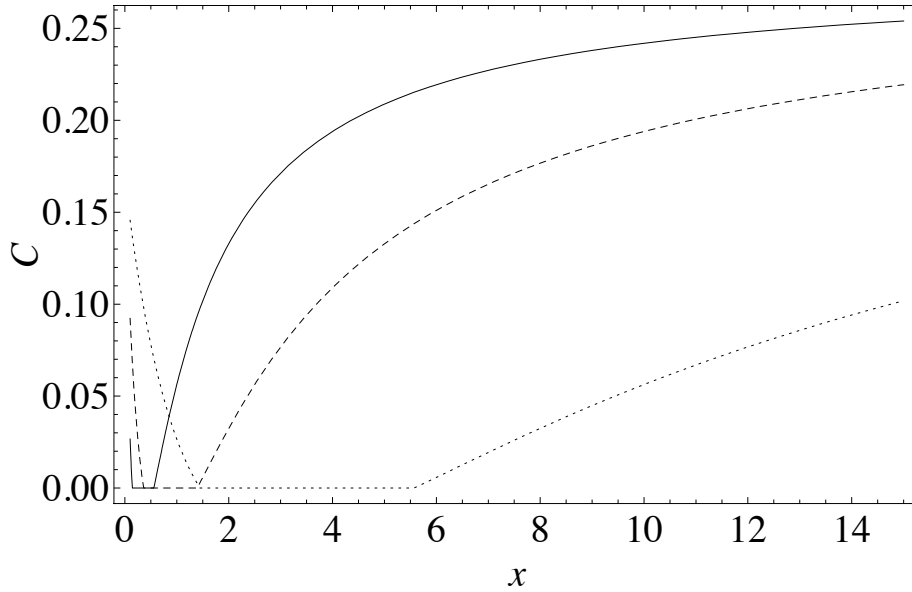


Figure 3.14: Concurrence $\mathbb{C}(\rho_{AB})$ in front of $x = r/ct$ for $p = 0.98$ and $z = \Omega r/c = 2 \cdot 10^6$ (solid line), $5 \cdot 10^6$ (dashed line) and $2 \cdot 10^7$ (dotted line). In the latter case sudden death and revival of entanglement occur for $x > 1$.

After tracing over all the states of the field, the density matrix of the atomic state ρ_{AB} takes the form (in the basis $\{|ee\rangle, |eg\rangle, |ge\rangle, |gg\rangle\}$):

$$\rho_{AB} = \frac{1}{N} \begin{pmatrix} \rho_{11} & 0 & 0 & \rho_{14} \\ 0 & \rho_{22} & \rho_{23} & 0 \\ 0 & \rho_{23}^* & \rho_{33} & 0 \\ \rho_{14}^* & 0 & 0 & \rho_{44} \end{pmatrix} \quad (3.74)$$

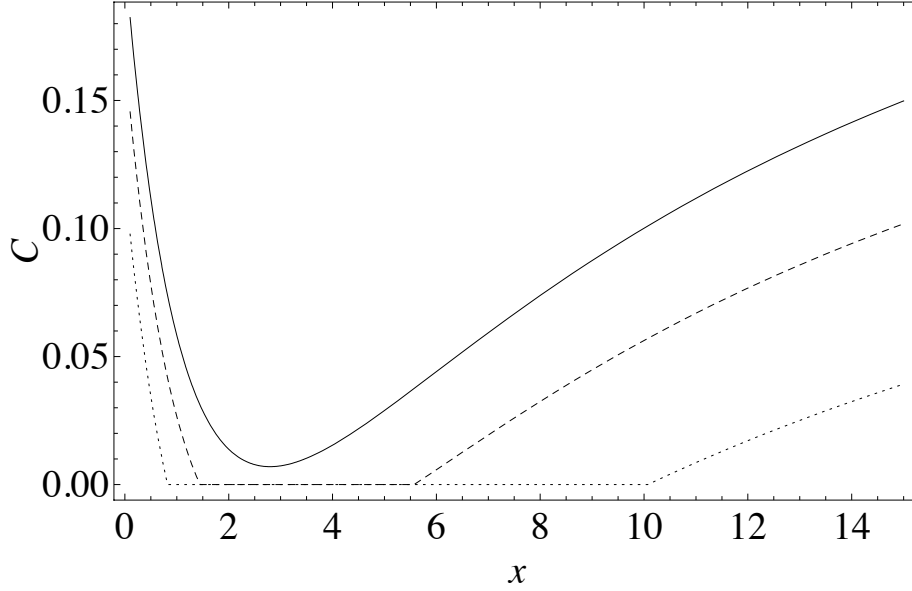


Figure 3.15: Concurrence $\mathbb{C}(\rho_{AB})$ in front of $x = r/ct$ for $z = \Omega r/c = 2 \cdot 10^7$ and $p = 0.97$ (solid line), $p = 0.98$ (dashed line) and $p = 0.99$ (dotted line). In the first case, entanglement decreases as t grows up to a minimum value and begin to grow since then. This behavior becomes entanglement sudden death and revival when the minimum value is 0 for higher values of p . $\mathbb{C}(\rho_{AB})$ tends to 0 as $x \rightarrow \infty$ and $p \rightarrow 1$.

where

$$\begin{aligned}
\rho_{11} &= |\alpha(1 + A') + \beta X''|^2 + |\alpha F' + \beta G''|^2, \\
\rho_{22} &= \rho_{33} = |\alpha|^2 |U|^2 + |\beta|^2 |V|^2 + 2 \operatorname{Re}(\alpha \beta^* l^*) \\
\rho_{44} &= |\alpha b + \beta(1 + A'')|^2 + |\alpha G' + \beta F''|^2, \\
\rho_{14} &= |\alpha|^2 ((1 + A') X'{}^* + F' G'^*) + |\beta|^2 ((1 + A'')^* X'' \\
&\quad + G'' F''^*) + \alpha \beta^* ((1 + A')(1 + A'') + F' F''^*) \\
&\quad + \beta \alpha^* (X'' X'{}^* + G'' G'^*) \\
\rho_{23} &= |\alpha|^2 U_B U_A^* + |\beta|^2 V_A V_B^* + 2 \operatorname{Re}(\alpha \beta^* U V^*) \\
N &= \rho_{11} + \rho_{22} + \rho_{33} + \rho_{44}
\end{aligned} \tag{3.75}$$

where

$$\begin{aligned}
|U|^2 &= |U_A|^2 = |U_B|^2, \\
|V|^2 &= |V_A|^2 = |V_B|^2, \\
l &= U_A V_B^* = U_B V_A^*
\end{aligned} \tag{3.76}$$

and

$$UV^* = U_A^* V_A^* = U_B V_B^*. \quad (3.77)$$

The computation of A' , X' , etc. can be performed following the lines given in the Appendix A, where they are computed for the initial state $|eg\rangle$ and only for $\Delta m = 0$. In terms of $z = \Omega r/c$ and $x = r/ct$, being r the interatomic distance, we find:

$$\begin{aligned} A' &= \frac{4iKz^3}{3x} \left(\ln\left(1 - \frac{z_{max}}{z}\right) + i\pi \right), \\ A'' &= \frac{-4iKz^3}{3x} \ln\left(1 + \frac{z_{max}}{z}\right) \\ X' &= X''^* = \frac{\alpha d_i d_j}{\pi e^2} (-\nabla^2 \delta_{ij} + \nabla_i \nabla_j) I, \end{aligned} \quad (3.78)$$

with $K = \alpha |\mathbf{d}|^2 / (e^2 r^2)$ and $I = I_+ + I_-$, where:

$$\begin{aligned} I_{\pm} &= \frac{-i e^{-i\frac{z}{x}}}{2z} \left[\pm 2 \cos\left(\frac{z}{x}\right) e^{\pm iz} Ei(\mp iz) + e^{-iz(1 \pm \frac{1}{x})} \right. \\ &\quad \left. Ei\left(iz\left(1 \pm \frac{1}{x}\right)\right) - e^{iz(1 \pm \frac{1}{x})} Ei\left(-iz\left(1 \pm \frac{1}{x}\right)\right) \right] \end{aligned} \quad (3.79)$$

for $x > 1$, having the additional term $-2\pi i e^{iz(1-1/x)}$ otherwise.

$|U|^2$, $|V|^2$, l , $U_B U_A^*$, $V_A V_B^*$ and UV^* have been computed in Section 3.1. Besides:

$$\begin{aligned} G' &= U_B U_A' + U_A U_B', G'' = V_A V_B' + V_B V_A' \\ F' &= \theta(t_1 - t_2) (V_A(t_1) U_A'(t_2) + U_A(t_1) V_A'(t_2) \\ &\quad + V_B(t_1) U_B'(t_2) + U_B(t_1) V_B'(t_2)) \\ F'' &= \theta(t_1 - t_2) (U_A(t_1) V_A'(t_2) + U_A'(t_1) V_A(t_2) \\ &\quad + U_B(t_1) V_B'(t_2) + U_B'(t_1) V_B(t_2)) \end{aligned} \quad (3.80)$$

where the primes in the U 's and V 's are introduced to discriminate between the two single photons.

We will use the concurrence $\mathbb{C}(\rho)$ [38] to compute the entanglement, which for a X-state like (3.74) is given by (3.33). If we take

$$\alpha = \sqrt{p}, \beta = \sqrt{1-p}, \quad (3.81)$$

we find that ESD appears at a range of values of p that decreases with increasing r , in agreement with [68]. Although this would suggest that ESD disappear for r large enough, we find that there are high values of p for which ESD exists for arbitrary large r . In Fig. 3.14, we represent $\mathbb{C}(\rho_{AB})$ in front of x for different values of z and $p = 0.98$. ESD occurs at $z/x = \Omega t$ of the order of 10^7 . Thus, as z (that is r) grows, ESD is shifted to higher values of x . It is also interesting to analyze the phenomenon of entanglement revival, discovered in these systems in [68]. We find that the dark periods [68] between death and revival has

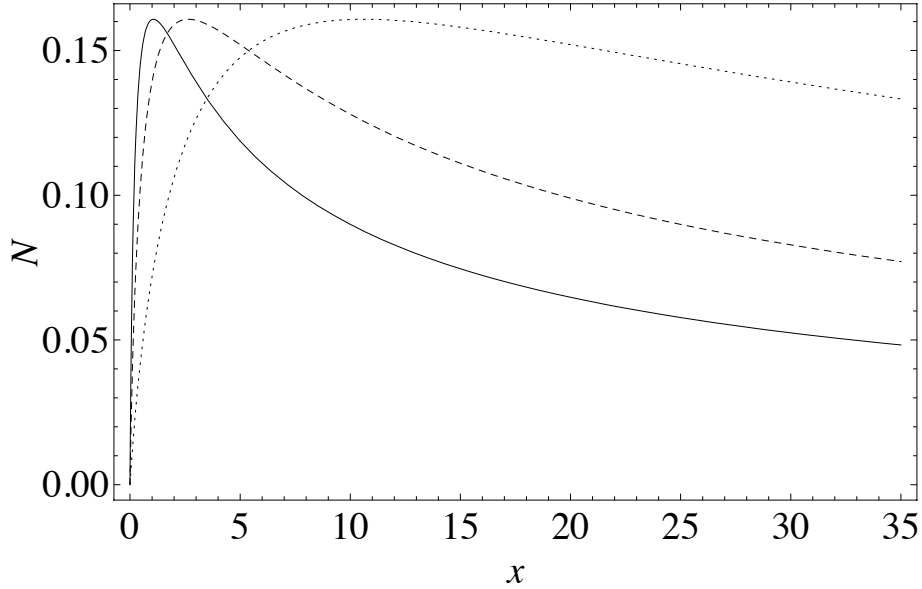


Figure 3.16: Negativity $\mathbb{N}(\rho_{BF}) = \mathbb{N}(\rho_{AF})$ in front of $x = r/ct$ for $p = 0.98$ and $z = \Omega r/c = 2 \cdot 10^6$ (solid line), $5 \cdot 10^6$ (dashed line) and $2 \cdot 10^7$ (dotted line). Entanglement increases from 0 at $x \rightarrow \infty$ up to a maximum value and then decreases and vanishes eventually.

larger time durations for increasing z . Besides, although in [68] the revival is described as a consequence of the photon exchange, for r sufficiently large both the ESD and the revival can occur for $x > 1$, where photon exchange is not allowed. We think that the explanation for entanglement revival is closer to the spirit of [66, 72] where entanglement revival between noninteracting atoms is interpreted as coming from entanglement transfer between different parts of the system. We shall discuss this point in the following sections. In Fig. 3.15 we sketch the dependence with p . Although sudden death and revivals appear in a very restricted range of the parameter, they are only a particular case of the generic behavior of entanglement observed in a wider range, which can be described as disentanglement up to a minimum value and growth of quantum correlations since then.

3.3.4 Atom-field entanglement

Tracing (3.70) over states of atom A (B) the reduced atom-field density matrix ρ_{BF} (ρ_{AF}) is obtained. Taking the basis $\{|e0\rangle, |e1\rangle, |e2\rangle, |g0\rangle, |g1\rangle, |g2\rangle\}$,

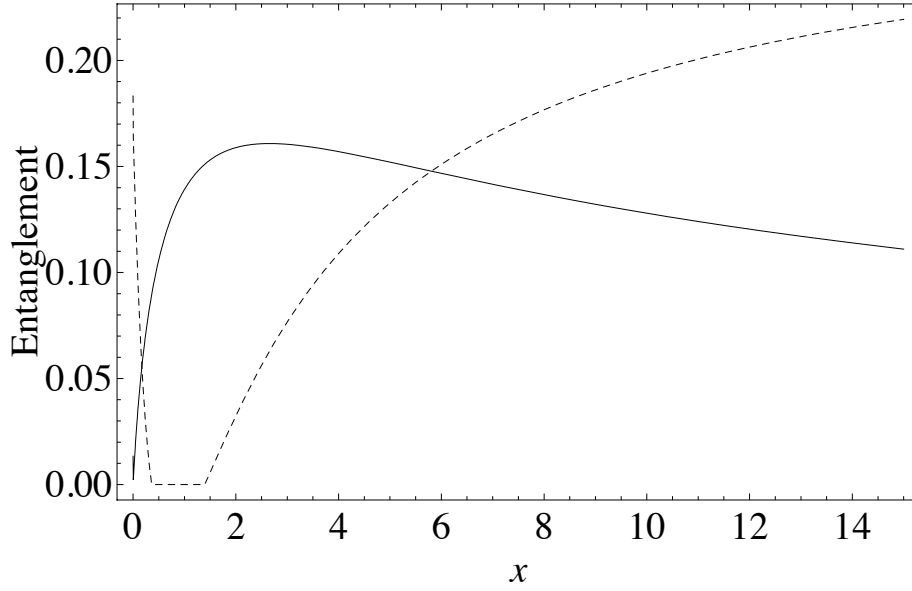


Figure 3.17: Negativity $\mathbb{N}(\rho_{BF}) = \mathbb{N}(\rho_{AF})$ (solid line) and concurrence $\mathbb{C}(\rho_{AB})$ (dashed line) in front of $x = r/ct$ for $p = 0.98$ and $z = \Omega r/c = 5 \cdot 10^6$. Entanglement atom-atom cycle is clearly correlated with the atom-field cycle, although the sum is not a conserved quantity. Although atom-field entanglement may change while the other remains zero, both entanglements cannot increase or decrease at the same time.

we have:

$$\rho_{BF} = \rho_{AF} = \frac{1}{N'} \begin{pmatrix} \rho'_{11} & 0 & \rho'_{13} & 0 & \rho'_{15} & 0 \\ 0 & \rho'_{22} & 0 & \rho'_{24} & 0 & \rho'_{26} \\ \rho'_{13*} & 0 & \rho'_{33} & 0 & \rho'_{35} & 0 \\ 0 & \rho'_{24*} & 0 & \rho'_{44} & 0 & \rho'_{46} \\ \rho'_{15*} & 0 & \rho'_{35*} & 0 & \rho'_{55} & 0 \\ 0 & \rho'_{26*} & 0 & \rho'_{46*} & 0 & \rho'_{66} \end{pmatrix} \quad (3.82)$$

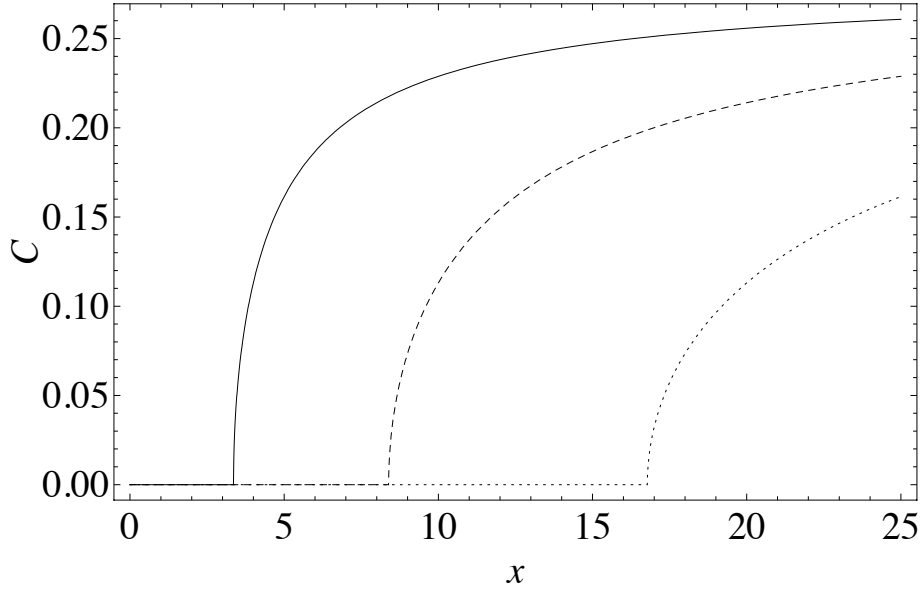


Figure 3.18: I concurrence $\mathbb{C}_{A-BF} = \mathbb{C}_{B-AF}$ in front of $x = r/ct$ for $p = 0.98$ and $z = \Omega r/c = 2 \cdot 10^5$ (solid line), $5 \cdot 10^5$ (dashed line) and $1 \cdot 10^6$ (dotted line). Entanglement disappears faster than the entanglement between the atoms (Fig. 3.14) and remains 0 since then.

with

$$\begin{aligned}
\rho'_{11} &= |\alpha(1 + A') + \beta X''|^2, \rho'_{22} = \rho'_{55} = \rho_{22} \\
\rho'_{33} &= |\alpha F' + \beta G''|^2, \rho'_{44} = |\alpha X' + \beta(1 + A'')|^2 \\
\rho'_{66} &= |\alpha G' + \beta F''|^2, \rho'_{13} = (\alpha(1 + A') + \beta X'')(\alpha F' + \beta G'') \\
\rho'_{15} &= (\alpha(1 + A') + \beta X'')(\alpha U_B + \beta V_A)^* \\
\rho'_{24} &= (\alpha U_A + \beta V_B)(\beta(1 + A'') + \alpha X')^* \\
\rho'_{26} &= (\alpha U_A + \beta V_B)(\alpha G' + \beta F'')^* \\
\rho'_{35} &= (\alpha F' + \beta G'')(\alpha U_B + \beta V_A)^* \\
\rho'_{46} &= (\alpha X' + \beta(1 + A''))(\alpha G' + \beta F'')^* \\
N' &= \rho'_{11} + \rho'_{22} + \rho'_{33} + \rho'_{44} + \rho'_{55} + \rho'_{66}
\end{aligned} \tag{3.83}$$

There are no operational generalizations of concurrence for mixed states in 2×3 dimensions like the ones in Eq. (3.82). We will use the negativity [39] $\mathbb{N}(\rho)$, which is the absolute value of the sum of the negative eigenvalues of the partial transposes of a state ρ . For the 2×2 and 2×3 cases $\mathbb{N}(\rho) > 0$ is a necessary and sufficient condition for ρ to be entangled.

Up to second order in perturbation theory, we have that $N' = N$ and that

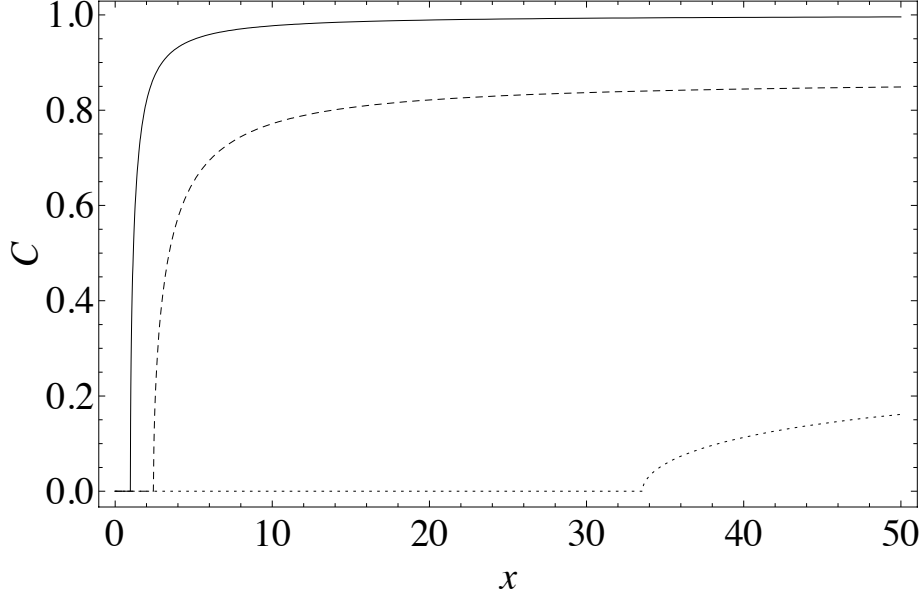


Figure 3.19: I concurrence $\mathbb{C}_{A-BF} = \mathbb{C}_{B-AF}$ in front of $x = r/ct$ for $z = \Omega r/c = 2 \cdot 10^6$ and $p = 0.50$ (solid line), $p = 0.75$ (dashed line) and $p = 0.98$ (dotted line). Entanglement sudden death occurs for a wider range than the entanglement between the atoms (Fig. 3.15).

the nonzero eigenvalues of the partial transposes of both ρ_{BF} and ρ_{AF} are

$$\lambda_{\pm} = \frac{\rho'_{11} + \rho'_{55} \pm \sqrt{(\rho'_{11} - \rho'_{55})^2 + 4|\rho'_{24}|^2}}{2N'} \quad (3.84)$$

and

$$\lambda'_{\pm} = \frac{\rho'_{44} + \rho'_{55} \pm \sqrt{(\rho'_{44} - \rho'_{22})^2 + 4|\rho'_{15}|^2}}{2N'} \quad (3.85)$$

being zero the other two. In Eqs. (3.84) and (3.85) only the terms up to second order are retained. Therefore, if $|\rho'_{24}|^2 > \rho'_{11}\rho'_{55}$ then $\lambda_- < 0$ and if $|\rho'_{15}|^2 > \rho'_{22}\rho'_{44}$ then $\lambda'_- < 0$. In Fig. 3.16 we represent $\mathbb{N}(\rho_{BF}) = \mathbb{N}(\rho_{AF})$ in front of x for same values of p and z of Fig. 1. We see that the negativity grows from 0 at $x \rightarrow \infty$ ($t = 0$) to its maximum value and then starts to decrease and eventually vanishes, following the opposite cycle to the entanglement of ρ_{AB} .

Although it would be interesting to look for conservation rules of entanglement like the ones in [66, 72, 73], this search is beyond the focus of this paper since in our study we are using different entanglement measures in Hilbert spaces of different dimensions. Besides, except for the concurrence between atoms A and B , the rest of the concurrences in the mentioned papers have not obvious counterparts in our case. But it is clear that in general the entanglement cycle between atoms is correlated with the entanglement cycle between each atom and

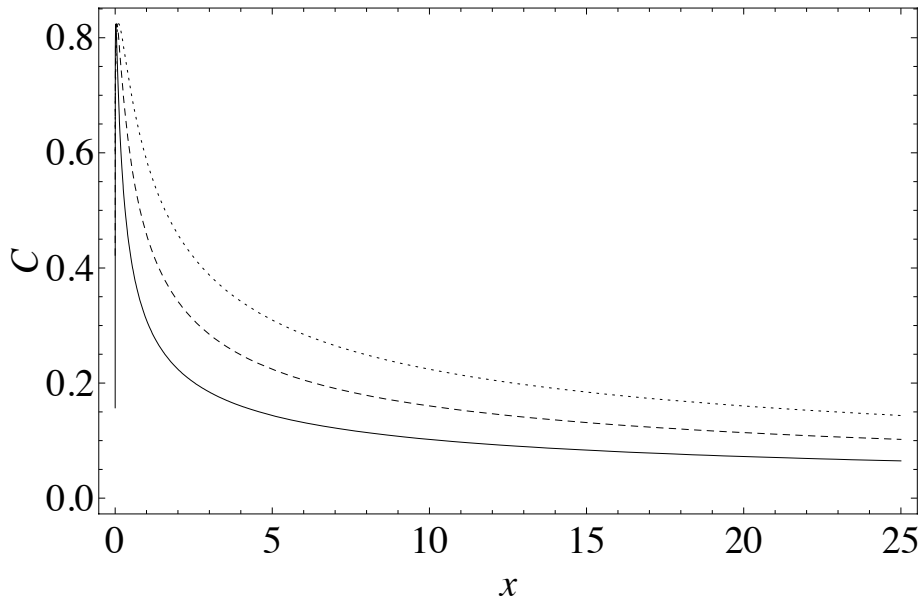


Figure 3.20: I concurrence \mathbb{C}_{F-AB} in front of $x = r/ct$ for $p = 0.98$ and $z = \Omega r/c = 2 \cdot 10^5$ (solid line), $5 \cdot 10^5$ (dashed line) and $1 \cdot 10^6$ (dotted line). Entanglement grows from 0 to its maximum value at $x \approx 0.1$ and then decreases.

the field, as can be seen in Fig. 3.17 in a particular case. Although atom-field entanglement may change while the other remains zero, both entanglements cannot increase or decrease at the same time.

3.3.5 Tripartite entanglement

Tripartite entanglement has been widely studied in terms of the entanglement of the different bipartitions $A-BC$, $B-AC$, $C-AB$ in the system [81, 82, 83], where A , B and C stand for the three parties. Here, we will compute the I concurrences [84] \mathbb{C}_{A-BF} , \mathbb{C}_{B-AF} , \mathbb{C}_{F-AB} , where

$$\mathbb{C}_{J-KL} = \sqrt{2(1 - \text{Tr} \rho_J^2)}, \quad (3.86)$$

where J runs from A to F and KL from BF to AB respectively, being ρ_J the reduced density matrix of J . A and B stand for the atoms, and F for the field.

Tracing (3.9) over BF (AF), we find the following density matrices ρ_A (ρ_B):

$$\rho_A = \rho_B = \frac{1}{N_A} \begin{pmatrix} \rho_{A11} & 0 \\ 0 & \rho_{A22} \end{pmatrix} \quad (3.87)$$

where

$$\rho_{A11} = \rho'_{11} + \rho'_{33} + \rho_{22} \quad (3.88)$$

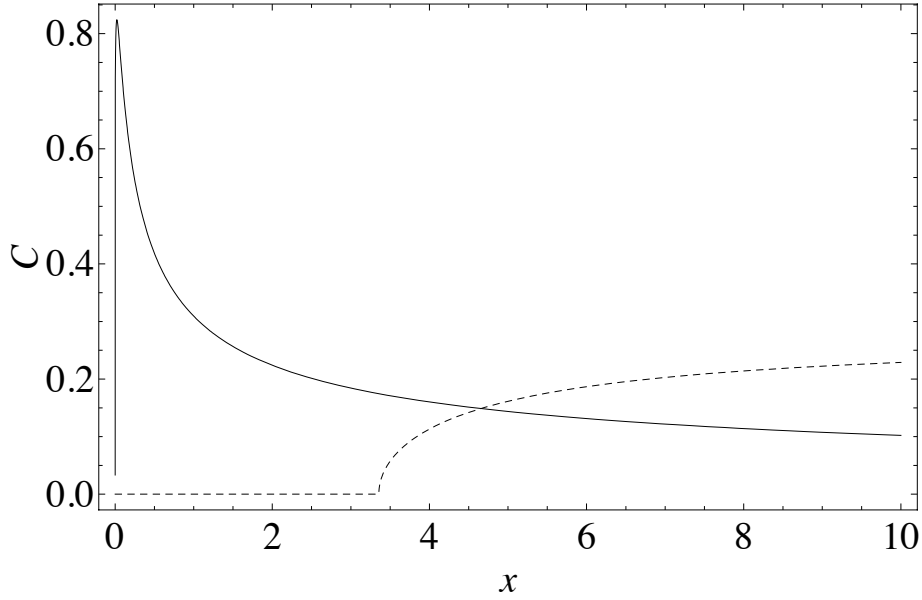


Figure 3.21: I concurrence \mathbb{C}_{F-AB} (solid line) and $\mathbb{C}_{A-BF} = \mathbb{C}_{B-AF}$ (dashed line) in front of $x = r/ct$ for $z = \Omega r/c = 2 \cdot 10^5$ and $p = 0.98$. Both magnitudes cannot increase or decrease at the same time.

and

$$\rho_{A22} = \rho'_{44} + \rho'_{66} + \rho_{22} \quad (3.89)$$

and $N_A = \rho_{A11} + \rho_{A22}$. In Fig. 3.18 we sketch the behavior of \mathbb{C}_{A-BF} and \mathbb{C}_{B-AF} in front of x for different values of z . Entanglement vanishes before the death of the entanglement between A and B , and does not have a revival. Besides, ESD appears in a wider range of p , as can be seen in Fig. 3.19. Now, tracing (3.70) over AB we obtain the reduced density matrix of the field ρ_F :

$$\rho_F = \frac{1}{N_F} \begin{pmatrix} \rho_{F11} & 0 & \rho_{F13} \\ 0 & \rho_{F22} & 0 \\ \rho_{F13}^* & 0 & \rho_{F33} \end{pmatrix} \quad (3.90)$$

where

$$\begin{aligned} \rho_{F11} &= \rho'_{11} + \rho'_{44}, \quad \rho_{F22} = 2\rho_{22}, \\ \rho_{F33} &= \rho'_{33} + \rho'_{66}, \quad \rho_{F02} = \rho'_{13} + \rho'_{46}, \end{aligned} \quad (3.91)$$

and $N_F = \rho_{F11} + \rho_{F22} + \rho_{F33}$. In Fig. 3.20 we represent \mathbb{C}_{F-AB} in front of x for the same values of z and p as in Fig. 3.18. Entanglement grows from 0 to a maximum value at $x \approx 0.1$ and then decreases. The growth of \mathbb{C}_{F-AB} is correlated with the decrease of \mathbb{C}_{A-BF} and \mathbb{C}_{B-AF} in the same way as the magnitudes analyzed in the previous section, as can be seen in Fig. 3.21 for a particular case.

3.3.6 Conclusions

We have analyzed in a previously unexplored spacetime region the entanglement dynamics of a system consisting in a pair of neutral two-level atoms A and B interacting with a common electromagnetic field F . At $t = 0$ atoms are in the Bell state $\sqrt{p}|ee\rangle + \sqrt{1-p}|gg\rangle$ and the field in the vacuum state. The evolution of this state has been considered within the non-Markovian, non-RWA approach of quantum electrodynamics up to second order in perturbation theory. We find ESD and revival of entanglement in the reduced state of the atoms, in a range of p that decreases with the interatomic distance r , in agreement with the results obtained with master equations [68]. For r large enough, we find that the revival of entanglement can occur with $r > ct$ and therefore is not a consequence of photon exchange between the atoms. We find that this phenomenon is strongly related to the transfer of entanglement between the different subsystems of two parties that coexist in the entire system: we obtain sort of entanglement cycle for the atom-field reduced states opposite to the atom-atom one. We have considered also the different bi-partitions of the system, namely $A - BF$, $B - AF$ and $F - AB$, finding similar relationships between their entanglement cycles.

Chapter 4

Circuit QED as a quantum simulation of matter-radiation interaction beyond RWA

“GALILEO: I improved it. LUDOVICO: Yes, sir. I am beginning to understand science. [...] Yes, a pretty red. When I saw it first it was covered in green.” (Bertold Brecht, *Galileo*.)

The experimental implementation of the theoretical results introduced in Chapter 3 is extremely challenging, mostly because of the impossibility of turning the interaction on and off at will, among other reasons. In this chapter we will move to the framework of circuit QED, which can be understood as 1-D version of matter-radiation interaction with artificial atoms and photons, with the advantage of experimental amenability. An important feature of circuit QED is that stronger values of the coupling strength can be achieved, entering into the so-called “ultrastrong” coupling regime in which effects beyond RWA become accessible to experiment. An important consequence of this will be analyzed in section 4.1, in which a possible experimental protocol to detect with certainty ground state qubit self-excitations is introduced. In section 4.2 we present an experiment proposal to test the entanglement generation between superconducting qubits coupled to a quantum field initially in the vacuum state, that is the circuit QED version of some of the results presented in chapter 3.

4.1 Detecting ground state qubit self-excitations in circuit QED: slow quantum anti-Zeno effect

4.1.1 Introduction

The model of a two-level system interacting with one or more harmonic oscillators can be implemented in circuit QED combining a superconducting qubit with a microwave resonator or a transmission line [34, 35, 85]. Compared to experiments in Quantum Optics with microwave cavities [86, 87] or with trapped ions [88], the superconducting circuit experiments have one important advantage: the strength of the qubit-photon coupling. The fact that superconducting resonators and superconducting qubits follow essentially the same physical laws makes it possible not only to reach the strong coupling regime [35, 85], in which multiple Rabi oscillations are possible within the decoherence of the cavity or the qubit, $g \gg \kappa, \gamma$, but also entering the ultrastrong coupling regime, $g \sim \omega$, in which the internal and interaction energies become similar [89, 90]. In this new regime the dynamics is very fast and the usual approximations such as the Rotating Wave Approximation (RWA) in the Jaynes-Cummings model break down [91, 92, 93].

One of the most astounding predictions of the ultrastrong coupling regime is that a single qubit can distort its electromagnetic environment, giving rise to a ground state in which the qubit is dressed with photons. As we will show in the following sections, in the case of a qubit and a single harmonic oscillator, this translates into a state which is a superposition of a desexcited qubit and a vacuum, with other states in which the qubit, the oscillator or both are populated with excitations and photons, respectively [92, 94, 95]. This is a completely non-RWA effect which requires large values of the coupling to be observed. More precisely, the excitation probability grows approximately as $p_e \propto (g/\omega)^2$ and g has to become comparable to the energies of a photon, $\hbar\omega$, or of a qubit, $\hbar\omega_0$, making the interaction dynamics both very strong and very fast. From the experimental point of view it would thus seem unfeasible to probe a physics that takes place at speeds of $\omega \sim 1 - 10$ GHz, while the typical measurement apparatus in circuit-QED have response times which are much slower, of about 50 ns. There are four routes to escape this problem: making the ultrastrong coupling switchable by design [96], dynamically turning it off by external drivings [97], engineering faster measurement apparatus or looking for new ways to extract information out of slow measurement devices.

In this section we take the slow route, showing that is possible to extract valuable information from the fast dynamics of the system with current measurement technologies. We will study what happens to an ultra-strongly coupled qubit-cavity system when the qubit is subject to repeated measurements by a detector with a slow repetition rate that is only capable of performing weak measurements of the state of the qubit. The main goal is to detect the qubit in its excited state starting from the ground state of the system. The first measure-

ment has already a small probability of success, as commented in the previous paragraph. In case of failure the system is projected to a non-equilibrium state which rapidly exhibits a dynamics with an oscillatory probability of excitation, mainly due to non-RWA transitions from the ground state of the qubit $|g\rangle$ to the excited one $|e\rangle$. By means of performing repeated measurements, we will show that the detector is able to probe these usually considered as “virtual” excitations of the qubit and the cavity and at the same time reveal information of the interaction model. More precisely, the repeated measurements accumulate information exponentially fast and behave like an anti-Zeno effect [98] in which the qubit is projected onto its excited state, revealing those ground-state excitations that we were looking for. We show that this anti-Zeno “decay” $|g\rangle \rightarrow |e\rangle$, is very efficient and does only require a *short number of repeated measurements* with a repetition rate which is much slower than in the standard anti-Zeno effect.

Like other proposals for probing the ultrastrong coupling limit [94], (see also section 4.2), the anti-Zeno dynamics in this work is supported by the counter-rotating terms in the qubit-resonator interaction, using as seed the ground state excitations of these systems. The phenomenon is absent in the limit of RWA in Jaynes-Cummings models. Let us remark that the non-RWA effects are being extensively studied not only in the ultrastrong coupling regime of circuit-QED but also in other fields like Quantum Optics [99]. Models of repeated measurements on superconducting qubits were considered for instance in Ref. [100] and have been implemented in the lab [101, 102].

The structure of this section is as follows. In 4. 1. 2 we will show that the eigenstates of the hamiltonian, and in particular the ground state of a qubit-cavity system in the ultrastrong coupling regime are not separable, $|g, 2n\rangle$ or $|e, 2n + 1\rangle$, but linear combinations of these vacua and excitations. More precisely, the qubit-resonator ground state contains a contribution of $|e, 1\rangle$ which grows with the coupling strength and becomes relevant in the ultrastrong coupling regime, $g \sim \omega$. We will see that after a few ideal periodic projective measurements of the qubit state, the probability of finding that it is in the state $|g\rangle$ tends quickly to 0, even if an uncertainty in the time taken by the measurement is considered. In section 4.1.2.5 we will consider a realistic model of measurement in which large amounts of errors are allowed, showing the robustness of our method. Section 4.1.2.6 is devoted to the analysis of the role of relaxation and dephasing. We conclude in section 4.1.3 with a summary of our results.

4.1.2 Detecting ground state qubit self-excitations

4.1.2.1 The Rabi model

We will consider the following Hamiltonian, corresponding to a qubit-cavity system

$$H = H_0 + gH_I = \hbar\omega a^\dagger a + \frac{\hbar\omega_0}{2}\sigma^z + \hbar g\sigma^x(a + a^\dagger), \quad (4.1)$$

where $\hbar\omega_0$ is the energy splitting between the two levels of the qubit $|e\rangle$ and $|g\rangle$, ω the frequency of the photons in the cavity or resonator field and g the coupling strength.

In the weak and strong coupling regimes, in which the coupling $g \ll \omega, \omega_0$ is only compared to the decay rates of the cavity and the qubit, one may treat H_I as a small perturbation on top of the bare qubit and resonator states. In this limit the counter-rotating terms $a^\dagger\sigma^+$, $a\sigma^-$ average out, and the total Hamiltonian becomes equivalent to the Jaynes-Cummings model, whose ground state is a separable combination of the qubit ground state and a cavity vacuum, $|g, 0\rangle$.

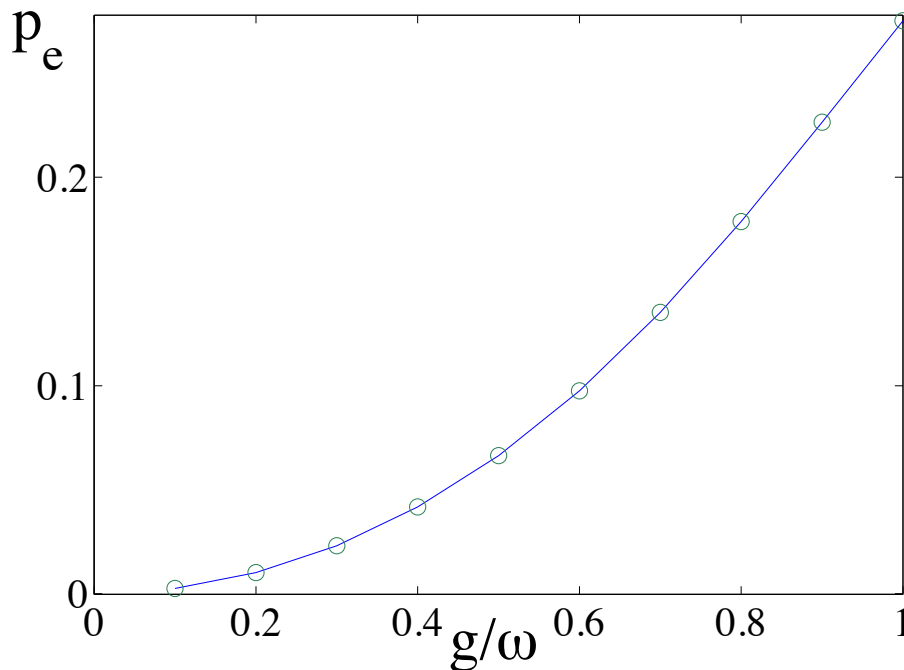


Figure 4.1: (Color online) Probability of excitation for of a qubit p_e (blue,solid) vs. the dimensionless ratio g/ω , for a qubit-resonator system [Eq. (4.1)] in the ground state of a ultrastrong coupled limit $\omega = \omega_0 = 1$ GHz. This line is undistinguishable from a quadratic fit (green,dashed).

In this work we are interested however in the ultrastrong coupling regime, in which g approaches the qubit and photon frequencies, ω and ω_0 . In this case it is more convenient to look at the state space in the language of parity subspaces [94], and treat H_0 and H_I on equal footing. Within this picture, the Hilbert space splits up in two different chains of states coupled by H_I , and in particular the ground state of the system becomes a linear combination of states in the even parity sector

$$|G\rangle = c_0 |g0\rangle + c_1 |e1\rangle + c_2 |g2\rangle + c_3 |e3\rangle + \dots \quad (4.2)$$

where the coefficients c_i depend on g, ω, ω_0 .

4.1.2.2 Detecting excitations with one measurement

One of the goals of this paper is design a protocol for measuring the tiny excitations in the ground states $|c_1|^2 + |c_3|^2 + |c_5|^2 + \dots$ in Eq. (4.2). Let us assume for now that we have a good measurement apparatus and that we perform a single measurement of the qubit in the ground $|G\rangle$ of the system. In Fig. 4.1 we plot the probability of finding the qubit excited after just one measurement

$$p_e = \langle \hat{P}_e \rangle_G =: \langle |e\rangle \langle e| \rangle_G \quad (4.3)$$

against different values of the coupling strength, assuming always $\omega = \omega_0$ and $g/\omega \leq 1$. For the strongest couplings the values of p_e are sizable. Moreover, we have:

$$p_e = \lambda \frac{g^2}{\omega^2}, \quad (\omega = \omega_0, \frac{g}{\omega} \leq 1) \quad (4.4)$$

This quadratic behavior comes as no surprise. The main contribution to p_e is $|c_1|^2$. If we think of $|G\rangle$ as the free vacuum $|g, 0\rangle$ dressed by the interaction H_I , then $|c_1|$ may be computed from perturbation theory in interaction picture, the leading term being proportional to $|\langle e, 1 | H_I | g, 0 \rangle|^2$. It is interesting to see how these contributions quickly grow as g approaches ω , but that at the same time the signal in current experiments with 10% coupling strengths, might have a too small excitation signal to be accurately detected.

This work is born from the idea that perfect projective measurements in c-QED might be too difficult, as existing measurement apparatus may be too slow or not have enough sensitivity to capture those excitations. The constraint of time is found, for instance, in flux qubit measurement devices based on SQUIDs, which roughly work as follows: A very short current pulse is sent to the SQUID, instantaneously changing its potential from a periodic function to a washboard potential. In this brief period of time, one of the flux qubit states which is sitting inside the SQUID may provide, through its intrinsic current and flux, enough additional energy for the SQUID to tunnel into a voltage state. This stochastic process is random in time and does not have a 100% success rate. Moreover, it requires an additional sustained current that keeps the SQUID in that voltage state during an integration time large enough for the electronics to realize that the measurement succeeded. Adding the excitation and integration phases, the best experimental setups bring the detection time down to tens of nanoseconds, which is still slower than the qubit-resonator dynamics ~ 1.6 ns for a 600 MHz coupling, and much shorter for the qubit and resonator periods, $1/\omega$.

An additional complication of the ultrastrong coupling limit is that an arbitrary measurement device might not have enough good coupling to either the qubit or the resonator in the ultrastrong coupling regime. If we assume that both quantum systems interact so strongly that their eigenstates are highly entangled states with large energy gaps, $\sim g, \omega, \omega_0$, the detector could have problems coupling to those states and breaking their energy level structure. In

other words, the measurement device couples through an operator, σ^z , which typically represents a perturbation of the qubit-resonator model, and if that perturbation, which aims at breaking the linear combinations (4.2), is not strong enough, it might not extract any information from the system, or the amount of information might be reduced, becoming an off-resonant, weak dispersive measurement.

All these considerations brought us to the idea of using more than one measurement steps in the same experiment, with the aim of increasing the amount of information that it is extracted from the same state. This can be done because the kind of measurements done in experiments are non-destructive: the same qubit can be continued to be measured at another time. It is true, however, that the interval between measurements might carry a strong, fast and almost chaotic dynamics [Fig. 4.2], arising from the fact that the measurement brings the system into a non-equilibrium state, even if it did not produce any information. We will show that this is not a limitation, but a plus, and that the repeated measurements may characterize the intermediate dynamics.

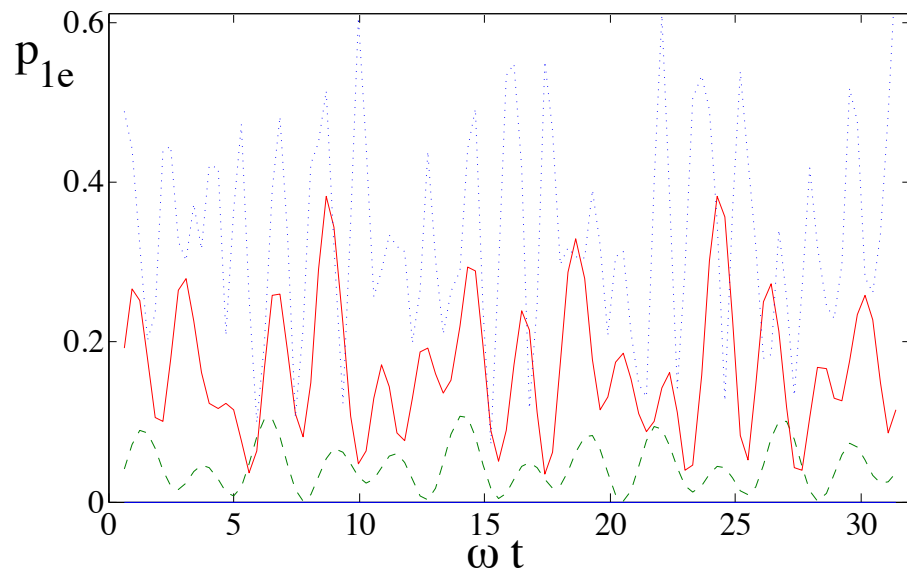


Figure 4.2: (Color online) After the qubit has been measured once, the qubit in the qubit-resonator system is left in a non-equilibrium state, $|\Psi\rangle$. Here we plot the probability of excitation for the qubit p_{1e} as a function of the dimensionless time ωt , shortly after that measurement. We show three situations, $\omega = \omega_0 = 1$ GHz and $g/\omega = 1/3$ (dashed), $g/\omega = 2/3$ (solid) and $g/\omega = 1$ (dotted), which exhibit fast dynamics.

4.1.2.3 Repeated measurements: survival probability

If we measure the qubit once, the measurement apparatus does not click and we are working with a perfect projective measurement, we conclude that the qubit-resonator system has been projected onto the state

$$|\Psi\rangle = \sum_n \hat{c}_{2n} |g, 2n\rangle, \quad (4.5)$$

which is a (normalized) linear combination of deexcited qubits and some photons in the cavity. By measuring the ground state in an improper basis, we have created a non-stationary state that will evolve very quickly, with frequencies that are close to g, ω and ω_0 . Lacking any other relaxation mechanism than the cavity and qubit decoherence times, these oscillations will be sustained for a large period of time, causing the qubit to get reexcited multiple times. The excitation probability

$$p_{1e}(t, 0) = \langle \Psi(t) | \hat{P}_e | \Psi(t) \rangle, \quad (4.6)$$

may be computed from the initially measured state as

$$|\Psi(t)\rangle \propto e^{-iHt} (1 - \hat{P}_e) |G\rangle. \quad (4.7)$$

As Fig. 4.2 shows, p_{1e} exhibits very fast oscillations, but also average to a nonzero value, which is always close to the ground state excitation probability of the qubit, $p_e = \sum_n |c_{2n+1}|^2$. Consequently, if we perform a second measurement at a later time t_1 we will have again a certain probability of success $p_{1e}(t_1, 0)$ of detecting the state $|e\rangle$, and a certain probability of failure $p_{1g}(t_1, 0) = 1 - p_{1e}(t_1, 0)$. In the latter case the system is projected to a new state with a new time dependent probability $p_{2e}(t_2, t_1)$, and so on. After a few measurements we can define the survival probability as the probability that we have never detected a state $|e\rangle$ in the qubit

$$P_g^N = p_g p_{1g}(t_1, 0) p_{2g}(t_2, t_1) \dots p_{Ng}(t_N, t_{N-1}). \quad (4.8)$$

A key idea in the interpretation of this formula is the fact that the intermediate probabilities p_{ng} are on average very similar, and almost independent of the timespan among measurements. For the range of couplings that are within intermediate reach in experiments, $g/\omega \sim 0.1 - 1$, we have verified numerically and perturbatively that this probability is well approximated by a quadratic law

$$p_{ng} \sim 1 - \chi_n \frac{g^2}{\omega^2} \quad (4.9)$$

with minor differences among realizations, χ_n . The accumulation of products in Eq. (4.8) leads to an approximately exponential decrease of the survival probability

$$P_g^N \sim \prod_{n=1}^N \left(1 - \chi_n \frac{g^2}{\omega^2} \right) \sim \exp \left(-N \bar{\chi} \frac{g^2}{\omega^2} \right), \quad (4.10)$$

as long as $\bar{\chi} \frac{g^2}{\omega^2} \ll 1$. This exponential behavior is typical of the so called anti-Zeno effect, in which repeated measurements of a quantum system accelerate the transition of a quantum system between two states. In our case the repeated measurements are rather creating a non-unitary evolution that excites the qubit from $|g\rangle$ to $|e\rangle$ using as seed the nonzero excitation probability $p_{1e} = \sum_n |c_{2n+1}|^2$ which is present in the equilibrium state of the qubit-resonator system. This last point is particularly important because this anti-Zeno evolution is impossible when the ground state of the qubit and the resonator is the vacuum $|g, 0\rangle$. In this case g/ω is so small, and p_{1e} so close to zero, that all measurements will give no signal at all and the qubit will remain in the state $|g\rangle$ for the duration of the experiment. As we will see in the following, there is a key difference between the effects described in this section and the standard anti-Zeno effect: we need only a few measurements and they can be widely spaced in time.

In the following sections we will summarize extensive numerical studies of the anti-Zeno dynamics. We have contrasted these with various semi-analytical methods, one of which, the use of truncated Hilbert spaces, helps us in understanding the reason for this behavior. For the range of couplings of current interest, $g/\omega \sim 0.1 - 1$, it suffices to take two photons, and the ground, $|G\rangle$, plus the two excited states $|E'\rangle, |E''\rangle$ within the same parity subspace. All states can be expanded as in Eq. (4.2) with coefficients c_i, c'_i, c''_i , as linear combinations of $|g0\rangle, |e1\rangle, |g2\rangle$. After the first measurement, the qubit will end up in an excited state with probability $|c_1|^2$ and it will remain in the unexcited state with $|c_0|^2 \simeq 1 - |c_1|^2$, ending up in a combination

$$\hat{P}_g |G\rangle = c_0 |G\rangle + c'_0 |E'\rangle + c''_0 |E''\rangle + \dots \quad (4.11)$$

The crudest approximation would be to neglect all excited state contributions and assume that after each measurement, either the state $|e\rangle$ is detected, or the system ends up in $|G\rangle$. In this case the survival probability would be exactly exponential

$$P_g^N = (1 - |c_1|^2) \prod_{i=1}^N |c_0|^2 = |c_0|^{2N+2}. \quad (4.12)$$

In practice, however, the combined system does not end up only on the ground state, but gets excited state contributions from $|E'\rangle, |E''\rangle$. When we average the contributions over the period in which the measurement takes place, we find that already after the first measurement step, the excited states add up to the total probability, $\langle p_{1e} \rangle_T = |c_1|^2 |c_0|^2 + |c'_1|^2 |c'_0|^2 + |c''_1|^2 |c''_0|^2 + \dots$, enhancing the original behavior.

4.1.2.4 Numerical experiments

We have verified the anti-Zeno dynamics and the exponential law (4.10) by means of exact numerical simulations in which we compute the outcome of repeated measurements on a qubit-resonator Dicke model (4.1). We will now explain the main results of this study.

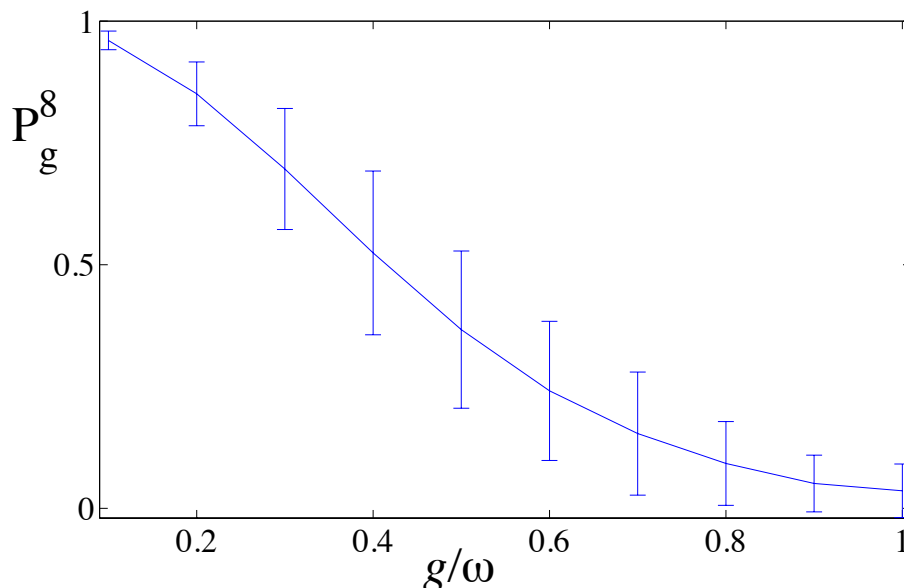


Figure 4.3: Survival probability after eight measurements P_g^8 vs. g/ω , with $\omega = \omega_0$. The measurements are performed with periods $T_1, T_2 = \sqrt{2}T_1$ and averaged over 100 values of T_1 within the interval $2\pi[0.1, 5]$. Note how the law approximates the Gaussian behavior in Eq. (4.10).

From an experimental point of view it might be interesting to maximize the exponent $\bar{\chi}$, optimizing the measurement repetition rate to hit all the maxima in the evolution of the excitation probability [See Fig. 4.2]. However we found that this is very difficult and demands a lot of precision on the measurement apparatus; for small errors or some measurement randomization this procedure drives the apparatus into exactly the opposite regime: always hitting the minima of excitation. Seeking a more robust, less demanding approach we opted for using two incommensurate periods, T_1 and $T_2 \simeq \sqrt{2}T_1$, simulating measurement at times

$$t_n \in \{T_1, T_1 + T_2, 2T_1 + T_2, 2T_1 + 2T_2, \dots\}, \quad (4.13)$$

and at most optimizing the value of T_1 .

With this approach, and exploring different values of T_1 , we have studied the survival probability and concluded that the exponential laws are really accurate. As shown in Fig. 4.3, if we fix the total number of measurements to be $N = 8$ and sample various periods, T_1 , we recover on average the Gaussian behavior $\exp(-N\bar{\chi}g^2/\omega^2)$ deduced in Eq. (4.10). Instead of fixing the number of measurements, we can also study the same law and verify the exponential decay with respect to N . This is shown in Figs. 4.4a-b, where we plot the accumulated survival probability, P_g^N , as a function of time, and fit it against the

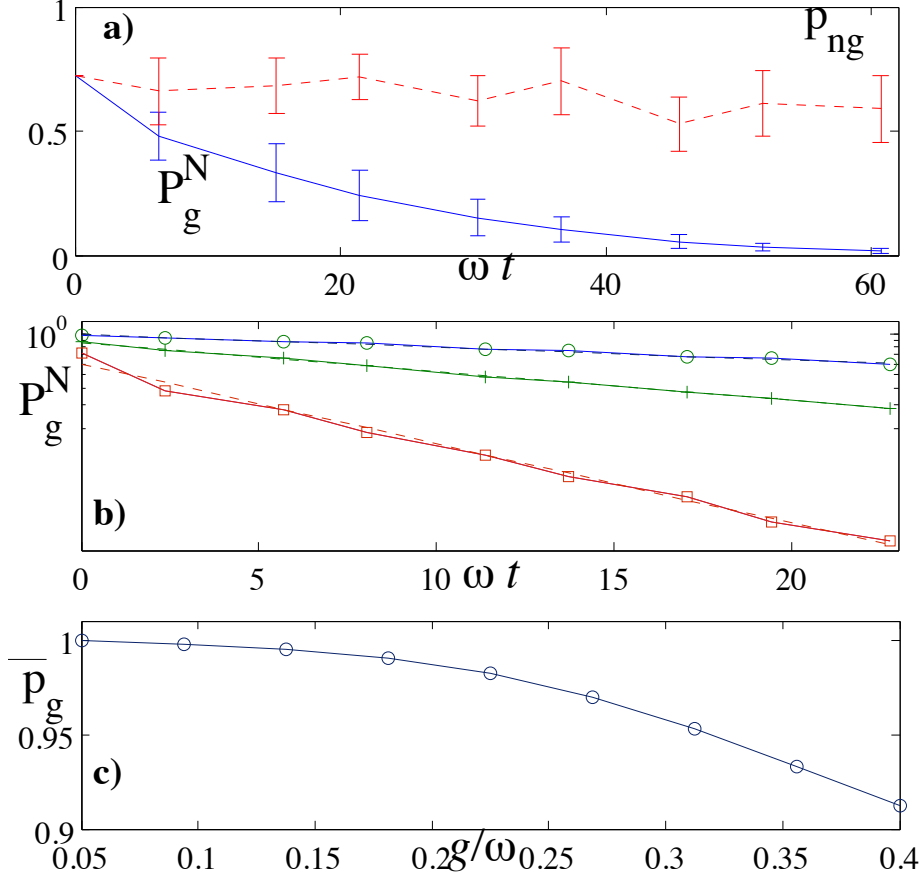


Figure 4.4: (a) Probability after the n -th single measurement, p_{ng} , (dashed) and accumulated survival probability, $P_g^N = \prod_{n=1}^N p_{ng}$ (solid) vs. dimensionless time ωt . We use $g/\omega = 1$ and perform measurements with approximate periods $\omega T_1 = \omega T_2/\sqrt{2} = 2\pi$, averaging over random perturbations of the actual measurement time, t_n , within the interval $\omega t_n + [-0.2\pi, +0.2\pi]$. (b) Survival probability P_g^N (solid lines) and the corresponding exponential fits (dashed lines) for $g/\omega = 1/3$ (circles), $2/3$ (crosses) and 1 (squares). (c) Mean value \bar{p}_g (solid) and the corresponding quadratic fit (dashed) vs. dimensionless coupling strength $\frac{g}{\omega}$. All plots assume $\omega = \omega_0$ and (b,c) use $\omega T_1 = 3\pi/4$

same exponential (4.10).

It is important to remark that the exponential decay is a robust signature that survives even when the measurement does not take place at precise times, t_n , from the list given before (4.13). This has been verified by simulating multiple runs in which t_n is randomly perturbed around its average value, and

computing the survival probability. We want to remind the reader the importance of this robustness, because some measurement apparatus such as SQUIDs behave stochastically and produce a signal at a random time that can not be determined a-priori. The fact that the measurement protocol and the resulting physical behavior are independent of a precise control is encouraging.

The accuracy of the exponential law (4.10) suggests that the survival probability of a single measurement remains constant throughout a single experiment, $p_g \simeq p_{ng} \forall n$. This is qualitatively confirmed by Fig. 4.4a, where we show that these values oscillate around a mean one that is close to the average population of $|g\rangle$ in the ground state, i. e. to p_g . This suggests us to consider average values and approximate

$$\bar{p}_g = \sum_n \frac{p_{ng}}{N} \simeq 1 - \bar{\chi} \frac{g^2}{\omega^2} \quad (4.14)$$

which has the expected quadratic behavior. This estimate is confirmed by Fig. 4.4c, where the quadratic fit is almost undistinguishable from the actual behavior. The final question which remains to be answered is whether the expo-

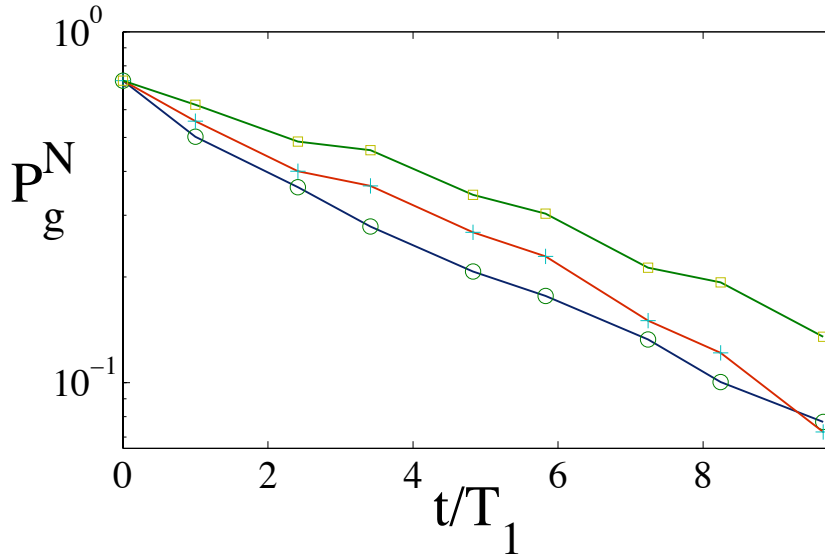


Figure 4.5: Survival probability P_g^N vs. t/T_1 , with $g = \omega = \omega_0$ GHz and $\omega T_1 = \pi$ (blue, circles), 2π (red, crosses) and 3π (green, squares). Each marker corresponds to a measurement.

nent $\bar{\chi}$ depends on the frequency of the measurements or not. For that we have fixed the coupling strength and explored three values of the period, T_1 , studying the average exponential behavior. The result is shown in Fig. 4.5, collapsing all numerical simulations in the dimensionless quantity t/T_1 , and finding that they have very similar slopes.

4.1.2.5 Weak measurements

So far we have considered ideal projective measurements, introducing only some stochasticity in the time at which the measurement event is produced. We will now add another ingredient to our measurement model, which is the possibility that the detector only performs a partial measurement, leaving the state “untouched” with a nonzero probability, ϵ .

We can easily model an imperfect detector using the formalism of completely positive maps, operations that transform density matrices into density matrices. If ρ and ρ' are the states of the qubit-resonator system before and after the measurement, we will write, up to normalization

$$\rho' = (1 - \epsilon)(\mathbf{1} - \hat{P}_e)\rho(\mathbf{1} - \hat{P}_e) + \epsilon\rho. \quad (4.15)$$

This is read as follows. With probability ϵ the measurement device will do nothing, leaving the state untouched. With probability $(1 - \epsilon)$ the measurement device will detect the state of the qubit. In this case it will either give us a positive signal, moment at which we will stop the experiment, or it will not produce anything at all, and we will continue with the projected state $(\mathbf{1} - \hat{P}_e)\rho(\mathbf{1} - \hat{P}_e)$, that has the qubit deexcited, $|g\rangle$.

This qualitative model describes measurements from a SQUID [101, 102], where we place ourselves on the verge of metastability and assume that if the qubit is in the excited state, $|e\rangle$, the SQUID will tunnel to the voltage state with probability $(1 - \epsilon)$, giving no signal for $|g\rangle$. Note that with probability ϵ the SQUID may not tunnel and then we will gain no information about the qubit or the resonator.

In Fig. 4.6 we analyze the impact of ϵ in our previous results. Even for large errors $\epsilon = 0.2$ we retain the exponential behavior observed in Fig. 4.4a, with acceptable error bars that decrease with increasing number of measurements — in other words, the qubit is still efficiently projected to the excited state.

4.1.2.6 Relaxation and dephasing

Throughout this work we have considered in the numerical simulations the model given by the Hamiltonian in Eq. (4.1) which do not include effects like relaxation or qubit dephasing, usually included in master equation approaches.

We want to remark that it is still an open question, both experimentally and theoretically, to understand and model the dissipation and decoherence processes of quantum circuits in the presence of ultrastrong qubit-cavity coupling. One popular approach [103, 104] is to combine the usual photon leakage mechanism from quantum optics models, $\mathcal{L}(\rho) \sim 2a\rho a^\dagger - a^\dagger a\rho - \rho a^\dagger a$, with the qubit-cavity Hamiltonian. Note that in such a combination, the asymptotic states of the dissipation (the vacuum) and of the interaction (populated cavity) are incompatible, and one may find excitations induced by the dissipative terms, an infinite stream of photons leaking out of the cavity and other controversial phenomena.

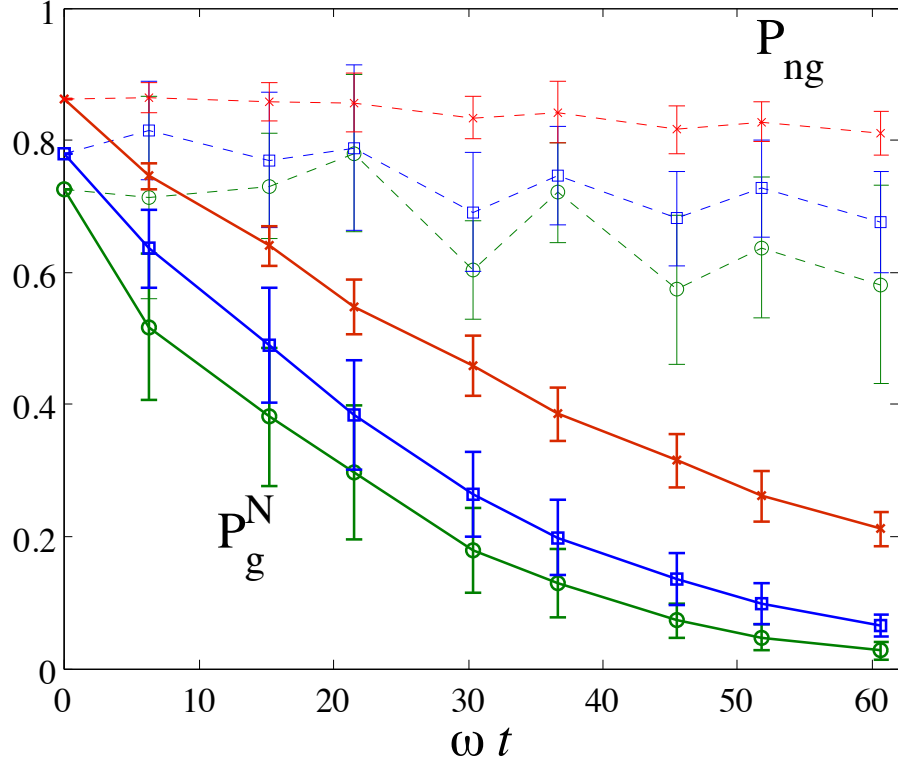


Figure 4.6: (Color online) Survival probability P_g^N (solid lines) and p_{ng} (dashed lines) vs. ωt , with $g = \omega = \omega_0 = 1$ GHz, $\omega T_1 = 2\pi$ and $\epsilon = 0.2, 0.1$ and 0 (crosses, squares and circles, respectively). The probability of a measurement at a time $\omega t = \omega t_0$ is averaged over 20 random values within the interval $[\omega t_0 - 0.2\pi, \omega t_0 + 0.2\pi]$

These effects disappear when one rederives the master equation from first principles, using the qubit-cavity eigenstates of the ultrastrong coupling model and the usual zero temperature baths. In the resulting models the main relaxation mechanisms are found to be the decay to the ground state $|G\rangle$ and a dephasing of the joint cavity-qubit states—in other words, dissipation and decoherence in the proper basis—. If we assume this reasonable model, then we can conclude that the exponential laws derived in this manuscript are not significantly distorted. To begin with, relaxation to the ground state $|G\rangle$ just makes the experiment closer to the truncated Hilbert space model considered in Sect. 4.1.2.3, and in particular to the exponential law from Eq. (4.12). For strong couplings, decoherence amounts to random modulations of the qubit-cavity energy levels, without significantly affecting the populations, $|c_i|^2$. Since this is the most relevant quantity in all the previous discussions, we can also

expect that, up to minor changes in the rates, the anti-Zeno effect will also survive.

4.1.3 Conclusions

We have considered a system consisting in a superconducting qubit coupled to a closed transmission line, operating in the ultrastrong coupling regime. The ground state in such scheme is not just a product of the ground states of the qubit and the cavity, as is the case for weaker couplings. On the contrary, the vacuum of the system is dressed by the interaction and so it contains a relevant probability of finding the qubit excited. This probability is proportional to the square of the coupling strength. We have introduced a protocol for detecting that excitations with certainty, maximizing the small probabilities that are obtained with only one measurement.

Our main result is that, after a number of periodic measurements of the qubit, the probability of finding it in the ground state in all the measurements goes exponentially to zero, even if the measurements are weak and are performed with a slow repetition rate in comparison with the fast dynamics of the interaction. We refer to this as slow quantum anti-Zeno effect. Like the well known quantum anti-Zeno effect, the result is the acceleration of a transition, in this case the exotic transition $|g\rangle \rightarrow |e\rangle$, which becomes relevant in this regime due to the breakdown of the RWA. But this procedure is less experimentally demanding, since it requires a smaller number of measurements and a shorter duration of the period at which they are performed. We have shown that the protocol is robust to large errors in the measurement process, when a realistic SQUID readout is considered.

This is one of the first experimentally accessible consequences of the new ultrastrong coupling regime and can only be derived beyond the RWA. The physical nature of the ground state qubit self-excitations, commonly considered as a virtual process without possible experimental record, seems now to be clear. Moreover, although the ultrastrong coupling entails a very fast dynamics, we have shown that valuable information of the interaction can be extracted efficiently with the current slow and imperfect measurement technologies.

Finally, we want to remark that strong qubit excitations have also been found theoretically in models that combine the full Rabi coupling with traditional dissipative contributions [103, 104]. However, the form of those dissipative terms is questionable in non-RWA setups, and furthermore, there is no justification to equate the sparse measurement setup in this work to a particular dissipative model. This lack of equivalence between models manifests in the fact that, as we have seen numerically, the sparsely repeated measurements can hit certain resonances that invalidate the anti-Zeno dynamics.

4.2 Entanglement dynamics via propagating microwave photons

4.2.1 Introduction

Quantum mechanics does not allow us in general to consider two arbitrary distant systems as separate [2]. In some cases there exist quantum correlations that cannot be generated by local operations and classical communication between remote systems. Time enters this picture through two different questions. The first one is related to the speed bound of a hypothetical superluminal influence which could explain all quantum correlations, estimated to be $10^4 c$ in a recent experiment [105]. The second question is of a more practical nature inside the quantum theory [9, 12, 10] (and Chapter 3 of this Thesis) : what is the speed at which two distant systems become entangled?

Quantum field theory (QFT) fulfills the principle of microscopic causality by which two space-like separated events cannot influence each other [106] and thus cannot be used to transfer information [46, 14]. We may then ask whether microcausality also sets a limit on the speed at which entanglement can be created between two separate systems. More precisely, can two subsystems, supported at regions (\mathbf{x}, t) and (\mathbf{x}', t') , become entangled while they are still space-like separated? Or in simple terms, can finite quantum correlations develop before signals arrive? As we have analyzed in Chapter 3, the answer to this far reaching question is yes, it is possible. After all, Feynman propagators are finite beyond the light cone and even before photon arrival there exist correlations between the vacuum fluctuations at any two space-like separated events.

In this section we demonstrate that circuit QED is arguably one of the most suitable fields to study the dynamics of entanglement between distant systems. One reason is the existence of various choices of high quality superconducting qubits, the so-called artificial atoms [107, 108, 109, 110]. Another reason is the possibility of coupling those qubits strongly with traveling photons using microwave guides and cavities [34, 35, 85]. Furthermore, those coupling strengths can reach the ultrastrong coupling regime [111, 112, 113, 89, 90], where the qubit-photon interaction approaches the energies of the qubit and photons. In this case, the rotating-wave approximation (RWA) breaks down and a different physical structure emerges. Such regimes can be activated and deactivated [96], facilitating the creation of a fairly large amount of entanglement in a time-dependent way, as we will see in this work.

We will discuss some of the preceding questions in the framework of a precise circuit QED setup, see Fig. 4.7, consisting on two well separated superconducting qubits coupled ultra-strongly to an open transmission line [Fig. 4.7b]. The waveguide provides a continuum of microwave photons propagating with uniform velocity, v , mediating an interaction between the qubits. Given an initial separable state in which only qubit A is excited, we have studied the evolution of correlations and related it to the propagation of photons between qubits. The main results are: (i) Outside the light cone, that is in region I of Fig. 4.7a where

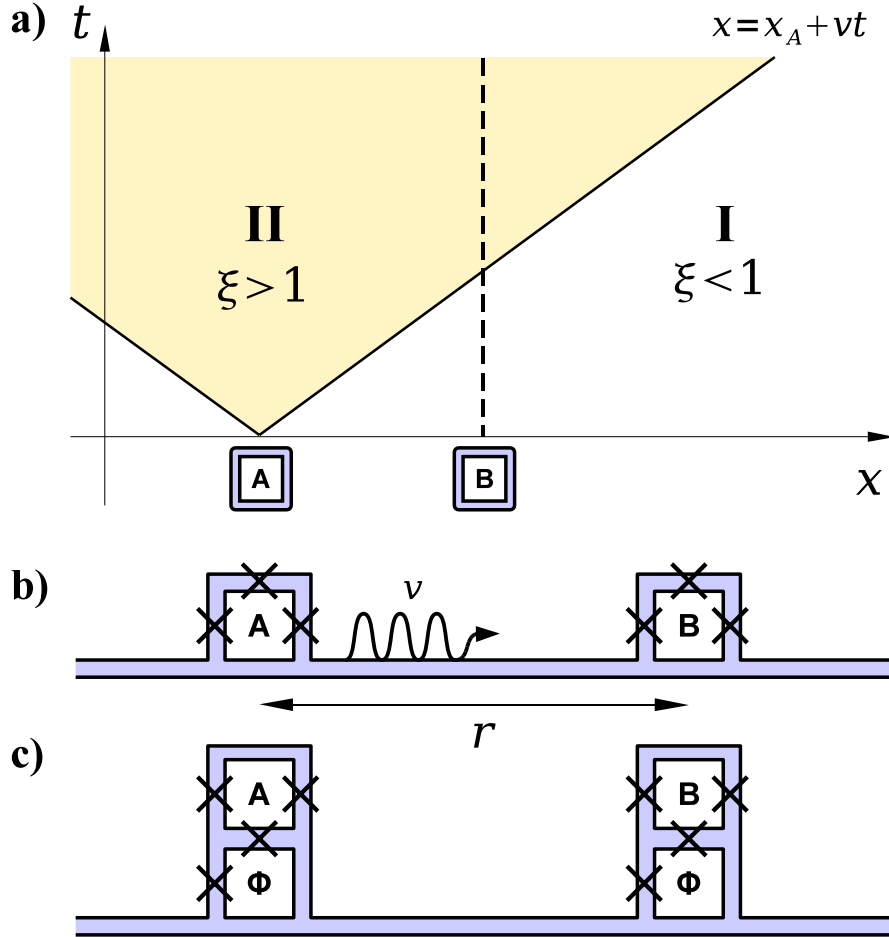


Figure 4.7: (a) Qubits that interact via traveling photons with finite velocity v can be space-like (I, white) or time-like (II, shaded) separated, depending on the value of $\xi = vt/r$. While only in II they are causally connected, entanglement may appear already in region I. (b) A possible implementation of these ideas consists of flux qubits ultra-strongly coupled to a common transmission line. (c) With a slight modification, the coupling of the qubits to the line can be dynamically tuned via fast magnetic fluxes, Φ (Color online).

$\xi = vt/r < 1$, the excitation probability of qubit B is independent of the distance r to qubit A. (ii) Still in region I, entanglement between the qubits always takes a finite value and grows with time. (iii) Once the qubits are time-like separated, that is as soon as we cross into region II, entanglement grows faster than the excitation probability of qubit B and takes sizeable values. Result (i) is a manifestation of the fact that our Quantum Field Theory (QFT) model satisfies

microscopic causality, which formally translates into the vanishing of commutators associated with observables at space-like separations, $[\mathcal{Q}(\mathbf{x}, t), \mathcal{Q}'(\mathbf{x}', t')] = 0$ for $|\mathbf{x} - \mathbf{x}'|^2 - c^2(t - t')^2 > 0$. Furthermore, it shows that two qubits which are space-like separated cannot be used to communicate superluminal information. Result (ii), on the other hand, reveals the fact that correlations between vacuum fluctuations at separate points can be established at arbitrarily short times, even though they are non-signalling and cannot transmit information.

It is important to remark that the previous questions have been posed theoretically using model detectors [9], two-level atoms [10] (and Chapter 3 of this Thesis), scalar fields [9, 12] and photons [10] (and Chapter 3 of this Thesis), yet no experimental test has been accomplished. However in this work, we show that the access to the ultrastrong couplings in circuit QED allows us to explore these ideas with very advantageous parameter ranges.

4.2.2 Superconducting qubits coupled to a quantum field

Our setup consists of two qubits, A and B , interacting via a quantum electromagnetic field. The qubits have two stationary states $|e\rangle$ and $|g\rangle$ separated by an energy $\hbar\Omega$ and interact with a one-dimensional field, which propagates along the line connecting them,

$$V(x) = i \int dk \sqrt{N\omega_k} [e^{ikx} a_k + \text{H.c.}]. \quad (4.16)$$

This field is described by a continuum of Fock operators

$$[a_k, a_{k'}^\dagger] = \delta_{kk'}, \quad (4.17)$$

and a linear spectrum,

$$\omega_k = v|k|, \quad (4.18)$$

where v is the propagation velocity of the field and plays the role of the speed of light. The normalization and the speed of photons depend on the microscopic details. In particular

$$v = 1/\sqrt{cl}, \quad (4.19)$$

where c and l are the capacitance and inductance per unit length.

We consider qubits that are much smaller than the relevant wavelengths, $\lambda = v/\Omega$, and lay well separated. Under these conditions we can split the Hamiltonian, $H = H_0 + H_I$, into a free part for the qubits and the field

$$H_0 = \frac{1}{2}\hbar\Omega(\sigma_A^z + \sigma_B^z) + \int dk \hbar\omega(k) a_k^\dagger a_k, \quad (4.20)$$

and a point-like interaction between them

$$H_I = - \sum_{J=A,B} d_J V(x_J). \quad (4.21)$$

Here x_A and x_B are the fixed positions of the atoms, and

$$d_J = d \times \sigma_J^x \quad (4.22)$$

is equivalent to the dipole moment in the case of atoms interacting with the electromagnetic field.

In what follows we choose the initial state

$$|\psi(0)\rangle = |eg0\rangle, \quad (4.23)$$

where only qubit A has been excited, while both B and the field remain in their ground and vacuum states, respectively. In the interaction picture given by the “free” Hamiltonian H_0 , the system evolves during a lapse of time t into the state

$$|\psi(t)\rangle = \mathcal{T}[e^{-i \int_0^t dt' H_I(t')/\hbar}] |eg\rangle \otimes |0\rangle, \quad (4.24)$$

\mathcal{T} being the time ordering operator. Up to second order in perturbation theory the final state can be written as

$$\begin{aligned} |\psi(t)\rangle = & [(1 + A) |eg\rangle + X |ge\rangle] \otimes |0\rangle + \\ & (U_A |gg\rangle + V_B |ee\rangle) \otimes |1\rangle \\ & + (F |eg\rangle + G |ge\rangle) \otimes |2\rangle + \mathcal{O}(d^3). \end{aligned} \quad (4.25)$$

The coefficients for the vacuum, single-photon, and two-photon states, are computed using the action ($J = A, B$)

$$\mathcal{S}_J^+ = -\frac{i}{\hbar} \int_0^t e^{i\Omega t'} \langle e_J | d\sigma_J^x | g_J \rangle V(x_J, t') dt' = -(\mathcal{S}_J^-)^\dagger \quad (4.26)$$

among different photon number states $|n\rangle$, $n = 0, 1, 2, \dots$, being

$$|n\rangle \langle n| = \frac{1}{n!} \int dk_1 \dots \int dk_n |k_1 \dots k_n\rangle \langle k_1 \dots k_n| \quad (4.27)$$

and

$$|k\rangle = a_k^\dagger |0\rangle. \quad (4.28)$$

Only one term corresponds to interaction

$$X = \langle 0 | T(\mathcal{S}_B^+ \mathcal{S}_A^-) | 0 \rangle. \quad (4.29)$$

This includes photon exchange only inside the light cone, $vt > r$, and vacuum fluctuations for all values of t and r , being

$$r = x_B - x_A \quad (4.30)$$

the distance between the qubits. The remaining terms are

$$\begin{aligned} A &= \frac{1}{2} \langle 0 | T(\mathcal{S}_A^+ \mathcal{S}_A^- + \mathcal{S}_B^- \mathcal{S}_B^+) | 0 \rangle \\ U_A &= \langle 1 | \mathcal{S}_A^- | 0 \rangle, V_B = \langle 1 | \mathcal{S}_B^+ | 0 \rangle, \\ F &= \frac{1}{2} \langle 2 | T(\mathcal{S}_A^+ \mathcal{S}_A^- + \mathcal{S}_B^- \mathcal{S}_B^+) | 0 \rangle, G = \langle 2 | T(\mathcal{S}_B^+ \mathcal{S}_A^-) | 0 \rangle. \end{aligned} \quad (4.31)$$

Here, A describes intra-qubit radiative corrections, while U_A, V_B, F and G correspond to single-photon emission events by one or more qubits.

All the above can be understood as the 1-D c-QED version of the formalism in chapter 3. The coefficients in Eq. (4.25) can be computed analytically (Appendix B) as a function of two dimensionless parameters, ξ and K . The first one,

$$\xi = vt/r, \quad (4.32)$$

was introduced before and it distinguishes the two different spacetime regions [Fig. 4.7a], before and after photons can be exchanged. The second parameter is a dimensionless coupling strength

$$K = \frac{4d^2N}{\hbar^2v} = 2 \left(\frac{g}{\Omega} \right)^2. \quad (4.33)$$

Note that the qubit-line coupling

$$g = \frac{d\sqrt{N\Omega}}{\hbar} \quad (4.34)$$

corresponds to the qubit-cavity coupling that appears by taking the same transmission line and cutting to have a length $L = \lambda$ thus creating a resonator [Refs. [35, 34]]. This formulation has the advantage of being valid both for inductive and capacitive coupling, the details being hidden in the actual expressions for d and N .

Tracing over the states of the field, we arrive at the following reduced density matrix

$$\rho_{AB} = \frac{1}{c} \begin{pmatrix} \rho_{11} & 0 & 0 & \rho_{14} \\ 0 & \rho_{22} & \rho_{23} & 0 \\ 0 & \rho_{23}^* & \rho_{33} & 0 \\ \rho_{14}^* & 0 & 0 & \rho_{44} \end{pmatrix}, \quad (4.35)$$

representing the two-qubit state in the basis formed by $|ee\rangle, |eg\rangle, |ge\rangle,$ and $|gg\rangle$. The coefficients with the leading order of neglected contributions are

$$\begin{aligned} \rho_{11} &= |V|_B^2 + \mathcal{O}(d^4), \quad \rho_{22} = 1 + 2\text{Re}(A) + \mathcal{O}(d^4) \\ \rho_{33} &= |X|^2 + |G|^2 + \mathcal{O}(d^6), \quad \rho_{44} = |U|_A^2 + \mathcal{O}(d^4) \\ \rho_{14} &= U_A^* V_B + \mathcal{O}(d^4) = \langle 0 | \mathcal{S}_A^+ \mathcal{S}_B^+ | 0 \rangle + \mathcal{O}(d^4) \\ \rho_{23} &= X^* + \mathcal{O}(d^4), \end{aligned} \quad (4.36)$$

and the state is normalized $c = \sum_i \rho_{ii}$.

Let us now remark the validity of the perturbative methods applied in this work. The leading corrections to $\mathcal{C}(\rho_{AB})$ (see (3.33)) come from the leading order corrections to $\rho_{23}, \rho_{11}, \rho_{44}$ (Eq. (4.36)). In the case of ρ_{23} we have

$$\rho_{23}(d^4) = (1 + A)X^* + FG^* \quad (4.37)$$

and

$$\rho_{23}(d^6) = \rho_{23}(d^4) + X_1 + X_2, \quad (4.38)$$

where X_1 comes from the interference of one and two photon exchange amplitudes and X_2 comes from the probability amplitude of three photon exchange. A rough upper bound for these two terms is given by $2|X|^3$. For ρ_{11} and ρ_{44} they involve a number of photon emissions and re-absorptions by the same atom or by the other, giving a term

$$\rho_{11}\rho_{44}(d^6) = |U_A|^2|V_B|^2 + A_1 + A_2, \quad (4.39)$$

where rough upper bounds to A_1 and A_2 are $2|A||U_A|^2|V_B|^2$ and $2|X||U_A|^2|V_B|^2$ respectively. All these products are shown to be small for the regions of interest discussed here, $\xi < 2$. The same techniques can be extended to all orders in perturbation theory since the bounds to the different contributions can be grouped and treated as power series, giving rise to corrections that remain negligible as long as $|A|$, $|X|$, $|U_A|^2$ and $|V_B|^2$ are small enough, like in the parameter range explored in this work. Finally, note that similar calculations and results can be obtained in the case in which the qubits have close but different frequencies.

4.2.3 Entanglement dynamics and single photons

We will use the concurrence \mathcal{C} to compute the entanglement of the X-state in (4.35) which is given by (3.33).

Since all quantities depend only on two dimensionless numbers, ξ and K , we can perform a rather exhaustive study of the dynamics of entanglement between both qubits. To cover the widest possible spectrum of experiments, we have chosen coupling strengths (4.33) over three orders of magnitude,

$$\frac{K}{K_0} = 1, 10, 100, 1000. \quad (4.40)$$

The smallest value

$$K_0 = 1.5 \cdot 10^{-4}, \quad (4.41)$$

which corresponds to $g/\pi \simeq 175$ MHz and $\Omega/2\pi \simeq 10$ GHz, that is for instance a charge qubit in the strong coupling limit with a transmission line [34]. The largest value, $K = 1000 K_0$ corresponds to $g \simeq 2\pi \times 500$ MHz and $\Omega \simeq 2\pi \times 2$ GHz, and typically corresponds to a flux qubit directly coupled to a transmission line [112, 96], as shown in Fig. 4.7b-c.

In Fig. 4.8 we plot the value of the concurrence for two qubits which are separated a distance $r = \lambda/8$, using the couplings discussed before. Note how the entanglement jumps discontinuously to a measurable value right inside the light cone ($\xi > 1$), signaling the arrival of photons. Furthermore, even a certain amount of entanglement appears outside the light cone, before photons could be exchanged. This is best seen for the largest couplings, as Fig. 4.8b illustrates.

The dynamics looks even more exciting when we go back to lab time and space. Fig. 4.9 shows the concurrence and the excitation probability of qubit B,

$$p_B = |V_B|^2/c + \mathcal{O}(d^4), \quad (4.42)$$

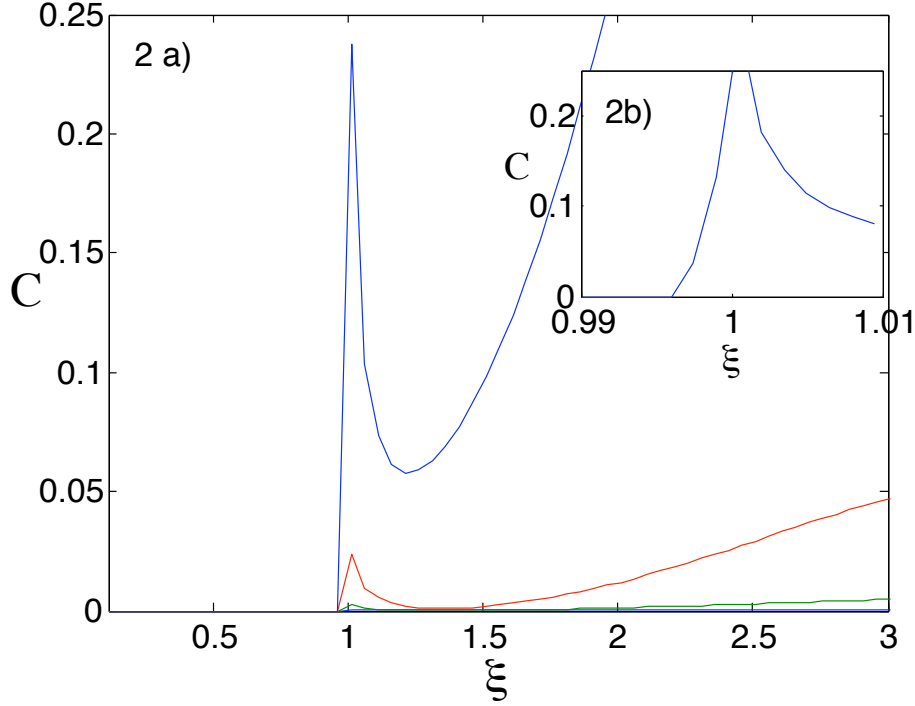


Figure 4.8: a) Concurrence vs. dimensionless separation ξ for $r = \pi v/4\Omega \sim \lambda/8$ and couplings $K = K_0, 10K_0, 100K_0$ and $1000K_0$ (bottom to top) b) Zoom around $\xi = 1$ for the strongest coupling $K = 1000K_0$. (Color online).

for two different separations, $r = \lambda/12$ and $r = \lambda/8$. The probability of excitation appears as independent of the qubit separation. This is exactly the case for the lowest order considered here, which only accounts for B self-interaction, and at all orders in perturbation theory [46] outside the light cone of this setup (region I in Fig. 4.7a). This is in full agreement with microcausality. However, as can be seen in Fig. 4.9, what was a tiny concurrence jumps to a sizable value when crossing the light cone $\Omega t = 2\pi/12$ and $\Omega t = 2\pi/8$. In other words, from the experimental point of view, it is the entanglement between the qubits and not the excitation probability p_B what best signals the presence of a light cone and a finite propagation speed.

4.2.4 Experimental implementation

In order to study the dynamics of quantum correlations between the two superconducting qubits, one has to perform a partial or full tomography of their state. In the first and simpler case, performing measurements in different basis should be enough to gather an entanglement quantifier, such as a Bell inequality

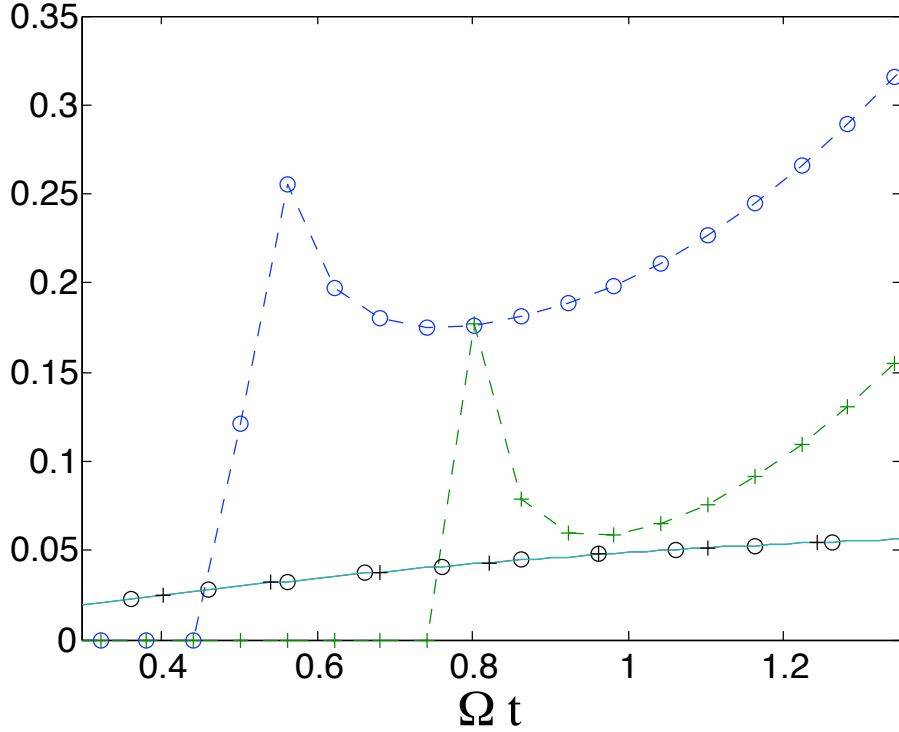


Figure 4.9: Concurrence (dash) and probability of excitation of atom B (solid) vs. dimensionless time, Ωt . Qubits are separated by $r = \lambda/12$ (circles) and $\lambda/8$ (crosses) and have a coupling strength $K = 1000K_0$. Note that, following microcausality, the excitation probabilities do not depend on the separation r outside the light cone (Color online).

violation or, as studied in this paper, the concurrence. This has to be repeated many times, not only to gather sufficient statistics, but also to resolve different of instants of time before and after the light-cone boundary. This may seem a daunting task, but thanks to the speed at which quantum circuits operate and their fast repetition rate, it will be as demanding as recent experiments realizing a controlled-NOT gate [114] or full two-qubit tomography [115].

The actual experimental challenge, though, arises from the need to perform quantum measurements of the qubit state and ensuring that this state is not altered by the ongoing dynamics. One possibility is to perform very fast measurements of the qubits, which means faster than $1/\Omega$. The typical response of measurement apparatus, which in the case of SQUIDS is around a few nanoseconds, sets an upper limit on the qubit and photon frequencies of a few hundreds of megahertz, though we expect this to be improved in the near future.

Another more reliable approach is to connect and disconnect the coupling

between the qubit and the transmission line. In this manner, we could prepare, entangle, and finally measure the qubits without interference or decay processes. If we work with flux qubits, a simple approach is to apply a very large magnetic flux on both qubits, taking the qubit away from its symmetry point. From a mathematical point of view, this amounts to adding a large contribution $E\sigma_{A,B}^x$ to the Hamiltonian. If done very quickly, the field projects the qubit on the same basis on which the coupling operates, eliminating the possibility of spontaneous emission. One would still need to combine the switching of this flux with short pulses that rotate the qubit basis in order to perform a complete set of measurements. The last and most elegant possibility is to effectively switch off all couplings between the qubit and the surrounding field. This can be achieved using a direct coupling between the qubit and the transmission line, with an scheme that incorporates an intermediate loop [Fig. 4.7c]. As Peropadre et al. show in a recent work [96], the result is a coupling that can be rotated and completely deactivated in a time of about 0.1 ns, that is the time needed to inject flux through the loop. The advantage is that, contrary to the case of a large external flux, the influence of the line is completely suppressed and makes it possible to easily rotate the qubits to perform all needed measurements.

4.2.5 Conclusions

Summing up, in this work we have proposed a circuit-QED experiment to study the dynamics of entanglement between two qubits that interact by exchanging traveling photons. Our work focuses on the existence of a finite propagation speed, the appearance of a light cone, the notion of microcausality and the possibility of achieving entanglement both by means of the correlated fluctuations of the vacuum and by photon exchange. The resulting predictions have a wide interest that goes beyond the assessment of microcausality in the QED of quantum circuits, demonstrating that the open transmission line is a useful mediator of entanglement, much like cavities and zero-dimensional resonators. Furthermore, the experiment we propose is also among the simplest ones that can probe the effective QFT for waveguides, both asserting the existence of propagating single photons and probing the dispersion relation at the single-photon level. Finally, we have shown that entanglement via traveling photons works better for stronger qubit-line couplings, making it one of the first potential applications of the ultrastrong coupling regime [89, 90].

Chapter 5

Causality in matter-radiation interactions

“She was particularly exasperated by the behavior of subatomic particles. She wanted the universe to behave sensibly” (Martin Amis, *The pregnant widow*)

Throughout this thesis we have analyzed several features of nonlocality in Quantum Mechanics, like the generation and destruction of entanglement between qubits outside their mutual light cone. We have remarked many times that these effects do not represent a violation of causality of any kind. In section 5.1 of this chapter we will show explicitly that this is indeed the case, in the context of the so-called Fermi problem and the long-lasting controversy associated to it. Although the results are valid also for the 3-D interaction of real atoms and the electromagnetic field, we choose the theoretical framework of 1-D circuit QED in order to make a realistic experimental proposal. Since this proposal involves measurements of a qubit excitation probability at short times in a regime at which non-RWA contributions are relevant, in section 5.2 we deal with the effect of these contributions in the interpretation of the readouts.

5.1 The Fermi problem with artificial atoms in circuit QED

5.1.1 Introduction

Information cannot travel faster than light. But in quantum theory, as we have seen in chapters 3 and 4, correlations may be established between space-like separated events. We remark again that these facts are not contradictory,

since correlations need to be assisted with classical communication in order to transmit information.

The two physical phenomena above arise in a natural fashion in the following situation, which is the so-called Fermi problem [15], originally proposed by Fermi to check causality at a microscopic level. At $t = 0$ a two-level neutral atom A is in its excited state and a two-level neutral atom B in its ground state, with no photons present. If A and B are separated by a distance r and v is the speed of light, can A excite B at times $t < r/v$? Fermi's answer was negative but his argument had a mathematical flaw. When a proper analysis is carried on, fundamental quantum theory questions arise due to the interplay between causal signaling and quantum non-local phenomena.

These issues led to a controversy [16, 17, 116, 46] on the causal behavior of the excitation probability of qubit B , whose conclusions were never put to experimental test. A notorious claim on causality problems in Fermi's two-atom system was given in [16]. The reply of [17] was in the abstract language of algebraic field theory and the proof of strict causality of [46] is perturbative, although given to all orders in perturbation theory. The Fermi problem is usually regarded just as a gedanken experiment, and remains untested, essentially because interactions between real atoms cannot be switched on and off.

In this section we give a complete description of the problem in a physical framework in which predictions can be verified. This framework will be circuit QED which can be regarded as a 1-D version of Quantum Electrodynamics (QED) with two-level (artificial) atoms, a testbed which makes it possible to control the interaction and tune the physical parameters. We complete previous descriptions made of the problem and explain how there are no real causality issues for Fermi's two-atom system. We give an explicit non-perturbative proof of strict causality in these setups, showing that the probability of excitation of qubit B is completely independent of qubit A for times $t < r/v$ and for arbitrary initial states. As a matter of fact, this comes as a manifestation of the non-signaling character of the quantum theory [14]. We also show how this is compatible with the existence of nonlocal correlations at times $0 < t < r/v$, a fact pointed out in various theoretical proposals to entangle qubits at arbitrarily short times [9, 10] (and chapters 3 and 4 of this Thesis). More precisely, we give a non-perturbative proof of the fact that the probability of B being excited and A in the ground state is finite and r -dependent at any time, even for $t < r/v$. We provide also a physical and intuitive explanation of why the conclusions in [16], even if mathematically sound, do not apply to the causality problem. At the end of the Section we discuss the time dependence predicted in our model for the various excitation probabilities and suggest a feasible experimental test of causality using superconducting circuits.

5.1.2 There are no causality problem in Fermi's two-qubit system

In what follows we focus on a practical setup of circuit-QED, with two qubits, A and B , interacting via a quantum field. The qubits have two stationary states

$|e\rangle$ and $|g\rangle$ separated by an energy $\hbar\Omega$ and interact with a one-dimensional field, $V(x)$, (4.16) which propagates along a one-dimensional microwave guide that connects them. This field has a continuum of Fock operators $[a_k, a_{k'}^\dagger] = \delta(k-k')$, and a linear spectrum, $\omega_k = v|k|$, where v is the propagation velocity of the field. The normalization and the speed of photons, v (4.19) depend on the microscopic details such as the capacitance and inductance per unit length, c and l . We will assume qubits that are much smaller than the relevant wavelengths, $\lambda = v/\Omega$, and are well separated. Under these conditions the Hamiltonian, $H = H_0 + H_I$, splits into a free part (4.20) for the qubits and the field and a point-like interaction between them (4.21).

The original formulation of the Fermi problem begins with an initial state

$$|in\rangle = |e_A g_B 0\rangle \quad (5.1)$$

in which only qubit A has been excited, while B and the field remain in their ground and vacuum states, respectively. The total probability of excitation of qubit J is the expectation value of the projector onto the excited state

$$\mathcal{P}_J^e = |e_J\rangle \langle e_J|. \quad (5.2)$$

In the Heisenberg picture

$$P_{eJ} = \langle in | \mathcal{P}_J^e(t) | in \rangle, \quad J \in \{A, B\}. \quad (5.3)$$

We will prove that for $vt < r$ the probability P_{eB} is *completely independent of the state of qubit A for all initial states*. In the Heisenberg picture this amounts to showing that there appears no observable of A in the projector $\mathcal{P}_B^e(t)$ for $vt < r$. Our proof begins by solving formally the Heisenberg equations for \mathcal{P}_J^e

$$\mathcal{P}_J^e(t) - \mathcal{P}_J^e(0) = -\frac{d_J}{\hbar} \int_0^t dt' \sigma_J^y(t') V(x_J, t'). \quad (5.4)$$

Integrating the Heisenberg equations of the operators a_k and a_k^\dagger and inserting them in Eq. (3.3), the total field evaluated at x in Heisenberg picture is decomposed

$$V(x, t) = V_0(x, t) + V_A(x, t) + V_B(x, t) \quad (5.5)$$

into the homogenous part of the field

$$V_0(x, t) = i \int_{-\infty}^{\infty} dk \sqrt{N\omega_k} e^{i(kx - \omega t)} a_k + \text{H.c.} \quad (5.6)$$

and the back-action of A and B onto the field

$$\begin{aligned} V_J(x, t) &= \frac{-id_J N}{\hbar} \times \\ &\times \int_0^t \sigma_J^x(t') \int_{-\infty}^{\infty} \omega_k e^{ik(x-x_J) - i\omega_k(t-t')} dk dt' + \text{H.c.} \end{aligned} \quad (5.7)$$

Eqs. (5.4) translates into a similar decomposition for the probability \mathcal{P}_B^e with three terms

$$\mathcal{P}_B^e(t) = \mathcal{P}_{B0}^e(t) + \mathcal{P}_{BB}^e(t) + \mathcal{P}_{BA}^e(t) \quad (5.8)$$

which are proportional to V_0, V_B and V_A , respectively. The only explicit dependence on A may come from \mathcal{P}_{BA}^e through $V_A(x_B, t)$. Manipulating Eq. (5.7) gives

$$V_A(x_B, t) = \frac{-2\pi d_A N}{\hbar} \frac{d}{dr} \left[\sigma_A^x \left(t - \frac{r}{v} \right) \theta \left(t - \frac{r}{v} \right) \right] \quad (5.9)$$

where the Heaviside function θ shows that strictly $\mathcal{P}_{BA}^e(x_B, t) = 0$ for $vt < r$, and no such dependence is possible. We still have to analyze a possible implicit dependence on A through \mathcal{P}_{BB}^e , whose expression is

$$\begin{aligned} \mathcal{P}_{BB}^e(t) &= \frac{id_B^2 N}{\hbar^2} \int_0^t dt' \int_0^{t'} dt'' \sigma_B^y(t') \sigma_B^x(t'') \\ &\quad \int_{-\infty}^{\infty} dk \omega_k e^{-i\omega_k(t'-t'')} + \text{H.c.} \end{aligned} \quad (5.10)$$

The only implicit dependence could come through the evolution of $\sigma_B^{x,y}(t)$, but again this is not the case. Since

$$[\sigma_B^x, H_I] = 0, \quad (5.11)$$

the evolution of σ_B^x does not involve the field in any way, and for $\sigma_B^y(t)$ we have that

$$\dot{\sigma}_B^y(t) = \Omega \sigma_B^x(t)/2 - \frac{d_B}{\hbar} V(x_B, t) \sigma_B^z(t) \quad (5.12)$$

so using again Eq. (5.5) and Eq. (5.9) we see that the A -dependent part of \mathcal{P}_{BB}^e is 0 for $vt < r$. Thus \mathcal{P}_B^e may be finite but is completely independent of qubit A for $vt < r$, as we wanted to show.

So far, we have demonstrated that although $\mathcal{P}_B^e(t)$ is non-zero for $vt < r$, the only non-zero contribution is \mathcal{P}_{B0}^e , which is not sensitive to the qubit A and thus cannot be used to transmit information between the qubits. Now we will show that this result is compatible with the existence of correlations for $vt < r$. For instance, we consider the probability of finding qubit B excited and qubit A on the ground state $P_{eB,gA}$, which is:

$$P_{eB,gA} = \langle in | \mathcal{P}_B^e(t) \mathcal{P}_A^g(t) | in \rangle, \quad (5.13)$$

where

$$\mathcal{P}_A^g = \mathbf{1} - \mathcal{P}_A^e. \quad (5.14)$$

Using Eqs. (5.4), (5.5) and (5.8), we find a term in this probability which is proportional to $\mathcal{P}_{BB}^e \mathcal{P}_{AA}^g$ and thus to $V_B(x_B, t) V_A(x_A, t)$. From Eq. (5.7) we obtain:

$$V_J(x_J, t) = \frac{2\pi d_J N}{\hbar v} \frac{d}{dt} \{ \sigma_J^x(t) \theta(t) \} \quad (5.15)$$

Therefore, we conclude that in (5.13) there is an unavoidable dependence on A at any $t > 0$, but this is not a causality violation because correlations alone cannot transmit information.

At this point it remains a single question: How can the A -dependent part of P_{e_B} be zero while the one of P_{e_B, g_A} is nonzero for $vt < r$? To better understand it we need less formal results that rely on perturbative expansions, but we would like to remark here that the conclusions above are valid to all orders in perturbation theory. To obtain the total probability of excitation of qubit B

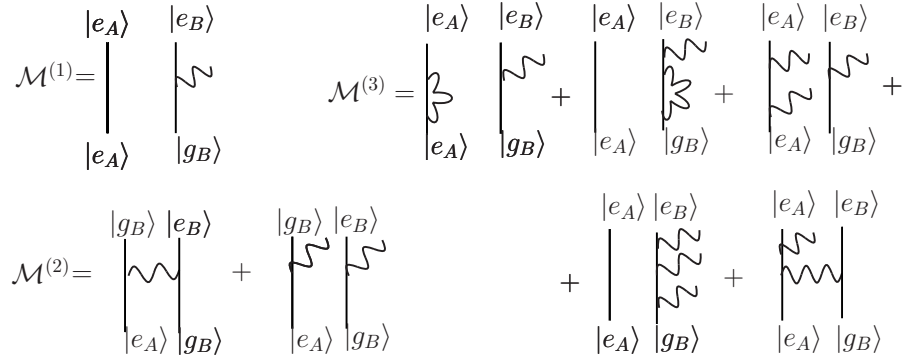


Figure 5.1: The terms of order d_J , d_J^2 and d_J^3 contributing to the amplitude for exciting qubit B .

P_{e_B} to a given order in perturbation theory, one has to expand to a certain order the operators appearing in Eqs. (5.4), (5.5), (5.7). The different terms in the expansion can be related to the probabilities of the different physical processes involved. Fig. 5.1 shows the diagrams of the different amplitudes contributing to P_{e_B} up to the fourth order in d_J . The lowest order amplitude contributing to a final excited B qubit is of order d_J , which means that terms up to order d_J^3 have to be considered. The only terms leading to this final state will be

$$\mathcal{M}^{(1)} = V_B, \quad \mathcal{M}^{(2)} = X + U_A V_B, \quad \mathcal{M}^{(3)} = A' V_B + U_A V_A V_B + V_B U_B V_B + \delta \mathcal{M}^{(3)} \quad (5.16)$$

where U_J (V_J) represent the amplitude for single photon emission at qubit J when the qubit is initially in the ground (excited) state, x is the amplitude for photon exchange, A_J are the radiative corrections of qubit J , and finally $\delta \mathcal{M}^{(3)}$ is the amplitude for photon exchange accompanied by a single photon emission at qubit A . Notice that some of these processes are only possible beyond the rotating wave approximation, which breaks down for strongly coupled circuit-QED setups [112] as the ones considered later. Keeping only terms up to fourth order, we have for the probability to get B excited at a time t

$$\begin{aligned} P_{e_B}(t) &= |\mathcal{M}^{(1)}|^2 + |\mathcal{M}^{(2)}|^2 + 2 \operatorname{Re}\{\mathcal{M}^{(1)*} \mathcal{M}^{(2)}\} \\ &+ 2 \operatorname{Re}\{\mathcal{M}^{(1)*} \mathcal{M}^{(3)}\} + \mathcal{O}(d^5) \end{aligned} \quad (5.17)$$

The final states in $\mathcal{M}^{(1)}$ are orthogonal to those in $\mathcal{M}^{(2)}$ and to the three photon terms in $\mathcal{M}^{(3)}$. Hence, their interference vanishes. Besides, we are only interested in the A -dependent part of the probability, so we can remove the r -independent terms left in (5.17), marking the remaining contributions with a superscript (r)

$$P_{eB}^{(r)}(t) = |\mathcal{M}^{(2)}|^2{}^{(r)} + 2\text{Re}\{\mathcal{M}^{(1)*} \delta\mathcal{M}^{(3)}\} + \mathcal{O}(d^5). \quad (5.18)$$

The first term actually gives $P_{eB,gA}$ up to the fourth order, it is positive and A -dependent at all times, as shown in Fig. 5.2a. The second term is not a projector onto any physical state, but an interference term which has the effect of canceling out exactly the first term for $vt < r$ but not for $vt > r$ (cf. Fig. 5.2b). In a nutshell, interference seems to be the physical mechanism that operates at all orders in perturbation theory to give the causal behavior of the total probability of excitation that we had previously shown. (See Appendix C for more details on the computation of $\delta\mathcal{M}^{(3)}$.)

These perturbative results cast new light on the controversy on the Fermi problem and help us understand *why* our results do not contradict those of Hegerfeldt [16]. Hegerfeldt proved mathematically that the expectation value of an operator consisting of a sum of projectors cannot be zero for all the times $vt < r$, unless it is zero at any time. Indeed, the expectation value of $\mathcal{P}_B^e(t)$ cannot be zero for all $vt < r$, for it always contains the contribution \mathcal{P}_{B0}^e from Eq. (5.6). However, as we showed non-perturbatively, the actual relevant question for causality is whether the expectation value of $\mathcal{P}_{BA}^e(t)$ vanishes for $vt < r$ or not, since only this part of the probability is sensitive to qubit A and could be used to transmit information. Besides, according to our above perturbative results to fourth order, the r -dependent part of the probability, that is the expectation value of $\mathcal{P}_{BA}^e(t)$, is not a mere sum of projectors, but also contains interfering terms. Thus, Hegerfeldt's result does not apply and $\mathcal{P}_{BA}^e(t)$ can be zero for $vt < r$ as is actually the case. Both results are in accord with a general fact of Relativistic Quantum Field Theory: two global states can not be distinguished locally with the aid of a local projector annihilating one of the states, since the local observable algebras are Type III von Neumann algebras (See [17, 116] for a discussion).

5.1.3 Experimental proposal

We will now suggest an experiment to check the causal behavior of P_{eB} . For this we need to control the interaction time at will to access the regions at both sides of $t = r/v$. This, which is highly unrealistic with real atoms, becomes feasible in circuit-QED. While the ideas are valid for both inductive and capacitive couplings, we will focus on using a pair of three-junction flux qubits [117, 118]. Each of the qubits is governed by the Hamiltonian

$$H_{0J} = \frac{1}{2}\epsilon_J\sigma_J^z + \frac{1}{2}\Delta_J\sigma_J^x. \quad (5.19)$$

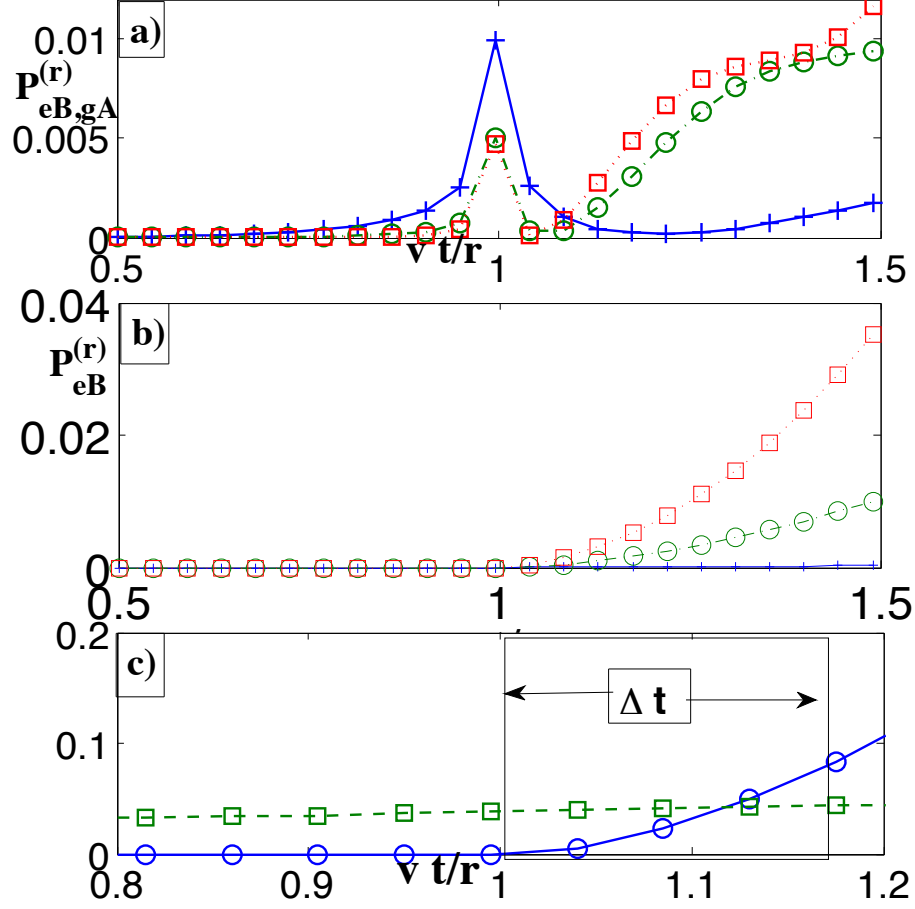


Figure 5.2: (a) $P_{eB, gA}^{(r)}$ and (b) $P_{eB}^{(r)}$ versus vt/r for $\Omega r/v = \frac{\pi}{2}$ (blue, crosses), π (red, squares), and 2π (green, circles) with $K_{A,B} = 0.0225$. For $vt < r$ the qubits are spacelike separated, but there are correlations between them and figure (b) shows the expected causal behavior. (c) $P_{eB}^{(r)}$ (blue, circles) and $|\mathcal{M}^{(1)}|^2$ (green, squares) vs. vt/r for $K_A = 0.20$, $K_B = 0.04$ and a separation of one wavelength $r = 2\pi v/\Omega_{A,B}$. With this data and $\Omega/2\pi \simeq 1\text{GHz}$ we have $\Delta t \simeq 1\text{ns}$. (Color online)

The energy $\epsilon_J = 2I_p \delta\Phi_{xJ}$, is approximately linear in the external magnetic flux, $\delta\Phi_{xJ}$, measured from the degeneracy point, and we assume that the gap Δ_J is fixed. The result is a qubit energy difference

$$\Omega_J(\delta\Phi_{xJ}) = \sqrt{(2I_p \delta\Phi_{xJ})^2 + \Delta_J^2}. \quad (5.20)$$

The coupling between the qubit and the microwave photons is ruled by the dimensionless ratio

$$K_J = \frac{4d_J^2 N}{\hbar^2 v} = 2(g/\Omega_J)^2. \quad (5.21)$$

Here

$$g_J = \frac{d_J \sqrt{N\Omega}}{\hbar} \quad (5.22)$$

is the coupling strength between a qubit and the cavity that would be obtained by cutting the transmission line to be perfectly resonant with the qubit transition. These numbers enter the qubit excitation probability computed before (5.18) through the product

$$P_{eB}^{(r)}(t) \propto K_A K_B. \quad (5.23)$$

Since

$$K_J \propto 1/\Omega_J, \quad (5.24)$$

we may use the external fluxes to move from a weakly coupled regime with no qubit excitations, $\Omega_J \ll g$, to the maximum coupling strength, $\Omega_J \simeq \Delta_J$ ($\delta\Phi_{xJ} = 0$).

Let us first discuss how to prepare the initial state (5.1) of the Fermi problem. We assume that the system starts in a ground state of the form $|g_A g_B 0\rangle$. This is achieved cooling with a large negative value of $\delta\Phi_{xJ}$ on both qubits, which ensures a small value of g/Ω_J and K_J . We estimate that couplings $g/\Omega_J < 0.15$ and $\Omega_J \sim 1.5\text{GHz}$ lower the probability of finding photons in the initial state below 5×10^{-3} , both for vacuum and thermal excitations. Both magnetic fluxes are then raised up linearly in time,

$$\delta\Phi_{xJ} = \alpha_J t, \quad (5.25)$$

to prepare the qubits. Using a Landau-Zener analysis [119] of the process we conclude that an adiabatic ramp

$$\alpha_B \ll \pi \Delta_B^2 / 4\hbar I_p \quad (5.26)$$

of qubit B followed by a diabatic ramp [120, 121]

$$\alpha_A \gg \Delta_A^2 / \hbar 2I_p \quad (5.27)$$

of qubit A , leads to the desired state $|e_A g_B 0\rangle$ with a fidelity that can be close to 1, depending only of α_A , α_B as derived from the Landau-Zener formula:

$$P_J = e^{-\frac{2\pi}{\hbar} \frac{(\frac{\Delta_I}{2})^2}{2I_p \alpha_J}}. \quad (5.28)$$

Note that the minimum gap Δ_B has to be large enough to ensure that the qubit-line coupling of B remains weak and the qubit does not “dress” the field with photons.

Once we have the initial state, both magnetic fluxes must take a constant value during the desired interaction time. After that, measurements of the probability of excitation of qubit B can be performed with a pulsed DC-SQUID scheme [122, 102]. The timescale of the “jump” of the probability around $t = r/v$ for qubit frequencies in the range of GHz and a separation of one wavelength $r = 2\pi v/\Omega$ is

$$\Delta t \simeq 1ns \tag{5.29}$$

[Fig. 5.2c]. Although the total measurement of the SQUID may take a few μs , the crucial part is the activation pulse ($\sim 15ns$) in which the SQUID approaches its critical current and may switch depending on the qubit state. During this activation period the SQUID and the qubit are very strongly coupled ($g \sim GHz$), [122] and the qubit is effectively frozen. The time resolution of the measurement is thus determined by the ramp time of the activation pulse, which may be below nanoseconds. Among the sources of noise that are expected, the short duration of the experiment, well below T_1 and T_2 of usual qubits, makes the ambient noise and decoherence pretty much irrelevant. Thermal excitations of the qubits and the line may be strongly suppressed by using larger frequencies ($> 1.5GHz$). The most challenging aspect is the low accuracy of SQUID measurements, which are stochastic, have moderate visibilities [122] and will demand a large and careful statistics.

On the technical side, it is important to choose carefully the coupling regimes. If we wish to compare with perturbation theory, we need $K_J \ll 1$. However, at the same time the product $K_A K_B$ must take sizable values for $P_{eB} \propto K_A K_B$ to be large. And we need to discriminate the causal signal from the r -independent background of the probability of excitation, whose main contribution is $|\mathcal{M}^{(1)}|^2 \propto K_B$. Thus, a good strategy would be to work with $K_A > K_B$. In Fig. 5.2c we show that it is possible to achieve a regime in which the perturbative approximations are still valid and the r -dependent part of P_{eB} is comparable to $|\mathcal{M}^{(1)}|^2$ in the spacetime region of interest $vt \simeq r$.

5.1.4 Conclusions

In this section, we have considered a system of two superconducting qubits coupled to a transmission line, which can be suitably described in the framework of 1-D QED with two-level (artificial) atoms. Starting from an initial state with qubit A excited, qubit B in the ground state and no photons, we have illustrated the causal character of the model showing that the probability of excitation of qubit B is completely independent of qubit A when $vt < r$. We have also shown that this is in agreement with the existence of nonlocal correlations and we have used perturbative computations to see the physical mechanism underlying the causal behavior. Finally, we have suggested an experiment feasible with current technology that would solve the controversy on the Fermi problem.

5.2 Quantum fluctuations and short-time quantum detection

5.2.1 Introduction

A counterintuitive direct consequence of the breakdown of the RWA is that a detector in its ground state interacting with the vacuum of the field has a certain probability of getting excited and emitting a photon. There is however not a widespread consensus on the physical reality of this effect. Introducing counterrotating terms is interpreted by some to be a problem as the processes described by those terms seem virtual. It seems difficult to accept that a detector in a ground state in the vacuum could get excited. As a matter of fact, there have been attempts of suggesting effective detector models by imposing this phenomenon to be impossible [123]. We should however recall here that these peculiar effects should not be that disconcerting. They are linked to the fact that the initial state considered has not definite energy, since the state “detector and field in their ground states” is not an eigenstate of the full Hamiltonian beyond RWA. Indeed, in section 4.1 we have devised an experimental protocol to detect the trace of this ground-state qubit self-excitations in a simplified-setup with a qubit in a cavity.

In this section we will keep using the theoretical framework applicable to circuit QED, without imposing any additional constraint. We will study the following setup: a source A initially excited, a detector B initially in the ground state and both interacting with the electromagnetic field in its vacuum state. If the detector clicks at a given time, does it mean that the source is now in the ground state? This problem amounts to compute the probability of decay of the source, conditioned to the excitation of the detector. We will show that, unlike Glauber’s RWA detector in which this conditioned probability would be equal to 1 at any time, this circuit QED detector only achieves this value at long times due to the impact of non-RWA effects, like the ground-state qubit self-excitations described above. We will see how these theoretical results have to be taken into account for the interpretation of the readouts of real ongoing experiments.

5.2.2 What does a detector’s click mean?

More precisely, let us consider an initial moment $t = 0$ where A is excited, B is in its ground state and there are no excitations in the transmission line, that is, the initial state would be Eq. 5.1. After a certain time t , if we measure qubit B and it results excited, that would naïvely lead us to think A has decayed and produced a photon which has then later been absorbed by B . We intend to prove otherwise by quantifying what information about the state of A can be extracted by knowing qubit B state after a certain time t . For that we will compute the probability $P_{gA/eB}(t)$ of A to have decayed at a certain instant t ,

conditioned we have measured B excited at that same moment:

$$P_{gA/eB}(t) = \frac{P_{eB,gA}}{P_{eB}}, \quad (5.30)$$

$P_{eB,gA}$ being the probability of A being in the ground state and B excited and P_{eB} the total probability of excitation of B , as they have been defined in the previous section 5.1. Within RWA $P_{gA/eB} = 1$ at any time. But beyond RWA and up to the fourth order in perturbation theory, we have seen in the previous section that P_{eB} is given by Eq. 5.17 and that

$$P_{eB,gA} = |\mathcal{M}^{(2)}|^2 \quad (5.31)$$

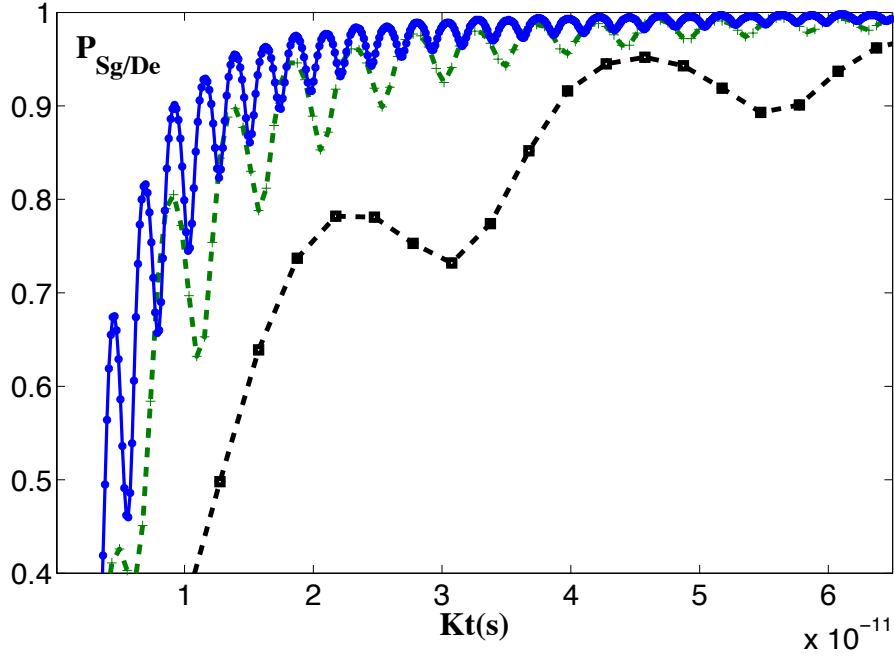


Figure 5.3: $\mathcal{P}_{gA/eB}(t)$ (5.30) in front of Kt for three different values of the coupling strength of $K = K_A = K_B = 7.5 \cdot 10^{-3}$ (solid, blue, circles), $1.5 \cdot 10^{-2}$ (dashed, green, crosses), $7.5 \cdot 10^{-2}$ (dashed, black, squares). In the three cases $2\pi \frac{\tau}{\lambda} = 1$ and $\Omega/(2\pi) = 1 \text{ GHz}$ ($\Omega = \Omega_A = \Omega_B$).

The effect of the non-RWA contributions to the evolution of $\mathcal{P}_{gA/eB}(t)$ can be seen in Figs.5.3 and 5.4, where the consequences of changing the coupling and the distance between qubits are considered. The first thing we notice in Fig.5.3 is that for short times the information provided by the detector is not

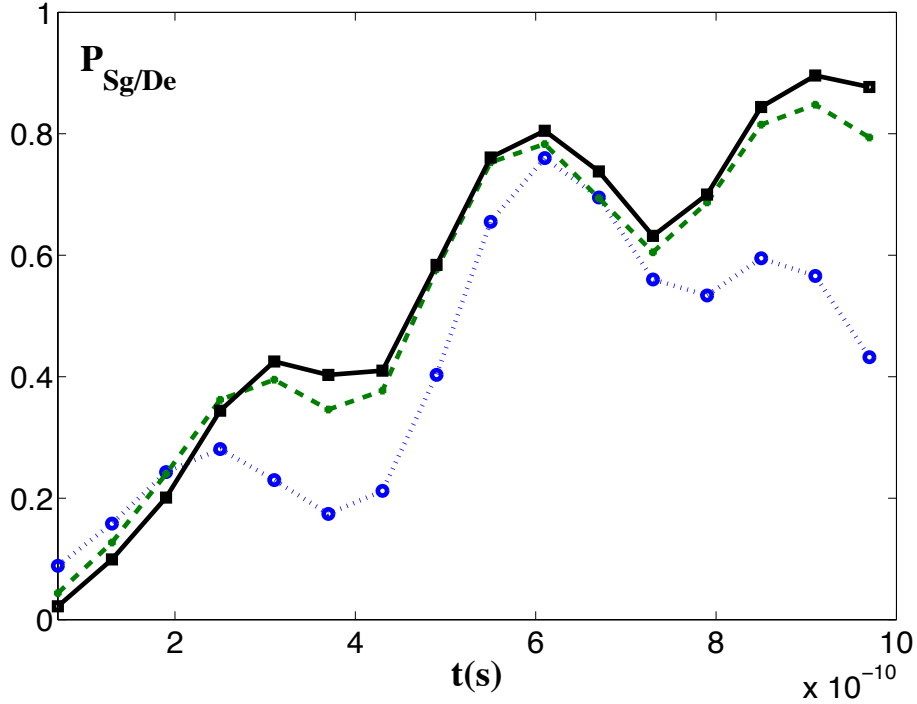


Figure 5.4: $\mathcal{P}_{gA/eB}(t)$ (5.30) in front of t in s for three different values of the distance $2\pi\frac{r}{\lambda} = 0.5$ (dotted, blue, circles), 0.75 (dashed, green, crosses), 1 (solid, black, squares). In the three cases the coupling strength $K = K_A = K_B = 1.5 \cdot 10^{-2}$ and $\Omega/(2\pi) = 1 \text{ GHz}$ ($\Omega = \Omega_A = \Omega_B$).

very much related to the state of the source, that is, self-excitations and other non-RWA phenomena dominate over the photon exchange between source and detector. For the cases considered, only at interaction times $t \gtrsim 1 \text{ ns} \simeq 1/\Omega$ the conditioned probability converges to the RWA prediction, that is, the excitation of the detector is a reliable way to detect the decay of the source. Since the non-RWA contributions are more relevant for large couplings and short distances, the convergence is faster as the distance grows and the couplings diminish, as can be seen in Figs.5.3 and 5.4. It is convenient to remark here that the ripple frequency we see for instance in Fig. 5.3 comes from higher harmonics of the qubit frequency Ω ($= \Omega_A = \Omega_B$ in our case) and so does not represent the emergence of a new time-scale. It can be thought as a process similar to that of a Rabi oscillation, where the qubits would be absorbing in cycles (in a self-deexcitation fashion) the photons previously emitted in self-excitations.

The above theoretical results could have an impact in real experiments of circuit QED. In particular, a typical setup to measure the internal state of a flux qubit coupled to a transmission line consists of a SQUID surrounding the qubit.

Although the total measurement process could take up to tens of nanoseconds, most of the time the coupling SQUID-qubit is much stronger than K , [122] and the dynamics qubit-transmission line is effectively frozen. Thus this dynamics is only important during the activation of the SQUID, a process that may be in the nanosecond regime. For those measurement times, as we have proved, self-excitation effects cannot be disregarded and should manifest themselves.

Besides, it should, in principle, be possible to prepare experiments in the near future to test our predictions directly. We here intend to give just a rough sketch. Such experiments would involve the preparation of the system at $t = 0$ in the initial state of Eq. 5.1, the switching of the interaction for a certain time t (in the line of previous proposals, as in section 5.1) and then the SQUID-measurement of both qubits A and B . By repeating the experiment several times, the result frequencies should theoretically match our probability predictions.

Chapter 6

Quantum simulations of relativistic dynamics. Majorana physics

“But is this really the poet” I asked. “There are two brothers, I know; and both have attained reputation in letters. The Minister I believe has written learnedly on the Differential Calculus. He is a mathematician, and no poet.” “You are mistaken; I know him well; he is both. As poet and mathematician, he would reason well; as mere mathematician, he could not have reasoned at all, and thus would have been at the mercy of the Prefect.” (Edgar Allan Poe, *The purloined letter*)

“Il mare mi ha rifiutato e ritornerò domani all'albergo Bologna, viaggiando forse con questo stesso foglio.” (Ettore Majorana, last letter to Prof. Carelli. English free translation: “The sea rejected me and I’ll be back tomorrow at Hotel Bologna traveling perhaps with this sheet.”)

In chapters 4 and 5 circuit QED was considered as a quantum simulation of matter-radiation interaction. In this chapter we will deal with different quantum simulations, in particular quantum simulations of Relativistic Quantum Mechanical systems. To this end, we will introduce in section 6.1 a new kind of pseudo-Hamiltonian, referred to as “Majorana Hamiltonian”. An example of this class is the object appearing in the Majorana equation, that is, the relativistic equation of a fermion with a Majorana mass term instead of the standard mass term of the Dirac equation. We will propose a trapped ion simulation of the 1-D version of this equation in section 6.2. Finally, in section 6.3 we will show a way to extend the quantum simulations of free relativistic quantum-mechanical systems to systems under the action of potentials, both for single-particle and bipartite systems, by simulating the potentials with free hamiltonians.

Note: Throughout this chapter we will use natural units ($\hbar = c = 1$)

6.1 On Majorana Hamiltonians

6.1.1 Introduction

The existence of spin 1/2 fermions that are their own antiparticles, a possibility opened up by Majorana [23], is under close scrutiny in terms of neutrino properties, theoretical schemes beyond the Standard Model or even in solid state systems [124]. These particles could have a mass with properties crucially different from those of the standard Dirac mass of charged fermions. Their very equation –called Majorana Equation– was introduced by Jehle [24] and by Case [125], who also made a thorough study of their behaviour under space-time transformations, quantized the field and also analyzed their possible (weak) interactions. Primers on these topics from a modern perspective can be found in Refs. [126, 127] and [128].

On studying the quantum mechanics of a fermion obeying the Majorana equation we have identified a structure of much more general applicability. In this section, we present this structure as a very general theoretical framework. We introduce a new kind of generalized Hamiltonians with different mathematical features of the textbook Hamiltonians: they are neither linear nor antilinear, and thus the definition of hermiticity is questionable. We will refer to them as Majorana Hamiltonians, since the Majorana equation is a good example, although their scope is more general. Our main result is that these objects enjoy the physically meaningful property of inducing a temporal evolution which conserves the norm, as expected from total probability conservation. However, this result comes with a bag of surprises: particles with a Majorana Hamiltonian do not have stationary states, probability amplitudes are thus not conserved and an initial global phase is observable in the evolution of the expectation values of physical magnitudes. Moreover, even the notion of density matrix is no longer adequate for a description of this new Majorana dynamics.

Alternatively, we will also show that all the above physics can be equivalently analyzed with a standard Hamiltonian in a real Hilbert space of higher dimensionality, which is actually the way in which a Majorana Hamiltonian would be implemented in the lab, as we will show in section 6.2. As we shall see, this complementary focus sheds light on the shocking features of the Majorana physics commented above.

6.1.2 Majorana Hamiltonians.

In what follows, we will present the general formalism, that will be illustrated in the text with some cases of the Majorana equation. We will refer to the following object as a Majorana Hamiltonian:

$$\hat{M}_\eta = \hat{A} + i\eta\hat{B}\hat{K}, \quad (6.1)$$

where η is a complex number such that

$$|\eta| = 1, \quad (6.2)$$

\hat{A} and \hat{B} are linear Hermitian operators and the novelty is in the complex conjugation operator \hat{K} , which obeys the following properties:

$$\hat{K}[\alpha\psi] = \alpha^*\psi^*, \quad \hat{K}^2 = \hat{1}, \quad (6.3)$$

and, for all ψ and ϕ in the Hilbert space,

$$(\phi, \hat{K}\psi) = (\psi, \hat{K}\phi). \quad (6.4)$$

The general antilinear product operator $\hat{B}\hat{K}$ results antiunitary if \hat{B} is unitary [129]. We restrict this last operator by the condition

$$\{\hat{K}, \hat{B}\} = 0, \quad (6.5)$$

i.e. \hat{K} and \hat{B} anticommute. We can express this by saying that \hat{B} is an imaginary operator (with respect to \hat{K}). Thus, \hat{M}_η is neither linear nor antilinear, but it is well defined on (a domain of) the Hilbert space.

A very important result is that if the evolution in a Hilbert space is governed by a Majorana operator, that is by the generalized Schrödinger equation

$$i\partial_t\psi = \hat{M}_\eta\psi = (\hat{A} + i\eta\hat{B}\hat{K})\psi, \quad (6.6)$$

then the norm is still conserved,

$$\partial_t(\psi(t), \psi(t)) = 0. \quad (6.7)$$

and we can still think of $|\psi|^2$ as a probability distribution. The proof is simple but subtle. First of all, the term with \hat{A} leads to norm conservation due to the standard hermiticity argument. Next, one can readily check that

$$(\psi, \hat{B}\hat{K}\psi) = -(\psi, \hat{B}\hat{K}\psi) = 0. \quad (6.8)$$

This last result follows from the Hermiticity of \hat{B} , the fact that \hat{K} and \hat{B} anticommute, and the relation $(\phi, \hat{K}\psi) = (\psi, \hat{K}^\dagger\phi)$. It is important to remark that while the norm is preserved, amplitudes are not.

The formalism introduced so far appears to respect all the postulates of quantum mechanics, but there is one usual convention that will have to be dropped: the equivalence of state vectors under global phases. This follows from the fact that the constant η in Eq. (6.1) can be traded for a global phase change. In other words, if $\psi(t)$ is a solution of the generalized Schrödinger equation (6.6) associated to the phase η , then

$$\psi_1(t) = \eta^{-1/2}\psi(t) \quad (6.9)$$

will evolve according to a different operator,

$$\hat{M}_1 = \hat{A} + i\hat{B}\hat{K}, \quad (6.10)$$

and it will behave, in general, differently.

This inequivalent evolution of states initially related through a global phase entails that the standard description of mixed states with projector density matrices is not suitable. A mixed state in the present context will be a collection of couples whose elements are unitary vectors ψ_i and corresponding probabilities p_i , with evolution given by

$$\rho_M(t) = \{p_i, \psi_i(t)\}_{i=1}^N \quad (6.11)$$

with each $\psi_i(t)$ a solution of Eq. (6.6). This gives rise to the following interesting point: consider $\psi(0)$ and $\phi(0)$ such that

$$\phi(0) = \exp(i\varphi)\psi(0). \quad (6.12)$$

Then there exists a family of mixed states $\{(p, \psi(0)), (1-p, \phi(0))\}$ which result in identical measurements at time 0 but are nonetheless generically inequivalent under evolution. In other words, density matrices can be the adequate tool for the description or computation of static quantities; but not for dynamic ones. We will illustrate all the above in the Examples section 6.1.4.

6.1.3 Hamiltonization.

We shall now provide an alternative description of the previous results in terms of a doubled (real) Hilbert space. We introduce the objects

$$P_+ = \frac{1}{2}(1 + \hat{K}), \quad P_- = \frac{1}{2}(1 - \hat{K}), \quad (6.13)$$

which are not projectors due to the antilinearity of \hat{K} though satisfy the useful relations

$$\hat{P}_\pm^2 = \hat{P}_\pm. \quad (6.14)$$

Using these operators we reconstruct the isomorphism

$$\psi \in \mathcal{H} \rightarrow \Psi = \begin{pmatrix} \hat{P}_+ \psi \\ -i \hat{P}_- \psi \end{pmatrix} = \begin{pmatrix} \text{Re } \psi \\ \text{Im } \psi \end{pmatrix} \in \mathcal{H}^{(2)}, \quad (6.15)$$

between the complex Hilbert space \mathcal{H} and the direct sum $\mathcal{H}^{(2)}$ of two real Hilbert spaces, $\hat{P}_+ \mathcal{H}$, $-i \hat{P}_- \mathcal{H}$. The norm is conserved under the isomorphism, naturally, but it is important to notice that the inner products are not preserved, namely,

$$(\Phi, \Psi) = \text{Re}[(\phi, \psi)]. \quad (6.16)$$

An alternative way of writing the isomorphism is as [130]

$$\Psi = \text{Re } \psi \otimes |0\rangle + \text{Im } \psi \otimes |1\rangle, \quad (6.17)$$

and demanding that the coefficients be real. Note that the reverse mapping, from the doubled real Hilbert space to the initial one is achieved explicitly as

$$\psi = V\Psi = (\hat{1}_{\mathcal{H}} \quad i\hat{1}_{\mathcal{H}}) \Psi = \text{Re } \psi + i\text{Im } \psi. \quad (6.18)$$

In order to compute how the previous isomorphism acts on operators, we have to introduce the real and imaginary parts of an arbitrary operator,

$$\hat{O} = \text{Re } \hat{O} + i \text{Im } \hat{O}, \quad \begin{cases} \text{Re } \hat{O} &= \frac{1}{2}(\hat{A} + \hat{K}\hat{A}\hat{K}) \\ \text{Im } \hat{O} &= \frac{i}{2}(\hat{K}\hat{A}\hat{K} - \hat{A}) \end{cases}. \quad (6.19)$$

Both the real and imaginary parts of a linear operator are also linear, but while the real part is Hermitian, $\text{Im } \hat{O}$ is anti-Hermitian. Using these components the Hermitian operator \hat{O} acting on \mathcal{H} is mapped onto an operator

$$\hat{O}^{(2)} = \begin{pmatrix} \text{Re } \hat{O} & -\text{Im } \hat{O} \\ \text{Im } \hat{O} & \text{Re } \hat{O} \end{pmatrix} = \text{Re } \hat{O} \otimes \mathbf{1}_2 - i \text{Im } \hat{O} \otimes \sigma_2, \quad (6.20)$$

acting on $\mathcal{H}^{(2)}$ that has all components real with respect to the induced complex conjugation.

Using these tools we can find the evolution equation for the mapped vector $\Psi \in \mathcal{H}^{(2)}$, up from the Majorana Hamiltonian (6.6). Taking for simplicity the operator without phase, \hat{M}_1 , we obtain the Schrödinger-like equation

$$i\partial_t \Psi = \begin{pmatrix} i \text{Im } \hat{A} & \hat{B} + i \text{Re } \hat{A} \\ \hat{B} - i \text{Re } \hat{A} & i \text{Im } \hat{A} \end{pmatrix} \Psi = \hat{M}^{(2)} \Psi. \quad (6.21)$$

This equation deserves a detailed explanation. First of all, the operator $\hat{M}^{(2)}$ is designed to act on the doubled complex Hilbert space $\mathcal{H} \oplus \mathcal{H}$, which contains our real Hilbert space, $\mathcal{H}^{(2)}$, as a subset. Second, note the operator $i\hat{M}^{(2)}$ is real and thus if $\Psi(0)$ is initially real, then it remains so throughout the evolution. In other words, if $\Psi(0) \in \mathcal{H}^{(2)} \subset \mathcal{H} \oplus \mathcal{H}$, it remains in the real sector at all times, preserving our isomorphism. Finally, while the doubled Hamiltonian $\hat{M}^{(2)}$ is Hermitian and its eigenvalues are real, this only happens *when this operator is defined on the complex doubled Hilbert space $\mathcal{H} \oplus \mathcal{H}$* . As a consequence of this and the fact that $\hat{M}^{(2)}$ is purely imaginary, the eigenvectors corresponding to nonzero eigenvalues are necessarily nonreal, so they live outside $\mathcal{H}^{(2)}$. It follows that \hat{M}_1 does not have any eigenvectors with nonzero eigenvalues, and the evolution under its generalized Schrödinger equation will of necessity be either constant or nonstationary. In other words, the Majorana Hamiltonians and Eq. (6.6) have no stationary states.

Now we can understand the role of global phases in Majorana physics in a different way. Two states in the original Hilbert space \mathcal{H} related by a global phase are mapped to states which are no longer related by a global phase in $\mathcal{H}^{(2)}$, but by a rotation

$$\begin{aligned} \phi(0) &= \exp(i\varphi)\psi(0) \\ \updownarrow &= \updownarrow \\ \Phi(0) &= \exp(-i\sigma_2\varphi)\Psi(0). \end{aligned} \quad (6.22)$$

Thus clearly $\Phi(t)$ and $\Psi(t)$ evolve in a non-equivalent way, as do $\phi(t) = V\Phi(t)$ and $\psi(t) = V\Psi(t)$.

6.1.4 Examples

We now apply our formalism to a series of cases whose first examples were given in the 1+1 Majorana equation [24, 125]:

$$i \partial_t \psi = \alpha p \psi \pm i m \sigma_2 K \psi, \quad (6.23)$$

where α is one of the Pauli matrices σ_i ($i = 1, 2, 3$), depending on the chosen representation of the Clifford algebra (see Appendix D). This equation is derived by replacing the ψ in the mass term of the usual Dirac equation by its charge conjugate ψ^C , as we will see with more detail in the next section and in the Appendix D. For simplicity and without loss of generality, we will use now the example with $p = 0$ and $m = 1$:

$$i \partial_t \psi = i \sigma_2 \psi^*. \quad (6.24)$$

Let us see how the previous statements are realized in (6.24). One can readily compute the solution, which is given by

$$\psi(t) = \cos t \psi(0) + \sin t \sigma_2 \psi(0)^*. \quad (6.25)$$

Norm conservation is an immediate consequence of the antisymmetry of σ^2 . On the other hand, amplitudes are not conserved: consider

$$\psi(0) = \begin{pmatrix} 1 \\ 0 \end{pmatrix}, \phi(0) = \begin{pmatrix} 0 \\ 1 \end{pmatrix}. \quad (6.26)$$

It is then the case that

$$(\phi(t), \psi(t)) = i \sin 2t. \quad (6.27)$$

The family of transformations given by (6.25) is not a family of linear or anti-linear isometries [131]; we could define an evolution operator

$$\hat{U}(t) = \cos t \hat{1} + \sin t \sigma_2 \hat{K}, \quad (6.28)$$

which is not unitary.

Let us, as before, study the case (6.24). Consider two initial vectors,

$$\psi(0) = \begin{pmatrix} 1 \\ 0 \end{pmatrix}, \phi(0) = \exp(i\varphi) \psi(0). \quad (6.29)$$

We then obtain

$$\psi(t) = \begin{pmatrix} \cos t \\ i \sin t \end{pmatrix}; \phi(t) = \begin{pmatrix} e^{i\varphi} \cos t \\ i e^{-i\varphi} \sin t \end{pmatrix}. \quad (6.30)$$

Furthermore, this phase is observable through the evolution in time of a measurable magnitude. Consider for instance the expectation value of the Hermitian operator σ_2 as a function of time:

$$\langle \sigma_2 \rangle(t) = \sin(2t) \cos(2\varphi). \quad (6.31)$$

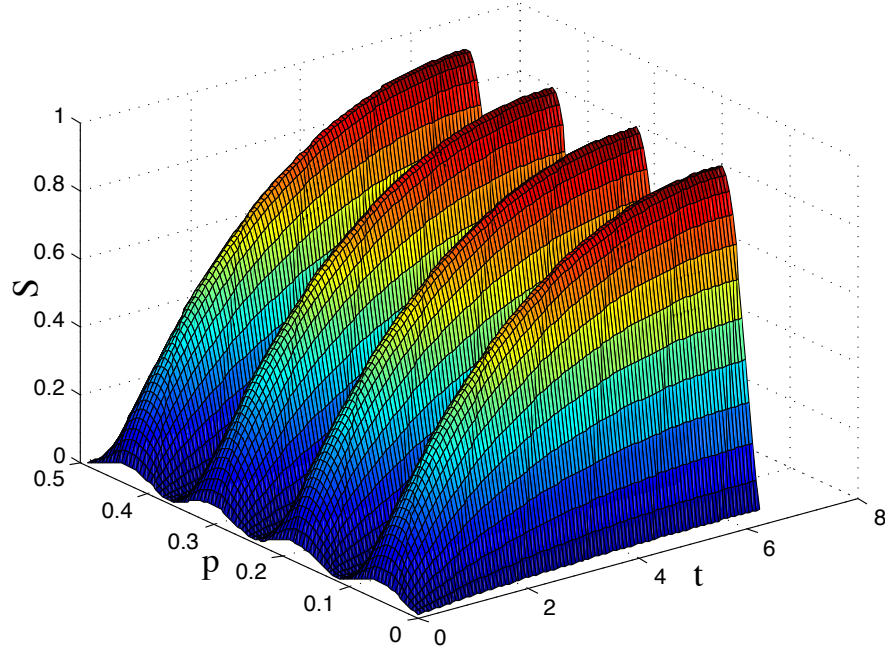


Figure 6.1: Von Neumann entropy of the state $\rho(t)$ Eq. (6.32) for $\varphi = \pi/2$ in front of p and t . In the standard quantum mechanical picture, this would be a pure state for any value of p and t and so entropy would be zero.

We now consider the mixed state defined by $\psi(t)$ with probability p and $\phi(t)$ with probability $1 - p$. If $\varrho(t)$ is the density matrix that would correspond to $\psi(t)$, then the density matrix $\rho(t)$, corresponding to the mixed state at time t , is

$$\rho(t) = \varrho(t) + (1 - p) \sin \varphi \sin(2t) (\cos \varphi \sigma_1 - \sin \varphi \sigma_2) . \quad (6.32)$$

The von Neumann entropy of this mixed state is depicted in Fig. 6.1 as a function of time and p for the case of $\varphi = \pi/2$. In the standard quantum mechanical picture, the initial state would be considered as a pure state, and unitary evolution would conserve entropy. Indeed, if the state were the reduced state of a composite system this would mean that the global state is non-entangled. All the above suggests that the standard quantum information theory, as it is, does not fit to Majorana physics.

As a general example of the hamiltonization we can consider Eq. (6.1) with $\eta = 1$,

$$\hat{B} = m \sigma_2, \hat{A} = p_x \sigma_1 + p_y \sigma_2, \quad (6.33)$$

which accommodates both the 1+1 and 2+1 Majorana equation. Thus, using Eq. (6.21), we obtain the following Hamiltonian in the doubled real Hilbert

space:

$$\hat{M}^{(2)} = \begin{pmatrix} p_x \sigma_1 & i p_y \sigma_2 + m \sigma_2 \\ -i p_y \sigma_2 + m \sigma_2 & p_x \sigma_1 \end{pmatrix}, \quad (6.34)$$

which is the Hamiltonian of a Dirac equation with

$$\beta = \sigma_1 \otimes \sigma_2, \alpha^1 = \mathbf{1}_{2 \times 2} \otimes \sigma_1, \alpha^2 = -\sigma_2 \otimes \sigma_2. \quad (6.35)$$

It is straightforward to check that

$$\gamma^0 = \beta, \gamma^1 = \beta \alpha^1 = -i \sigma_1 \otimes \sigma_3, \gamma^2 = \beta \alpha^2 = -i \sigma_3 \otimes \mathbf{1}_{2 \times 2} \quad (6.36)$$

form a Clifford algebra, and also γ^0, γ^1 . Thus Majorana equation in 2+1 and 1+1 dimensions is mapped to a 3+1 Dirac equation with $p_z = 0$ and $p_y = p_z = 0$ respectively. This result is more general: with this techniques the 3+1 Majorana equation is mapped to a 7+1 Dirac equation with four components of the momentum set to 0.

As another example, let us consider the Hilbert space of qubits, where a general operator $\hat{A} = a_\mu \sigma_\mu$ with $\sigma_\mu = (\hat{1}, \vec{\sigma})$ and real a_μ will be decomposed as $\text{Re } \hat{A} = a_0 \hat{1} + a_1 \sigma_1 + a_3 \sigma_3$, $\text{Im } \hat{A} = -i a_2 \sigma_2$. Without losing generality, we can choose $\hat{B} = \sigma_2$. The scale of \hat{B} would be fixed by the timescale. Thus we can explicitly write

$$\hat{M}^{(2)} = \begin{pmatrix} a_2 \sigma_2 & \sigma_2 + i \text{Re } \hat{A} \\ \sigma_2 - i \text{Re } \hat{A} & a_2 \sigma_2 \end{pmatrix}, \quad (6.37)$$

whose eigenvalues appear in pairs,

$$\begin{aligned} \lambda_1 &= |\mathbf{a}| + \sqrt{1 + a_0^2}, \lambda_2 = -\lambda_1, \\ \lambda_3 &= |\mathbf{a}| - \sqrt{1 + a_0^2}, \lambda_4 = -\lambda_3. \end{aligned} \quad (6.38)$$

6.1.5 Conclusions and outlook.

Putting all together, we have introduced a new kind of generalized Hamiltonians Eq. (6.1). We refer to them as Majorana Hamiltonians since the Majorana equation is a good example, but the framework is far more general. These objects are neither linear nor antilinear and thus there is not a clear definition of hermiticity, but they induce a physical dynamics in which the norm is conserved. This new physics has very interesting features: for instance, initial global phases are relevant since they can be observed in the dynamics of expectation values of physical magnitudes. As a consequence, the notion of density matrix is not adequate for a dynamical description of the system, and has to be replaced. Alternatively, all this can be seen within the usual Quantum Mechanics framework, since a Majorana Hamiltonian can always be mapped to a standard Hamiltonian in a real Hilbert space of double dimensionality. A global phase transformation in the original Hilbert space is not mapped to a global phase transformation in the new one, which explains the differences in the evolution. This mapping between Hilbert spaces is actually the tool to implement Majorana Hamiltonians

and also antiunitary operations like time reversal, charge conjugation or partial transpose in the lab, as we will see in the next section. A deeper look into the physics of real Hilbert spaces will imply also a better understanding of the new Majorana physics, for instance the quantum information theory of Majorana systems, since it has been noted that quantum information properties in real Hilbert spaces are different from the standard ones [132], [133].

6.2 Quantum simulation of Majorana equation and unphysical operations

6.2.1 Introduction

The Majorana equation [24], [125] is a relativistic wave equation for fermions where the mass term contains the charge conjugate of the complex spinor, ψ_c ,

$$i\rlap{\not{D}}\psi = m\psi_c. \quad (6.39)$$

Here, $\rlap{\not{D}} = \gamma^\mu \partial_\mu$ and γ_μ are the Dirac matrices [20], while the non-Hamiltonian character stems from the simultaneous presence of ψ and ψ_c . The significance of the Majorana equation rests on the fact that it can be derived from first principles in a similar fashion as the Dirac equation [128]. Both wave equations are Lorentz invariant but the former preserves helicity and does not enjoy stationary solutions. The Majorana equation is considered a possible model [126] for describing exotic particles in supersymmetric theories –photinos and gluinos–, or in grand unified theories, as is the case of neutrinos. Indeed, the discussion of whether neutrinos are Dirac or Majorana particles still remains open [124]. Relativistic quantum models can be simulated, but they can also emerge as a natural description of certain systems, as happens with the 2+1 Dirac equation in graphene systems. Nevertheless, note that despite the similar naming, this work is neither related to the Majorana fermions (modes) in many-body systems, nor to the Majorana fermions (spinors) in the Dirac equation [126].

In order to simulate physics described by the Majorana equation, we have to solve a fundamental problem: the physical implementation of antilinear and antiunitary operations in a quantum simulator. In this section, we apply a mapping introduced in the previous section by which complex conjugation, an unphysical operation, becomes a unitary operation acting on an enlarged Hilbert space. The mapping works in arbitrary dimensions and can be immediately applied on advanced quantum simulation platforms. As a key application, we show how to simulate the Majorana equation in 1+1 dimensions and other unphysical operations –time reversal and complex conjugation– using only two trapped ions. This is completed with a recipe for measuring relevant observables and a roadmap towards more general scenarios, including the combination of Majorana and Dirac physics. Finally, we discuss further scopes of quantum simulations in the context of fundamental and relativistic quantum physics.

6.2.2 Quantum simulation of antiunitary operations

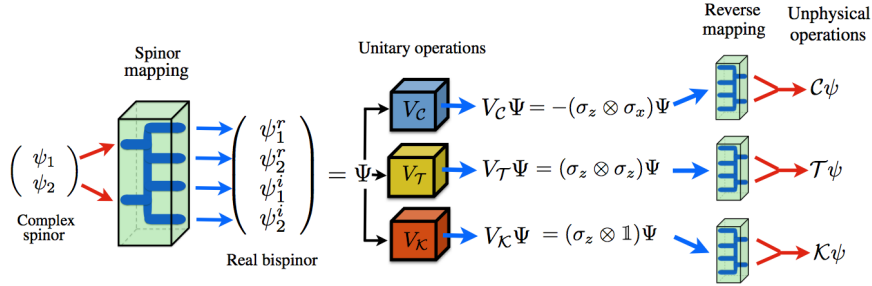


Figure 6.2: Diagram showing the different steps involved in the quantum simulation of unphysical operations in 1+1 dimensions.

6.2.3 Simulating antiunitary operations

There are three discrete symmetries [134] which are central to quantum mechanics and our understanding of particles, fields and their interactions: parity, \mathcal{P} , time reversal, \mathcal{T} , and charge conjugation, \mathcal{C} . None of these operations can be carried out in the real world: \mathcal{P} involves a global change of the whole physical space, while \mathcal{C} and \mathcal{T} are antiunitaries. However, there is no apparent restriction for implementing them in a physical system that simulates quantum mechanics. We will focus on the study of antiunitary operations, which can be decomposed into a product of a unitary, \mathcal{U}_C (for charge conjugation) or \mathcal{U}_T (for time reversal), and complex conjugation, $\mathcal{K}\psi = \psi^*$. We consider the mapping 6.15 of the quantum states of an n -dimensional complex Hilbert space, \mathbb{C}_n , onto an real Hilbert space, \mathbb{R}_{2n} . This mapping can be physically implemented by means of an auxiliary two-level system, such that $\mathbb{R}_{2n} \in \mathcal{H}_2 \otimes \mathcal{H}_n$. In this manner, the complex conjugation of the simulated state becomes a local unitary V_K acting solely on the ancillary space,

$$\mathcal{K}\psi = \psi^* \rightarrow V_K \Psi = (\sigma_z \otimes \mathbf{1}) \Psi, \quad (6.40)$$

and thus physically implementable. Furthermore, unitaries and observables can be also mapped onto the real space, (6.20) preserving unitarity and Hermiticity. In addition to complex conjugation, unitaries and Hermitian operators, the proposed simulator also accomodates the antiunitary operations

$$\mathcal{C} = \mathcal{U}_C \mathcal{K} \quad (6.41)$$

and

$$\mathcal{T} = \mathcal{U}_T \mathcal{K}. \quad (6.42)$$

To this end, we have to choose a particular representation (see Appendix D) that fixes the unitaries \mathcal{U}_C and \mathcal{U}_T , as will be shown below.

At this point, we possess the basic tools to simulate the Majorana equation in the enlarged space. The expression for the charge conjugate spinor is given by

$$\psi_c = \eta \mathcal{C} \gamma^0 \mathcal{K} \psi, \quad (6.43)$$

with \mathcal{C} a unitary matrix satisfying

$$\mathcal{C}^{-1} \gamma^\mu \mathcal{C} = -(\gamma^\mu)^T. \quad (6.44)$$

We illustrate now with the case of 1+1 dimensions (Appendix D). Here, a suitable representation of charge conjugation is

$$\psi_c = i \sigma_y \sigma_z \psi^*, \quad (6.45)$$

that is $\eta \mathcal{C} = i \sigma_y$, and the Majorana equation reads

$$i \partial_t \psi = \sigma_x p_x \psi - i m \sigma_y \psi^*, \quad (6.46)$$

where $p_x = -i \hbar \partial_x$ is the momentum operator. Note that Eq. (6.46) is not Hamiltonian, $i \hbar \partial_t \psi = H \psi$, as is the case of Schrödinger and Dirac equations. This is due to the presence of a complex conjugate operation in the right-hand side of Eq. (6.46), which is not a linear Hermitian operator. Through our mapping (6.15),

$$\begin{pmatrix} \psi_1 \\ \psi_2 \end{pmatrix} \in \mathbb{C}_2 \rightarrow \Psi = \begin{pmatrix} \psi_1^r \\ \psi_2^r \\ \psi_1^i \\ \psi_2^i \end{pmatrix} \in \mathbb{R}_4, \quad (6.47)$$

the Majorana equation for a complex spinor becomes a 3+1 Dirac equation with dimensional reduction, $p_y, p_z = 0$, and a four-component real bispinor

$$i \hbar \partial_t \Psi = [(1 \otimes \sigma_x) p_x - m \sigma_x \otimes \sigma_y] \Psi. \quad (6.48)$$

Note that, here, the dynamics preserves the reality of the bispinor Ψ and, in general, cannot be reduced to a single 1+1 Dirac particle. The result of Eq. (6.48) is even more general and the complex-to-real map in arbitrary dimensions transforms always a Majorana equation into a higher dimensional Dirac equation. Since Eq. (6.48) is a Hamiltonian wave equation, it can be simulated in a conventional quantum system while suitably encoding the Majorana dynamics.

The mapping of wavefunctions into larger spinors may allow us not only to implement Majorana equations in the lab, but also to explore exotic symmetries and unphysical operations, otherwise impossible in nature. From Eqs. (6.40), (6.45), and (6.47), for the 1+1 dimensional case, we can deduce that charge conjugation is implemented in the enlarged space via the unitary operation $V_{\mathcal{C}}$

$$\psi_c = \mathcal{C} \psi = \mathcal{U}_{\mathcal{C}} \mathcal{K} \psi \rightarrow V_{\mathcal{C}} \Psi = -(\sigma_z \otimes \sigma_x) \Psi. \quad (6.49)$$

We can do something similar with time reversal, defined as the change $t \rightarrow (-t)$. In this case, we expect [128] (Appendix D)

$$i \partial_\tau \psi'(\tau) = H \psi'(\tau), \quad (6.50)$$

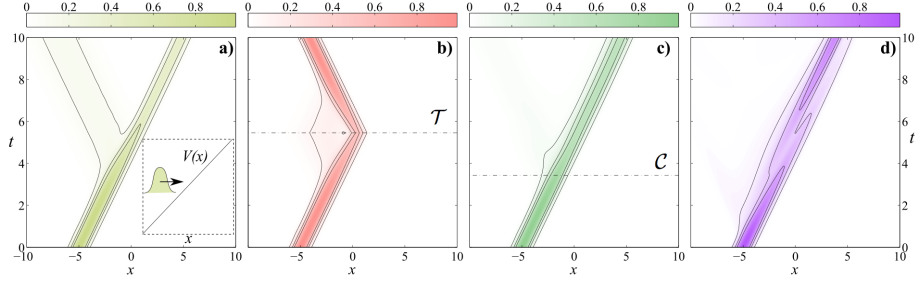


Figure 6.3: Scattering of a fermion against a linearly growing potential (inset). (a) Ordinary Klein process: a fraction of a Dirac fermion turns into an antiparticle, entering the potential. (b) At an instant of time we apply the time reversal operator \mathcal{T} causing the particle to retrace its own trajectory. (c) Similar to (b) but now we apply charge conjugation, converting the particle in its antiparticle. (d) Scattering of a Majorana fermion, which propagates through the potential. Parameters are $m = 0.5$ and $V(x) = x$, in dimensionless units.

where the time variable $\tau = -t$ and the modified spinor

$$\psi'(\tau) = \mathcal{T}\psi(t). \quad (6.51)$$

In order to preserve scalar products and distances, the time reversal operator must be an anti-unitary operator and thus decomposable as the product

$$\mathcal{T} = \mathcal{U}_{\mathcal{T}}\mathcal{K}. \quad (6.52)$$

In $1 + 1$ dimensions, imposing that the Hamiltonian be invariant under time reversal,

$$H' = \mathcal{T}^{-1}H\mathcal{T}, \quad (6.53)$$

implies that the unitary satisfies

$$\mathcal{U}_{\mathcal{T}}^{-1}(i\sigma_x\partial_x)\mathcal{U}_{\mathcal{T}} = -i\sigma_x\partial_x, \quad (6.54)$$

with a possible choice being

$$\mathcal{U}_{\mathcal{T}} = \sigma_z. \quad (6.55)$$

In other words, in the enlarged simulation space

$$\mathcal{T}\psi = \mathcal{U}_{\mathcal{T}}\mathcal{K}\psi \rightarrow V_{\mathcal{T}}\Psi = (\sigma_z \otimes \sigma_z)\Psi. \quad (6.56)$$

See Fig. 6.2 for a scheme of the simulated symmetries.

Equation (6.48), a Dirac equation in $3+1$ dimensions with dimensional reduction $p_y, p_z = 0$, can also be interpreted as a recipe for the quantum simulation of the Majorana equation in the laboratory. In a recent experiment, the dynamics of a free Dirac particle was simulated using a single trapped ion [22], a quantum

platform that has proved instrumental for quantum information implementations. Unfortunately, Eq. (6.48) has a more complex structure and a different setup is required, which is outlined in the Appendix E. Moreover, the encoded Majorana dynamics requires a systematic decoding via a suitable reverse mapping of observables, as we show below. In short, the real bispinor $\Psi \in \mathbb{R}_4$ can be encoded in the internal state of two ions, while the position and momentum of the Majorana particle are mapped onto the quadratures of a collective motional mode, e. g. the center-of-mass mode, of the ions [135, 22]. The Hamiltonian of Eq. (6.48) can be implemented term-by-term, in principle, in the trapped-ion system by a number of lasers coupling the motional and internal states of the ions. However, our proposal is valid for a general quantum simulator and we do not discard its implementation in other quantum platforms.

A relevant feature of the Majorana equation in 3+1 dimensions is the conservation of helicity. A reminiscent of the latter in 1 + 1 dimensions is the observable called hereafter as *pseudo-helicity*

$$\Sigma = \sigma_x p_x. \quad (6.57)$$

This quantity is conserved in the 1+1 Majorana dynamics of Eq. (6.46) but not in the 1+1 Dirac equation. We will use this observable to illustrate measurements on the Majorana wavefunction. The mapping for operators can be simplified if we are only interested in expectation values. Reconstructing the complex spinor

$$\psi = M\Psi \quad (6.58)$$

with matrix

$$M = \begin{pmatrix} \mathbf{1} & i\mathbf{1} \end{pmatrix} \quad (6.59)$$

associated with Eqs. (6.47) and (6.48), we can write the following equivalence

$$\langle O \rangle_\psi = \langle \psi | O | \psi \rangle = \langle \Psi | M^\dagger O M | \Psi \rangle =: \langle \tilde{O} \rangle_\Psi. \quad (6.60)$$

According to this, in order to measure the pseudo-helicity Σ , we have to measure

$$\tilde{\Sigma} = M^\dagger \sigma_x p_x M = (\mathbf{1} \otimes \sigma_x - \sigma_y \otimes \sigma_x) \otimes p_x \quad (6.61)$$

in the enlarged simulation space. In an ion trap implementation, the first term of this observable, $(\mathbf{1} \otimes \sigma_x) \otimes p_x$, is measurable with recently developed techniques [22]. The second term is a three-operator correlation, $(\sigma_y \otimes \sigma_x) \otimes p_x$, and will require a specific design with measurements involving short-interaction times [136], as explained in the Methods section.

We want to emphasize that the previous mappings and the implementation of discrete symmetries are not only valid for Majorana equations, but also for Dirac spinors. Equally interesting is the possibility of combining both Dirac and Majorana mass terms in the same equation [126],

$$i\partial\!\!\!/ \psi = m_M \psi_c + m_D \psi, \quad (6.62)$$

which still requires only two ions for a 1+1 quantum simulation. It also becomes feasible to have CP violating phases in the Dirac mass term, $m_D \exp(i\theta\gamma^5)$.

Furthermore, we could study the dynamics of coupled Majorana neutrinos with a term $\bar{M}\psi_c$, where \bar{M} is now a matrix and $\psi = \psi(x_1, x_2)$ is the combination of two such particles, simulated with three ions and two vibrational modes.

So far, we have presented a complete toolbox of unphysical operations, \mathcal{C} , \mathcal{T} , and \mathcal{K} , that are available in the proposed quantum simulator. We can combine all these tools to study dynamical properties of the transformed wavefunctions. To exemplify the kind of experiments that become available, we have studied the scattering of wavepackets against a linearly growing potential,

$$V(x) = \alpha x. \tag{6.63}$$

It is known that repulsive potentials are partially penetrated by Dirac particles [20], an effect called the Klein paradox [137, 138, 139]. This is shown in Fig. 6.3a, where a Dirac particle splits into a fraction of a particle, that bounces back, and a large antiparticle component that penetrates the barrier. This numerical experiment has been combined with the discrete symmetries and the Majorana equation. In Fig. 6.3b we show a Dirac wavepacket that suffers the time reversal operation some time after entering the barrier: all momenta are reversed and the wavepacket is refocused, tracing back exactly its original trajectory. In Fig. 6.3c we repeat the same procedure but using charge conjugation. This operation changes the sign of the charge turning a repulsive electric potential into an attractive one, which can be easily penetrated by the antiparticle. In our last example, Fig. 6.3d, we show the scattering of a Majorana particle. While the evolution is not so smooth—there are no plane wave solutions in the Majorana equation—, we can still identify a wavepacket penetrating the barrier, showing a counter-intuitive insensitivity to the presence of the barrier, that will be explained in the next section 6.3.

6.2.4 Conclusions

In summary, we have introduced a general method to implement the quantum simulation of unphysical operations and the non-Hamiltonian Majorana equation in a Hamiltonian system. To this end, we have designed a suitable mapping that enlarges the simulation space by means of an ancillary system to allow for complex conjugation, charge conjugation, and time reversal. We have exemplified the implementation of the 1+1 dimensional case in the context of trapped-ion physics. The flexibility of this protocol allows to explore a novel front of quantum simulations, that of unphysical operations and exotic quantum relativistic processes that go beyond ordinary Schrödinger and Dirac quantum mechanics.

6.3 Quantum simulation of relativistic potentials without potentials

6.3.1 Introduction

Last years had witnessed an increasing interest in simulating dynamics coming from the Relativistic Quantum Mechanics realm with physical systems of Quantum Optics, such as trapped ions. Striking theoretical predictions like *Zitterbewegung* and Klein paradox [137] has been observed in these simulations. In particular, the proposal of simulation with one trapped ion [135] of the single particle free 1-D Dirac equation has been successfully implemented in the lab [22]. This is also the case for the single particle 1-D Dirac equation with some external potential [138] whose simulation involves two ions [139]. In the last section we have proposed that the free Majorana equation and unphysical operations like complex conjugation, charge conjugation and time reversal can also be simulated with two trapped ions. Besides, two-body Dirac equations have been the subject of recent research [140].

In this section we will show that the same setups built up for the simulations of the free single particle Dirac and Majorana equations can also be used for simulations of these equations with the addition of some external potential, for a large class of potentials. This is based in the following idea, which is the main result of this paper: some states which are solutions of the Dirac or Majorana equation with the potential can be related through a phase transformation with a solution of the free corresponding equation. So, if we want to simulate the dynamics of a given state under certain potential the transformation tells us which is the state whose dynamics under the free equation does the job. In other words, the potential is codified in the phase involved in the transformation. The trick does not work for any potential, but only for potentials belonging to a certain class. In some cases, it works for potentials in the Majorana equation but not for the same potentials in the Dirac equation, which can be used to analyze the different character of Majorana and Dirac dynamics. In general, the transformation does not leave the probability density unchanged but this happens in some particular cases, showing us an additional amazing feature: under certain potentials the particle behaves as a free particle. We extend our results also to two-body equations.

Although our method works in principle in any dimension and any representation, we will focus in this work in the 1-D case and the particular representations commonly employed in the experiments.

6.3.2 One particle systems

Let us come to explain our results with more detail. We will consider the following 1-D Dirac equation in natural units:

$$i\dot{\psi} = -i\sigma_x\psi' + (\sigma_z m + V(x))\psi \quad (6.64)$$

where $\dot{}$, $'$ denote time and space partial derivatives respectively. In the same representation, Majorana equation looks like:

$$i\dot{\psi} = -i\sigma_x \psi' - i\sigma_y m\psi^* + V(x)\psi \quad (6.65)$$

In 1-D a general potential can be written down as [138]:

$$V = f_1(x) + f_2(x)\sigma_z + f_3(x)\sigma_y + f_4(x)\sigma_x \quad (6.66)$$

We start from the Eq.(6.65) with the potential in Eq.(6.66). We will analyze under what conditions a transformation of the form

$$\psi = \prod_j e^{-i\Theta_j(x)} \phi \quad (6.67)$$

where

$$\prod_j e^{-i\Theta_j(x)} = e^{-iF_1(x)\sigma_x} e^{-iF_2(x)\sigma_y} e^{-iF_3(x)\sigma_z} e^{-iF_4(x)} \quad (6.68)$$

can convert Eq. (6.65) in the corresponding free Majorana equation for ϕ . (Please recall that $e^A e^B \neq e^{A+B}$ unless $[A, B] = 0$, which in general is not the case here.) To this end we first notice that after applying Eq.(6.67) the LHS of Eq.(6.65) becomes:

$$\prod_j e^{-i\Theta_j(x)} i\dot{\phi} \quad (6.69)$$

while due to the anticommutation properties of the Pauli matrices the first term of the RHS transforms as:

$$\prod_j e^{-i\Delta_j(x)} (-i\sigma_x \phi)' + \left(\prod_j e^{-i\Delta_j(x)}\right)' (-i\sigma_x \phi) \quad (6.70)$$

with

$$\prod_j e^{-i\Delta_j(x)} = e^{-iF_1(x)\sigma_x} e^{iF_2(x)\sigma_y} e^{iF_3(x)\sigma_z} e^{-iF_4(x)}. \quad (6.71)$$

If we choose the F' s such that:

$$\begin{aligned} F'_1(x) &= f_1(x), F'_2(x) = -i f_2(x), \\ F'_3(x) &= i f_3(x), F'_4(x) = f_4(x). \end{aligned} \quad (6.72)$$

the second term of Eq.(6.70) cancels out the one coming from the third term of Eq.(6.65), that is, the potential is removed. Finally, if F_1 is real and F_2, F_3, F_4 imaginary, we have:

$$\sigma_y \left(\prod_j e^{-i\Theta_j(x)}\right)^* = \left(\prod_j e^{-i\Delta_j(x)}\right) \sigma_y. \quad (6.73)$$

Putting all together, we have that applying Eq.(6.67) in Eq.(6.65) we obtain the following equation for ϕ , provided that F_1 is real and the other F 's imaginary, and that they are related with the f 's in the potential through Eq.(6.72):

$$\prod_j e^{-i\Theta_j(x)} i\dot{\phi} = \prod_j e^{-i\Delta_j(x)} (i\sigma_x \phi' - i\sigma_y m\phi^*). \quad (6.74)$$

Then, if $F_2(x) = F_3(x) = 0$, ϕ verifies a free Majorana equation. That is, if we want to simulate the dynamics of a particle in the state $\psi(x, t)$ under the 1-D Majorana equation with a potential of the form $V(x) = f_1(x) + f_4(x)\sigma_x$, we only have to study the state $\phi(x, t)$ which is related to it through $\psi(x, t) = e^{-i F_1(x)\sigma_x} e^{-i F_4(x)\sigma_x} \phi(x, t)$. Since, F_1 is real and F_4 imaginary, we have the following relationship between the probability densities:

$$|\psi(x, t)|^2 = e^{-2i F_4(x)} |\phi(x, t)|^2. \quad (6.75)$$

So the probability density observed for ϕ can be easily related with the simulated probability density for ψ . Also, analogous relations can be derived, for instance for expectation values of observables. Of particular interest is the case in which $F_4(x) = 0$ (then $f_4(x) = 0$) and the probability density is the same for ψ and ϕ . Therefore, the probability density of a state under the potential is always the same as the one of a free state. We shall illustrate this with an example below. The method does not work in general for $F_2(x) \neq 0$, $F_3(x) \neq 0$ unless approximatively in the regions of space in which $F_2(x) \simeq 0$, $F_3(x) \simeq 0$, which does not necessarily entails $f_2(x) \simeq 0$, $f_3(x) \simeq 0$.

We now analyze the case of the 1-D Dirac equation Eq.(6.64). Using the same techniques as in the Majorana case, if we consider a potential with $f_1(x) = f_3(x) = 0$:

$$V(x) = f_2(x) \sigma_z + f_4(x) \sigma_x, \quad (6.76)$$

the transformation

$$\psi = e^{-i F_2(x)\sigma_y} e^{-i F_4(x)\sigma_x} \phi \quad (6.77)$$

transforms Eq.(6.64) into:

$$e^{-i F_2(x)\sigma_y} e^{-i F_4(x)\sigma_x} i \dot{\phi} = e^{i F_2(x)\sigma_y} e^{-i F_4(x)\sigma_x} (-i\sigma_x \phi' + \sigma_z m\phi), \quad (6.78)$$

and similar conclusions as in the Majorana case are reached for this class of potentials. But the absence of the complex conjugation in the mass term, prevents the possibility of extract a phase in the RHS if we include F_1 or F_3 , so potentials with f_1 and/or f_3 cannot be simulated, not even approximatively, with free Dirac Hamiltonians.

6.3.3 Examples

Now we will illustrate all the above with some examples. First, we will consider the 1-D Dirac and Majorana equations with a linear potential

$$V(x) = g x, \quad (6.79)$$

and the transformation:

$$\psi(x, t) = e^{\frac{-i g x^2}{2} \sigma_x} \phi(x, t). \quad (6.80)$$

In that case ϕ satisfies the free Majorana equation and $|\psi|^2 = |\phi|^2$, so any

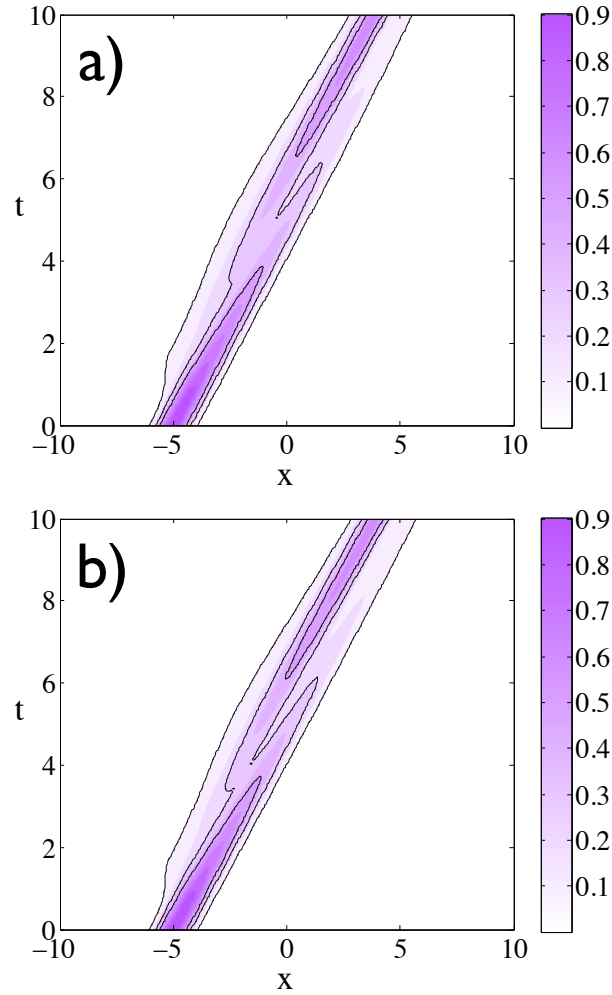


Figure 6.4: a) Evolution of a fermionic wavepacket under Eq.(6.65) with the potential of Eq.(6.79). b) Evolution of the corresponding state with the transformation in Eq.(6.80) under a free Majorana equation. In both cases: $m = 0.5$ and $g = 1$.

solution of the Majorana equation with potential has the same probability density of a solution of the free Majorana equation. The same transformation does not work in the Dirac case, shedding light to the different behavior of Majorana and Dirac particles against such potentials, as can be seen in Fig. 6.4. Notice that the Majorana equation does not have stationary solutions and that an initial global phase is not conserved as a global phase during the evolution, as commented in section 6.1. Thus Eq.(6.80) cannot be written in terms of the

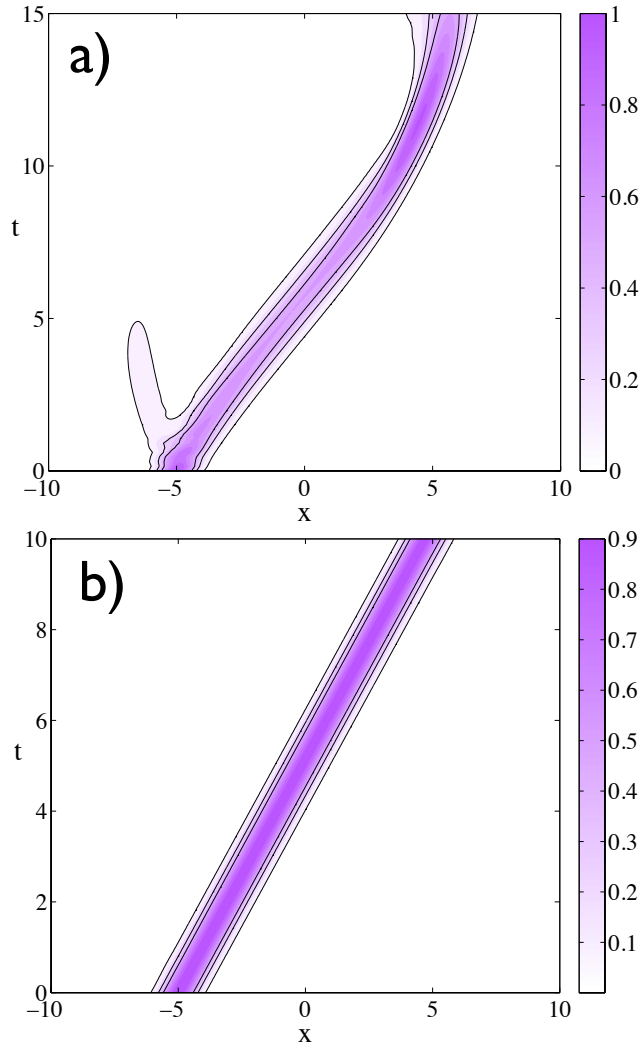


Figure 6.5: a) Evolution of a fermionic wavepacket under Eq.(6.64) with the potential of Eq.(6.81). b) Evolution of the corresponding state with the transformation in Eq.(6.80) under a free Dirac equation. In both cases: $m = 0.5$ and $g = -1$.

evolution of some $\psi(0)$ and $\phi(0)$. In other words, a solution ϕ of the equation with potential is always equivalent to some solution ψ of the free equation, but in general this ψ is a different state at each instant of time, not the evolution of one state $\psi(0)$. In Fig.6.5 we show that our method works as a good approximation in a certain region of space in the case of the Dirac equation with a

potential:

$$V(x) = g x \sigma_z, \quad (6.81)$$

and the corresponding transformation:

$$\psi(x, t) = e^{-\frac{g x^2 \sigma_y}{2}} \phi(x, t). \quad (6.82)$$

6.3.4 Bipartite systems

All the above can be extended to two-particle systems. For instance, it has been shown that a Lorentz-invariant two-body Dirac equation with an oscillator-like mutual interaction can be written in the center of mass reference frame [141]. In 1-D and the particular representation we are using, we have:

$$i\dot{\psi} = -\frac{i}{\sqrt{2}}(\alpha_1 - \alpha_2)(\psi' + m\omega x\beta_{12}\psi) + (\beta_1 + \beta_2)m\psi \quad (6.83)$$

with $\alpha_1 = \sigma_x \otimes \mathbf{1}$, $\alpha_2 = \mathbf{1} \otimes \sigma_x$, $\beta_1 = \sigma_z \otimes \mathbf{1}$, $\beta_2 \mathbf{1} \otimes \sigma_z$, $\beta_{12} = \sigma_y \otimes \sigma_y$, $x = (x_1 - x_2)/\sqrt{2}$. Thus the corresponding two-body Majorana oscillator equation is :

$$i\dot{\psi} = -\frac{i}{\sqrt{2}}(\alpha_1 - \alpha_2)(\psi' + m\omega x\beta_{12}\psi) - i(\hat{\beta}_1 + \hat{\beta}_2)m\psi^* \quad (6.84)$$

with $\hat{\beta}_1 = \sigma_y \otimes \mathbf{1}$ and $\hat{\beta}_2 = \mathbf{1} \otimes \sigma_y$. With the techniques explained above, we find that the transformation

$$\psi(x, t) = e^{-\frac{m\omega x^2 \beta_{12}}{2}} \phi(x, t). \quad (6.85)$$

transforms Eq.(6.84) into a quasi-free two-body Majorana equation:

$$e^{-\frac{m\omega x^2 \beta_{12}}{2}} i\dot{\phi} = e^{\frac{m\omega x^2 \beta_{12}}{2}} \left(-\frac{i}{\sqrt{2}}(\alpha_1 - \alpha_2)\phi' + (\hat{\beta}_1 + \hat{\beta}_2)m\phi^* \right) \quad (6.86)$$

Thus, in that case the situation would be similar to the one-particle example of Fig.6.5: Eq.(6.84) can be simulated with good approximation with a two-body free Majorana equation in a large region of space. Interestingly, the trick does not work for the two-body Dirac oscillator.

6.3.5 Conclusions

We have shown that Majorana and Dirac potentials can be simulated with free Hamiltonians, since there is a mapping between free states and states under the action of the potential. The method works better in the Majorana case, in which there are potentials that cannot be simulated with a free Dirac Hamiltonian, as has been illustrated with a particular case. This example also exhibits the peculiarity of conservation of probability density between free and non-free states, illuminating the issue of the different behavior of Majorana and Dirac particles against such a potential. In other cases the method works only as a good approximation in certain regions of space. We have extended our results to two-particle interacting systems.

Appendix A

In this appendix, we will give details on the computations of the quantities of interest in Chapter 3. We first start with A and X in (3.9). Both are a sum of second order transition amplitudes, which can be written as:

$$\left(\frac{-i}{\hbar}\right)^2 \sum_k \langle f | H_I | k \rangle \langle k | H_I | i \rangle \int_0^t dt_1 \int_0^{t_1} dt_2 e^{i(E_f - E_k)t_2/\hbar} e^{i(E_k - E_i)t_1/\hbar} \quad (\text{A.1})$$

being E_f , E_k and E_i the energies of the final $|f\rangle$, intermediate $|k\rangle$ and initial $|i\rangle$ states of the system, respectively. The sum over k is a sum over all the possible intermediate states of the system which in the case of fixed two-level atoms reduces to a sum over all the momenta and polarizations of the emitted photon. The time integrations in (A.1) are just

$$-\hbar^2 \left(\frac{e^{i(E_f - E_i)t/\hbar} - 1}{(E_f - E_k)(E_f - E_i)} - \frac{e^{i(E_k - E_i)t/\hbar} - 1}{(E_f - E_k)(E_k - E_i)} \right) \quad (\text{A.2})$$

The second term in (A.2) is usually neglected, but give rise to a very different short time behavior [53] ($\propto t^4$, not $\propto t^2$). Therefore, it is of interest for our purposes.

In order to obtain X we have to sum over the amplitudes for single photon emission at atom A (B) followed by absorption at atom B (A). The case where a photon is emitted and absorbed by the same atom corresponds to A , that we will consider below. Using the mode expansion for the electric field:

$$\mathbf{E}(\mathbf{x}) = i \sqrt{\frac{\hbar c}{2\varepsilon_0 (2\pi)^3}} \sum_{\lambda} \int d^3k \sqrt{k} (e^{i\mathbf{k}\cdot\mathbf{x}} \boldsymbol{\epsilon}(\mathbf{k}, \lambda) a_{k\lambda} - e^{-i\mathbf{k}\cdot\mathbf{x}} \boldsymbol{\epsilon}^*(\mathbf{k}, \lambda) a_{k\lambda}^\dagger), \quad (\text{A.3})$$

(with $[a_{k\lambda}, a_{k'\lambda'}^\dagger] = \delta^3(\mathbf{k} - \mathbf{k}') \delta_{\lambda\lambda'}$) taking into account (A.1) and (A.2), recalling that

$$\sum_{\lambda} \boldsymbol{\epsilon}_i^*(\mathbf{k}, \lambda) \boldsymbol{\epsilon}_j(\mathbf{k}, \lambda) = \delta_{ij} - \hat{k}_i \hat{k}_j, \quad (\text{A.4})$$

and using the tabulated integrals that we list at the end of the appendix, a somewhat tedious although straightforward computation leads to:

$$X = \frac{\alpha d^i d^j}{\pi e^2} (-\nabla^2 \delta_{ij} + \nabla_i \nabla_j) I \quad (\text{A.5})$$

α being the fine structure constant and

$$I = I_+ + I_-, \quad (\text{A.6})$$

which, in terms of the dimensionless parameters $z = \Omega r/c$ and $x = r/ct$ are

$$I_{\pm} = \frac{1 \pm \frac{1}{x}}{2} \{e^{iz}[Ei(-iz) - Ei(-iz(1 \pm 1/x))] + e^{-iz}[Ei(iz) - Ei(iz(1 \pm 1/x))]\} \quad (\text{A.7})$$

for $x > 1$, I having the extra term $i\pi(1 - 1/x)e^{-iz}$ for $x < 1$. We use the conventions of [54]. As noted in [53], the non-zero contributions for $x > 1$ come from the second term of (A.2). We display here the results of the derivatives in (A.5) only for the particular case where the dipoles are parallel along the z axis ($\mathbf{d}_A = \mathbf{d}_B = \mathbf{d} = d\mathbf{u}_z$) and the atoms are along the x axis, corresponding to the physical situation considered previously in, for instance, [10] and in this paper. Actually, $|E\rangle$ is a triply degenerate state $|E, m\rangle$ with $m = 0, \pm 1$ and our scheme holds for a transition with $\Delta m = 0$ [80]. Another independent possibility would be to consider transitions with $\Delta m = \pm 1$ that corresponds to $\mathbf{d} = d(\mathbf{u}_x \pm i\mathbf{u}_y)/\sqrt{2}$ [80]. We find that:

$$\begin{aligned} X = & -\frac{\alpha|\mathbf{d}|^2}{2\pi x r^2 e^2} \left\{ 4x \left(-1 + \frac{(-2+x^2)\cos\frac{z}{x}}{-1+x^2} \right) + e^{iz} [-2x z^2 Ei(-iz) \right. \\ & + (2+z(-2i+(-1+x)z)) Ei\left(-\frac{i(-1+x)z}{x}\right) \\ & + (-2+z(2i+z+xz)) Ei\left(-\frac{i(1+x)z}{x}\right) \\ & + 2e^{-iz} \left(Ei\left(\frac{i(-1+x)z}{x}\right) - Ei\left(\frac{i(1+x)z}{x}\right) \right) + \\ & z e^{-iz} [-2x z Ei(iz) + (2i+(-1+x)z) \\ & \left. Ei\left(\frac{i(-1+x)z}{x}\right) + (-2i+z+xz) Ei\left(\frac{i(1+x)z}{x}\right) \right] \} \quad (\text{A.8}) \end{aligned}$$

for $x > 1$, with the additional term $i\alpha e^{-iz} d^2 (2+z(2i+(-1+x)z))/(r^2 x)$ for $x < 1$.

Now we come to A , which is the sum of the radiative corrections of atoms A and B . As can be seen in the main text, A appears in our results only as a higher order correction to X . Therefore, instead of finding an exact expression for it, we are mainly concerned with removing the divergencies. We followed the standard treatment (see, for instance, [79]) which is valid for the times $\Omega t > 1$ we are considering. From (A.1), it is possible to arrive at:

$$\frac{-2i\alpha|d|^2 t}{3\pi e^2 c^2} \lim_{\epsilon \rightarrow 0^+} \int_0^\infty d\omega \omega^3 \left(\frac{1}{\Omega - \omega + i\epsilon} - \frac{1}{\Omega + \omega - i\epsilon} \right). \quad (\text{A.9})$$

Now, using in (A.9) the identities

$$\frac{\omega^3}{\Omega \pm \omega} = \pm(\omega^2 - \mp \Omega \omega + \Omega^2 - \frac{\Omega^3}{\Omega \pm \omega}), \quad (\text{A.10})$$

the first term of (A.10) cancels out the contribution of the Hamiltonian self-interaction terms Eq. (2.15), the second is the state-independent contribution

that can be absorbed in the definition of the zero of energy [79], the third cancels the counterterm coming from the mass renormalization [79] and finally the last term has logarithmic divergences and a cut-off, related with the fact that we are in the electric dipole representation could be imposed at $t_{min} = \frac{a_0}{c} = 1.76 \cdot 10^{-19} s$. Please notice that the times relevant in our computations are of the order of $t \cong \frac{10}{\Omega} \approx 4 \cdot 10^{-15} s$. Therefore:

$$A = \frac{2i\alpha|\mathbf{d}|^2 z^3}{3\pi L^2 e^2 x} \ln\left(\left|\frac{1 - \frac{z_{max}}{z}}{1 + \frac{z_{max}}{z}}\right|\right), \quad (\text{A.11})$$

with $z_{max}/z = c/(\Omega a_0)$.

Another quantity of interest is what we called l in the main text and it is given by (3.24) and (3.25). Performing the integration in (3.25), we obtained $M(z, x) = M_+(z, x) + M_-(z, x)$, where:

$$\begin{aligned} M_{\pm}(z, x) &= \frac{e^{i\frac{z}{x}}}{4\pi^2 z} \left\{ \sin\left(z\left(1 \pm \frac{1}{x}\right)\right) [ci(z) - ci\left(z\left(1 \pm \frac{1}{x}\right)\right)] - \right. \\ &\quad \left. \cos\left(z\left(1 \pm \frac{1}{x}\right)\right) [si(z) - si\left(z\left(1 \pm \frac{1}{x}\right)\right)] \right\} \end{aligned} \quad (\text{A.12})$$

The derivatives in (3.24) were performed in the same particular situation as in X .

$|U|^2 = \langle 0 | \mathcal{S}_A^+ \mathcal{S}_A^- | 0 \rangle$, and $|V|^2 = \langle 0 | \mathcal{S}_B^- \mathcal{S}_B^+ | 0 \rangle$, are just the two terms that contribute to A without the time ordering and therefore their divergencies are removed by the application of (A.9). Taking this into account, we obtain:

$$\begin{aligned} |U|^2 &= \frac{2\alpha|d|^2 z^2}{3\pi e^2 L^2} \left(-2 + \pi \frac{z}{x} + 2 \cos\left(\frac{z}{x}\right) + 2\left(\frac{z}{x}\right) si\left(\frac{z}{x}\right)\right) \\ |V|^2 &= \frac{2\alpha|d|^2 z^2}{3\pi e^2 L^2} \left(2 + \pi \frac{z}{x} - 2 \cos\left(\frac{z}{x}\right) - 2\left(\frac{z}{x}\right) si\left(\frac{z}{x}\right)\right) \end{aligned} \quad (\text{A.13})$$

F and G can be written in terms of previously computed quantities, taking into account that:

$$\begin{aligned} F &= \theta(t_1 - t_2) (u_A(t_1)v'_A(t_2) + v'_A(t_1)u_A(t_2) \\ &\quad + u_B(t_1)v'_B(t_2) + u'_B(t_1)v_B(t_2)) \\ G &= u_A v'_B + u'_A v_B, \end{aligned} \quad (\text{A.14})$$

being $V_A = \langle 1 | \mathcal{S}_A^+ | 0 \rangle$, and $U_B = \langle 1 | \mathcal{S}_B^- | 0 \rangle$. The primes are introduced to label two different single photons. Therefore, in the computation of $|F|^2$, $|G|^2$ and $F G^*$ we will only need, besides $|U|^2$, $|V|^2$ and l , the following:

$$\begin{aligned} V_A U_A^* &= V_B U_B^* = \frac{2\alpha|d|^2 z^2}{3\pi L^2} e^{i\frac{z}{x}} \sin \frac{z}{x} \\ V_A V_B^* &= \frac{\alpha d^i d^j}{\pi} (-\nabla^2 \delta_{ij} + \nabla_i \nabla_j) I' \end{aligned} \quad (\text{A.15})$$

being $I' = I'_+ + I'_-$, with:

$$\begin{aligned}
I'_\pm &= \frac{1 \pm \frac{1}{x}}{2} \{e^{iz} Ei(-iz(1 \pm \frac{1}{x})) + e^{-iz} Ei(iz(1 \pm \frac{1}{x}))\} \\
&- e^{\mp iz} Ei(\pm iz) \}
\end{aligned} \tag{A.16}$$

and $U_A U_B^* = V_A V_B^*$ when $x > 1$, with the additional term $-2\pi \sin z (1 - 1/x)$ when $x < 1$. Again the derivatives were performed as in X and l .

The following integrals are useful to obtain the results of this appendix [54]:

$$\begin{aligned}
\int_0^\infty d\omega \frac{e^{\pm i\omega\gamma}}{\omega + \beta} &= -e^{\mp i\gamma\beta} Ei(\pm i\gamma\beta) \\
\int_0^\infty d\omega \frac{e^{\pm i\omega\gamma}}{\omega - \beta} &= -e^{\pm i\gamma\beta} (Ei(\mp i\gamma\beta) \mp i\pi),
\end{aligned} \tag{A.17}$$

with $a > 0$, $arg \beta \leq \pi$.

Appendix B

In this appendix we will give further details on the computations of the relevant magnitudes $|X|$, $|U_A|^2$, $|V_B|^2$ which are necessary to compute the concurrence Eq.(3.33) in section 4.2. With Eqs. (4.26)- (4.29) and Eq. (4.17):

$$X = \frac{d^2 N v}{\hbar^2} \int_{-\infty}^{\infty} dk |k| (e^{ikr} I_{t_1} + e^{-ikr} I_{t_2}) \quad (\text{B.1})$$

with

$$I_{t_{1,2}} = \int_0^t dt_{2,1} \int_0^{t_{2,1}} dt_{1,2} e^{i\Omega(t_2-t_1)} e^{-iv|k|(t_{2,1}-t_{1,2})}. \quad (\text{B.2})$$

Notice that the term with I_{t_2} gives the non-RWA probability amplitude associated to a single photon emission of qubit B followed by an absorption of qubit A. Performing the time integrations, inserting them in Eq. (B.1) and after some algebra, X can be given as a combination of integrals of the form:

$$\begin{aligned} \int_0^{\infty} dk \frac{\cos(k\gamma)}{k+\beta} &= -\sin(\gamma\beta)si(\gamma\beta) - \cos(\gamma\beta)ci(\gamma\beta) \\ \int_0^{\infty} dk \frac{\cos(k\gamma)}{k-\beta} &= -\sin(\gamma\beta)si(\gamma\beta) - \cos(\gamma\beta)ci(\gamma\beta) \\ &\quad - \pi \sin(\gamma\beta) \\ \int_0^{\infty} dk \frac{\sin(k\gamma)}{k+\beta} &= \sin(\gamma\beta)Ci(\gamma\beta) - \cos(\gamma\beta)si(\gamma\beta) \\ \int_0^{\infty} dk \frac{\sin(k\gamma)}{k-\beta} &= -\sin(\gamma\beta)Ci(\gamma\beta) + \cos(\gamma\beta)si(\gamma\beta) \\ &\quad + \pi \cos(\gamma\beta) \end{aligned} \quad (\text{B.3})$$

with $\gamma, \beta > 0$ and the conventions in [54] for the si and Ci . Putting all together we find:

$$\begin{aligned}
X = & \frac{K}{2}(i\pi\rho\xi\sin(\rho) - e^{\frac{i\rho\xi}{2}}((1+i\tau_-)(C(\tau_-) - S(\tau_-) \\
& -\pi\sin(\tau_-)\Theta(1-\xi)) + (1-i\tau_+)(-C(\tau_+) - S(\tau_+) \\
& -\pi\sin(\tau_+)) + (-\tau_- + i)(-SC(\tau_-) + CS(\tau_-) + \pi \\
& \cos(\tau_-)) + (-\tau_+ - i)(-SC(\tau_+) + CS(\tau_+) + \pi\cos(\tau_+)) \\
& -2) - e^{\frac{-i\rho\xi}{2}}((1-i\tau_-)(-C(\tau_-) - S(\tau_-) - \pi\sin(\tau_-) \\
& \Theta(\xi-1)) + (1+i\tau_+)(-C(\tau_+) - S(\tau_+) + (\tau_- + i) \\
& (SC(\tau_-) - CS(\tau_-)) + (\tau_- - i)(SC(\tau_+) - CS(\tau_+) + \pi \\
& \cos(\tau_+)) - 2) - 2 - 2C(\rho) - 2S(\rho) - \rho(-2SC(\rho) \\
& + 2CS(\rho))
\end{aligned} \tag{B.4}$$

where ξ has been defined in Eq. (4.32),

$$\rho = \Omega r/v \tag{B.5}$$

is a dimensionless distance,

$$\begin{aligned}
\tau_- &= \rho(1-\xi) = \rho - \Omega t, \\
\tau_+ &= \rho(1+\xi) = \rho + \Omega t,
\end{aligned} \tag{B.6}$$

and we define

$$\begin{aligned}
C(x) &= \cos(x) Ci(x), S(x) = \sin(x) si(x), \\
CS(x) &= \cos(x) si(x), SC(x) = \sin(x) Ci(x).
\end{aligned} \tag{B.7}$$

Notice the dependence with the spacetime region through the factors with the Heaviside function Θ .

Now we come to the emission probabilities $|U_A|^2, |V_B|^2$, which are given by

$$|U_A|^2 = \langle 0 | \mathcal{S}_A^+ \mathcal{S}_A^- | 0 \rangle, |V_B|^2 = \langle 0 | \mathcal{S}_B^- \mathcal{S}_B^+ | 0 \rangle \tag{B.8}$$

Following similar techniques we find that

$$|U_A|^2 = f_+(\Omega t), |V_B|^2 = f_-(\Omega t), \tag{B.9}$$

where:

$$f_{\pm} = \frac{K}{2}(\pi\Omega t \pm 2(\cos(\Omega t) + \Omega t Si(\Omega t) - 1)) \tag{B.10}$$

where Si must not be mistaken by si , $Si = si + \pi/2$ as usual.

Finally, notice that A (Eq.(4.31)) is a sum of two terms like $|U_A|^2$ and $|V_B|^2$ with the time ordering operator T and that $U_A * V_B$ (Eq.(4.36)) is similar to X without T . The treatment of the divergencies has followed the lines sketched in Appendix A.

Appendix C

In this appendix the task is to compute the term $\delta\mathcal{M}^{(3)}$ introduced in section 5.1. This term is included in the whole third order amplitude

$$\begin{aligned} \mathcal{M}^{(3)} &= \left(\frac{1}{i\hbar}\right)^3 \sum_{\alpha\beta} \langle f|V|\alpha\rangle \langle \alpha|V|\beta\rangle \langle \beta|V|i\rangle \times \\ &\times \int_0^t dt_1 e^{iw_{f\alpha}t_1} \int_0^{t_1} dt_2 e^{iw_{\alpha\beta}t_2} \int_0^{t_2} dt_3 e^{iw_{\beta i}t_3} \end{aligned} \quad (\text{C.1})$$

where α, β stand for arbitrary sets of quantum numbers and the sum includes integrals over momenta and polarization sums. We start computing the time integrals:

$$\begin{aligned} &\int_0^t dt_1 e^{iw_{f\alpha}t_1} \int_0^{t_1} dt_2 e^{iw_{\alpha\beta}t_2} \int_0^{t_2} dt_3 e^{iw_{\beta i}t_3} = \\ &\frac{1}{(iw_{\beta i})(iw_{\alpha i})} \left[\frac{e^{iw_{f i}t} - 1}{iw_{f i}} - \frac{e^{iw_{f\alpha}t} - 1}{iw_{f\alpha}} \right] - \\ &\frac{1}{(iw_{\beta i})(iw_{\alpha\beta})} \left[\frac{e^{iw_{f\beta}t} - 1}{iw_{f\beta}} - \frac{e^{iw_{f\alpha}t} - 1}{iw_{f\alpha}} \right] \end{aligned} \quad (\text{C.2})$$

The last two lines in Eq.(C.2) contains all the time dependence along with that in the final and exchanged photon frequencies. Among all the terms that can interfere with V_B , we select only those that depend on the interatomic distance r whose contribution $\delta\mathcal{M}^{(3)}$ we will now compute. We first consider the three cases where the exchange ‘‘goes from A to B’’, where we display the frequencies that enter in Eq.(C.1) and Eq.(C.2) in terms of

$$\begin{aligned} \Sigma_f &= w_f + \Omega, \Delta_f = w_f - \Omega, \\ \Sigma &= w + \Omega \text{ and } \Delta = w - \Omega, \end{aligned} \quad (\text{C.3})$$

where w_f, w are the final and exchanged photon frequencies, and $\Omega = (E_e - E_g)/\hbar$ is two level frequency gap. The primed objects that will appear in the equations are associated to the energy E'_g of the intermediate atomic ground states; we will take $E'_g - E_g \rightarrow 0$ at the end of the calculations.

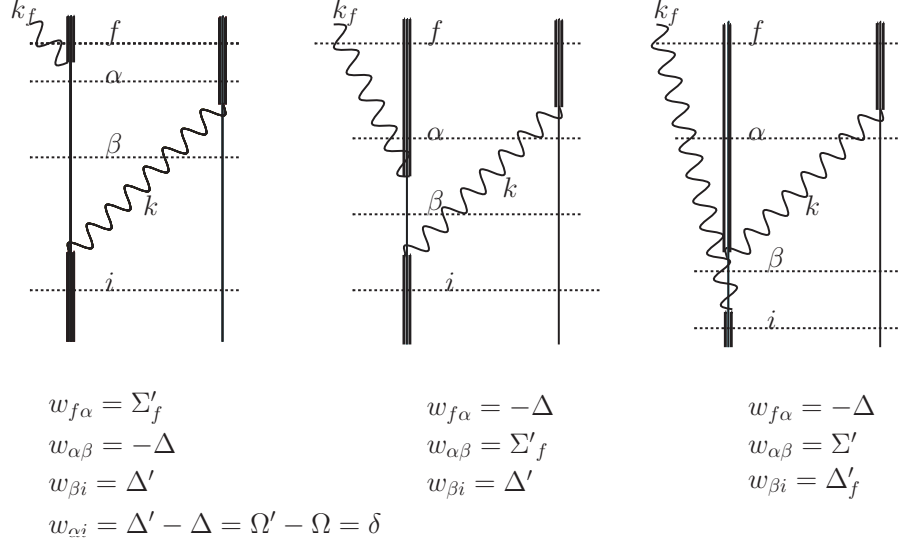


Figure C.1: The three diagrams contributing to $\delta\mathcal{M}^{(3)}$ in which qubit A emits

The contribution to $\mathcal{M}^{(3)}$ coming from Fig.2 can be written as

$$\begin{aligned}
& -\frac{1}{\hbar^3} V_{eg}^\dagger(\mathbf{x}_A) \underline{V_{eg}(\mathbf{x}_B)} V_{g'e}^\dagger(\mathbf{x}_A) \left\{ \frac{1}{\Delta'(\Sigma_f - \Sigma'_f)} (\mathcal{S}(\Sigma_f, t) \right. \\
& - \mathcal{S}(\Sigma'_f, t)) + \frac{1}{\Delta' \Delta} (\mathcal{S}(\Sigma'_f - \Delta, t) - \mathcal{S}(\Sigma'_f, t)) \left. \right\} - \\
& \frac{1}{\hbar^3} \underline{V_{eg}(\mathbf{x}_B)} V_{eg}^\dagger(\mathbf{x}_A) V_{g'e}^\dagger(\mathbf{x}_A) \left\{ \frac{1}{\Delta'(\Sigma_f + \Delta)} (\mathcal{S}(\Sigma_f, t) - \right. \\
& \mathcal{S}(-\Delta, t)) - \frac{1}{\Delta' \Sigma'_f} (\mathcal{S}(\Sigma'_f - \Delta, t) - \mathcal{S}(-\Delta, t)) \left. \right\} - \\
& \frac{1}{\hbar^3} \underline{V_{eg}(\mathbf{x}_B)} V_{fg}^\dagger(\mathbf{x}_A) V_{g'e}^\dagger(\mathbf{x}_A) \left\{ \frac{1}{\Delta'_f(\Sigma_f + \Delta)} (\mathcal{S}(\Sigma_f, t) - \right. \\
& \mathcal{S}(-\Delta, t)) - \frac{1}{\Delta'_f \Sigma'_f} (\mathcal{S}(\Sigma'_f - \Delta, t) - \mathcal{S}(-\Delta, t)) \left. \right\} \quad (C.4)
\end{aligned}$$

In the above formula $\underline{P(x) \cdots Q(y)}$ stands for the contraction of the operators P and Q , namely

$$\underline{V_{fi}(\mathbf{x}) \cdots V_{f'i'}^\dagger(\mathbf{y})} = \int dk N d_{fi} \cdots d_{f'i'} e^{ik(x-y)} \quad (C.5)$$

and the function \mathcal{S} is defined as

$$\mathcal{S}(z, t) = \frac{e^{izt} - 1}{z} \quad (C.6)$$

Finally, we recall some issues about the contractions. First, the frequency that appears in Eq.(C.5) and in the definitions for Δ and Σ is $w = vk$. Second, we can pull out the lone operator V^\dagger from the contractions. Third, we will consider real dipole moments, so that $V_{eg} = V_{ge}$, etc. This allows to factorize from equation (C.4) a common factor $-(1/\hbar^3)V^\dagger(x_A)\underline{V(x_B)}V^\dagger(x_A)I_A^B(w, t)$, where $I_A^B(w, t)$ contains all the terms within braces.

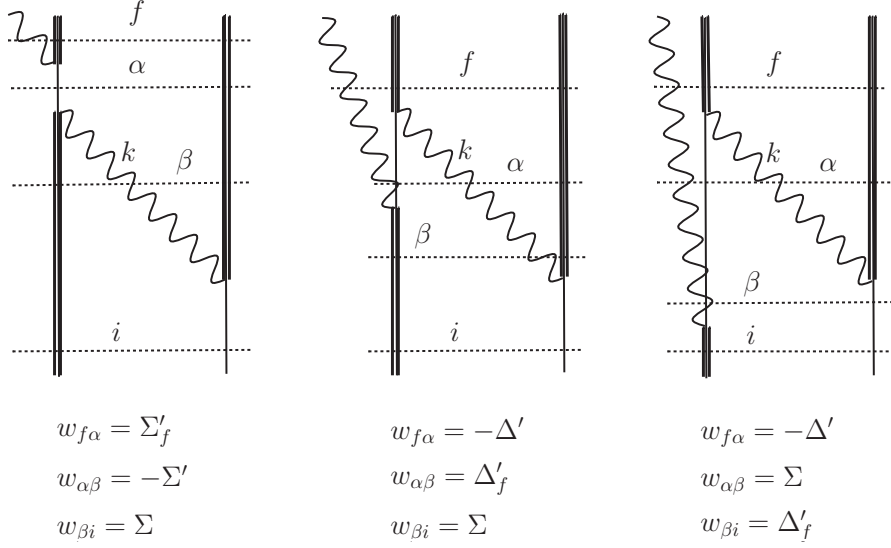


Figure C.2: The three diagrams contributing to $\delta\mathcal{M}^{(3)}$ in which qubit A absorbs

The cases where the exchange “goes from B to A” are depicted in Fig.3 below. From arguments similar to those of the previous case, we can factorize out the V terms obtaining $-(1/\hbar^3)V^\dagger(x_A)\underline{V(x_A)}V^\dagger(x_B)I_B^A(w, t)$, where

$$\begin{aligned}
I_B^A(w, t) &= \frac{1}{\Sigma(\Sigma_f - \Sigma'_f)}(\mathcal{S}(\Sigma_f, t) - \mathcal{S}(\Sigma'_f, t)) + \\
&\frac{1}{\Sigma\Sigma'}(\mathcal{S}(\Sigma'_f - \Sigma, t) - \mathcal{S}(\Sigma'_f, t)) + \frac{1}{\Sigma(\Sigma + \Delta'_f)} \\
&(\mathcal{S}(\Sigma_f, t) - \mathcal{S}(-\Delta', t)) - \frac{1}{\Sigma\Delta'_f}(\mathcal{S}(\Sigma'_f - \Delta', t) - \\
&\mathcal{S}(-\Delta', t)) + \frac{1}{\Delta'_f(\Sigma + \Delta'_f)}(\mathcal{S}(\Sigma_f, t)\mathcal{S}(-\Delta', t)) - \\
&-\frac{1}{\Delta'_f\Sigma}(\mathcal{S}(\Sigma - \Delta', t) - \mathcal{S}(-\Delta', t)) \tag{C.7}
\end{aligned}$$

Finally, the contribution of third order to the amplitude we are interested in is

given by

$$\begin{aligned} \delta\mathcal{M}^{(3)} &= -(1/\hbar^3)\{V^\dagger(x_A)\underline{V(x_B)}V^\dagger(x_A)I_A^B(w, t) + \\ &V^\dagger(x_A)\underline{V(x_A)}V^\dagger(x_B)I_B^A(w, t)\} \end{aligned} \quad (\text{C.8})$$

Appendix D

Majorana equation in 1+1 dimensions

We start from the Dirac equation in 1+1 dimensions and in covariant form [20]:

$$-i\gamma^0 \partial_0 \psi - i\gamma^1 \partial_1 \psi + m\psi = 0 \quad (\text{D.1})$$

with $\hbar = c = 1$ and the gamma matrices γ^μ , $\mu = 0, 1$ verifying the anticommutation rules of a Clifford algebra

$$\{\gamma^\mu, \gamma^\nu\} = 2g^{\mu\nu}, \quad (\text{D.2})$$

$g^{\mu\nu}$ being the 1+1 Minkowski metric. Multiplying by γ^0 and with the usual notation

$$\beta = \gamma^0, \alpha = \gamma^0 \gamma^1, \quad (\text{D.3})$$

we can write it in the Schrödinger-like form:

$$i\partial_t \psi = \alpha p \psi + m\beta \psi \quad (\text{D.4})$$

If we want α and β to be involutions ($\alpha^2 = \beta^2 = 1$) they must be Pauli matrices. In table D.1 we spell the six possible cases.

The Majorana equation is obtained by replacing the Ψ in the mass term of Eq. (D.1) or Eq. (D.4) by the charge conjugate Ψ^C . Then:

$$i\partial_t \psi = \alpha p \psi + m\beta \psi^C \quad (\text{D.5})$$

The charge conjugation is defined in the following way [128]:

$$\psi^C = \eta \tilde{C} \psi^* \quad (\text{D.6})$$

where the matrix \tilde{C} must verify

$$\tilde{C} \gamma_\mu^* \tilde{C}^{-1} = -\gamma_\mu \quad (\text{D.7})$$

β	γ^1	α	H	<i>Cases</i>
σ_x	$i\sigma_y$	$-\sigma_z$	$-\sigma_z p - im\sigma_y K$	I.a
	$i\sigma_z$	σ_y	$\sigma_y p - im\sigma_y K$	I.b
σ_y	$i\sigma_x$	σ_z	$\sigma_z p + im\sigma_y K$	II.a
	$i\sigma_z$	$-\sigma_x$	$-\sigma_x p + im\sigma_y K$	II.b
σ_z	$i\sigma_x$	$-\sigma_y$	$-\sigma_y p - im\sigma_y K$	III.a
	$i\sigma_y$	σ_x	$\sigma_x p - im\sigma_y K$	III.b

Table D.1: The six possible representations of the 1+1 Clifford algebra, with the corresponding Majorana Hamiltonian associated.

and η is an arbitrary phase. Now, defining

$$\tilde{C} = C \beta \quad (\text{D.8})$$

and using that

$$\beta \gamma_\mu^* \beta = \gamma_\mu^T \quad (\text{D.9})$$

if β is real or purely imaginary, we have:

$$C \gamma_\mu^T C = -\gamma_\mu \quad (\text{D.10})$$

and then C must commute with σ_y and anticommute with $\sigma_{x,z}$, so

$$C = \sigma_y \quad (\text{D.11})$$

for all representations, and

$$\tilde{C} = \sigma_y \beta. \quad (\text{D.12})$$

Therefore, the Majorana equation can be written in the following form:

$$i\partial_t \psi = \alpha p \psi + \eta m \tilde{\beta} \psi^* \quad (\text{D.13})$$

where $\tilde{\beta}$ is given by

$$\tilde{\beta} = \beta \tilde{C} = \pm \sigma_y \quad (\text{D.14})$$

and the plus sign corresponds to the representations in which $\beta = \sigma_y$ (Cases II in table D.1) and the minus to the ones with $\beta = \sigma_{x,z}$ (Cases I and III). Finally we define the antiunitary involution K [129], given by

$$\psi^* = K \psi \quad (\text{D.15})$$

and set the global phase to $\eta = i$ by convenience. Thus the Majorana equation is

$$i\partial_t \psi = \alpha p \psi \pm im\sigma_y K \psi \quad (\text{D.16})$$

where now the plus corresponds to II. In chapter 6 we choose the particular representation III. b and then

$$i\partial_t \psi = \sigma_x p \psi - im\sigma_y K \psi \quad (\text{D.17})$$

This last equation can alternatively be thought of as the dimensional reduction of one of the equations in which the 3+1 Majorana equation in Weyl representation can be decomposed.

Eq.(D.16) is a Schrödinger-like equation in which

$$H = \alpha p \pm im\sigma_y K \tag{D.18}$$

plays the role of a Hamiltonian. Hitherto we have considered the “free” Majorana equation, but we could add a potential V to Eq. (D.16), obtaining:

$$H' = V + \alpha p \pm im\sigma_y K \tag{D.19}$$

Appendix E

Implementation of the quantum simulation of the Majorana equation in trapped ions

We can simulate Eq. (6.48) using two trapped ions that are subject to two dynamical terms, coupling both to the internal states and motion of the ions. The kinetic part, $cp_x(\mathbf{1} \otimes \sigma_x)$, is created with a laser tuned to both the blue and the red motional sideband of an electronic transition [135, 138], and focussed on ion 2. The spin-spin interaction term, $\sigma_x \otimes \sigma_y$, is derived from detuned red and blue sideband excitations acting on each ion in addition to the previous one [142, 143]. The Hamiltonian describing this situation reads

$$\begin{aligned}
 H &= \hbar \frac{\omega_0}{2} \sigma_1^z + \hbar \frac{\omega_0}{2} \sigma_2^z + \hbar \nu a^\dagger a + \hbar \nu_r b^\dagger b \\
 &+ \hbar \Omega \left[(e^{i(qz_1 - \omega_1 t + \phi_1)} + e^{i(qz_1 - \omega'_1 t + \phi'_1)}) \sigma_1^+ + \text{H.c.} \right] \\
 &+ \hbar \Omega \left[(e^{i(qz_2 - \omega_2 t + \phi_2)} + e^{i(qz_2 - \omega'_2 t + \phi'_2)}) \sigma_2^+ + \text{H.c.} \right] \\
 &+ \hbar \tilde{\Omega} \left[(e^{i(qz_2 - \omega t + \phi)} + e^{i(qz_2 - \omega' t + \phi')}) \sigma_2^+ + \text{H.c.} \right].
 \end{aligned}
 \tag{E.1}$$

Here $z_{1,2} = Z \pm \frac{z}{2}$ are the ion positions, measured from the center of mass, Z , and relative coordinate, z . The phases of the lasers ϕ_i for $i = 1, 2$, (ϕ, ϕ'), are controlled to perform the interaction term (kinetic term). The frequencies of the center of mass and stretch mode are given by ν and $\nu_r = \sqrt{3}\nu$, while a^\dagger , a , b^\dagger , and b , are the corresponding creation and annihilation operators. Finally, Ω and $\tilde{\Omega}$ are the Rabi frequencies of the lasers within the bounds of applicability

of the rotating-wave approximation. With an appropriate choice of parameters

$$\begin{aligned}
\omega_1 &= \omega_0 + \nu_r - \delta & \omega &= \omega_0 - \nu & \phi_1 &= \pi/2 \\
\omega'_1 &= \omega_0 - \nu_r + \delta & \omega' &= \omega_0 + \nu & \phi'_1 &= \pi/2 \\
\omega_2 &= \omega_0 - \nu_r + \delta & \phi &= \pi & \phi_2 &= 0 \\
\omega'_2 &= \omega_0 + \nu_r - \delta, & \phi' &= 0, & \phi'_2 &= 0,
\end{aligned} \tag{E.2}$$

the Hamiltonian (E.1) in the interaction picture reads

$$\begin{aligned}
H &= \hbar\eta_r\Omega(\sigma_x \otimes \mathbf{1} - \mathbf{1} \otimes \sigma_y)(b^\dagger e^{i\delta t} + b e^{-i\delta t}), \\
&\quad + \hbar\eta\tilde{\Omega}(\mathbf{1} \otimes \sigma_x)i(a^\dagger - a)
\end{aligned} \tag{E.3}$$

where $\eta \equiv \eta_r 3^{1/4} \equiv \sqrt{\hbar/4m'\nu} \ll 1$ is the Lamb-Dicke parameter and m' the ion mass. In the limit of large detuning, we have

$$\delta \gg \eta_r\Omega\sqrt{\langle b^\dagger b \rangle}, \eta\tilde{\Omega}|\langle a^\dagger - a \rangle|. \tag{E.4}$$

We recover Eq. (6.48) with the momentum operator $p_x = i\hbar(a^\dagger - a)/2\Delta$ and the equivalences

$$c = 2\eta\Delta\tilde{\Omega}, \quad mc^2 = \frac{2\hbar\eta_r^2\Omega^2}{\delta}. \tag{E.5}$$

Here, $\Delta = \sqrt{\frac{\hbar}{4m'\nu}}$ is the size of the harmonic oscillator ground state. Note that it is possible to explore all velocity regimes. Introducing the ratio $\gamma = |mc^2/\langle cp_x \rangle|$,

$$\gamma = \frac{2(\eta_r\Omega/\delta)^2}{|\langle i(a^\dagger - a) \rangle|(\eta\tilde{\Omega}/\delta)}, \tag{E.6}$$

it is possible to tune the numerator and denominator independently so as to preserve the dispersive regime, while exploring simultaneously the range from $\gamma \simeq 0$ (ultrarelativistic limit) to $\gamma \rightarrow \infty$ (nonrelativistic limit).

We could also consider other implementations that do not require synchronization of laser phases for different beams. Consider, for example, the Hamiltonian

$$H = c\mathbf{1} \otimes (p_x\sigma_z) - mc^2\sigma_y \otimes \sigma_y, \tag{E.7}$$

which is equivalent to that of equation (6.48) up to local unitary rotations. Using a detuning of $\pm\nu/2$ for the blue and red sideband, respectively, in the laser focussed onto ion 2, leads to an interaction of the form $8\Delta\eta\tilde{\Omega}^2\mathbf{1} \otimes (p_x\sigma_z)/\nu$ and the equivalence $c = 8\Delta\eta\tilde{\Omega}^2/\nu$. The spin-spin interaction in the second term can be implemented by an additional global bichromatic light field acting on the red and blue sidebands of the stretch mode, similar to the case above. In the present case, however, the ions experience laser light with the same phase $\phi_1 = \phi_2 = \phi'_1 = \phi'_2 = 0$ and a single laser beam can be used.

Measurement of the pseudo-helicity

In experiments using trapped ions, the only observable that can be directly measured by fluorescence detection for each ion is σ_z , and additional laser pulses are needed to map other observables onto it. The application of a state-dependent displacement operation on ion 2, $U_2 = \exp(-ik(\mathbf{1} \otimes \sigma_y) \otimes p_x/2)$, generated by a resonant blue and red sideband, followed by a measurement of $\mathbf{1} \otimes \sigma_z$ is equivalent to measuring the observable

$$\begin{aligned} A(k) &= U_2^\dagger (\mathbf{1} \otimes \sigma_z) U_2 \\ &= \cos(k p_x) (\mathbf{1} \otimes \sigma_z) + \sin(k p_x) (\mathbf{1} \otimes \sigma_x). \end{aligned} \quad (\text{E.8})$$

Here, k is proportional to the probe time t_{probe} [22]. In order to measure the first term in Eq. (6.61), we note that $\left. \frac{d}{dk} \langle A(k) \rangle \right|_{k=0} \propto \langle (\mathbf{1} \otimes \sigma_x) \otimes p_x \rangle$. Therefore, this term can be measured by applying a short probe pulse to the ions and measuring the initial slope of the observable $A(k)$ [136, 22].

To measure the second term in Eq. (6.61), we have to apply a different state-dependent displacement operation to ion 1: $U_1 = \exp(-ik(\sigma_x \otimes \mathbf{1}) \otimes p_x/2)$, and measure the spin correlation $\sigma_z \otimes \sigma_x$, which requires an additional $\pi/2$ pulse on ion 2. Again taking the initial slope in this observable, we have

$$\left. \frac{\partial \langle \sigma_z \otimes \sigma_x \rangle}{\partial k} \right|_{k=0} = 2 \langle (\sigma_y \otimes \sigma_x) \otimes p_x \rangle. \quad (\text{E.9})$$

Conclusions

Throughout this Thesis, the specific results have been summarized at the end of each section. Now we will outline the most important results and conclusions.

Dynamics of entanglement

We have characterized the dynamics of the generation and destruction of entanglement between qubits mediated by a quantum field, focusing in the relationship with the spacetime region at which the qubits are placed. More precisely, we have considered a pair of two-level atoms -real or artificial, that is, superconducting qubits- A and B separated by a fixed distance r interacting through a quantum electromagnetic field.

- (Sections 3.1, 3.2 and 4.2) If the qubits are initially in a separable state, two different spacetime regions emerge from our computations. If $vt < r$ - t being the time of the interaction and v the propagation velocity of the field quanta- entanglement can be generated between the atoms due to the non-locality of the Feynman propagator - or in other language, “vacuum entanglement” - which give rise to correlations at any time. In the weak coupling regime, which is the case with real atoms and the electromagnetic field, we show that these correlations are only classical, but entanglement -even maximal- can be generated through a measurement of the state of the field. For stronger couplings, as is the case in 1-D circuit QED, a small amount of entanglement shows up even in the absence of a measurement. If $vt > r$, a very different behavior of entanglement appears due to photon exchange, making apparent that entanglement generation may be a good signature of single photon propagation, a fact of particular significance in the framework of circuit QED. In all the cases the point $vt = r$ plays the role of a frontier between two different spacetime regions regarding the behavior of entanglement dynamics. We have devised a detailed circuit QED proposal of an experiment to test all the above physics.
- (Section 3.3) If the qubits are initially entangled, we have characterized the remarkable phenomenon that a full Entanglement Sudden Death-Sudden Birth cycle can take place for $vt < r$. In this case, these entanglement destructions and revivals are related with the revivals and destructions of

the atom-field entanglement, that is to say, there is sort of an entanglement flux between the different pairs of the tripartite system atoms-field. That this can happen at times at which photon exchange is not allowed represent an additional insight on the nature of the generation and destruction of quantum correlations.

Non-RWA effects

We have seen that the reasons for going beyond the ubiquitous and celebrated Rotating Wave approximation are twofold. On the fundamental side, it is necessary to include all the non-RWA terms for a complete theoretical short-time analysis of the matter-radiation interaction or to properly deal with causality questions, although in these systems these effects are beyond experimental reach. On a more applied viewpoint, circuit QED in the ultrastrong coupling provides a framework in which the non-RWA effects are available to experiment. We have explored a striking consequence of working beyond RWA, the fact that a qubit in the ground state can get excited and emit a photon, even if the field is also in the vacuum state.

- (Section 4.1) In the simplified model of a circuit QED analog of a cavity QED system, we have introduced the “slow quantum anti-Zeno effect”, providing a full experimental proposal to detect a qubit in its excited state with certainty after a few measurements starting from the ground state of the whole system. The protocol is based in the certain probability of excitation already present in the system for strong enough couplings and in the non-equilibrium dynamics after a single measurement. This feasible and realistic experiment would shed light onto the physical reality of a phenomenon commonly considered as “virtual”.
- (Section 5.2) In the case of the full multimode Hamiltonian of circuit QED, we have analyzed the implications of the mentioned ground state qubit self excitations and in general the non-RWA dynamics in the interpretation of the measurements of the probability of excitation. In particular, we have seen that only for long interaction times we can say with certainty that a qubit detector’s click entails the decay of an excited source. For short -although experimentally accessible in circuit QED- times, non-RWA contributions dominate in the dynamics of the probability of excitation conditioned to the decay of the source, meaning that in this regime a click is more likely linked with a self-excitation.

Causality

We have revisited the old question -Fermi problem- on causality in matter-radiation interactions, which we can rephrase as follows: “Is the probability of excitation of the atom B causal?” To properly deal with this issue, we have first

to pose a different question: “What does causality mean?” As we have seen, quantum correlations may show up at superluminal rates, thus the probability of a given nonlocal state such as one atom in the excited state and the other in the ground state becomes non-zero at $vt < r$. Also we have to take into account the mentioned fact that an atom can get self-excited at any time. But all these is compatible with causality since cannot be used to transmit information faster than light. The relevant question is actually “Is the probability of excitation of atom B independent of atom A at times $t < r/v$?”

- (Section 5.1) We have shown that the answer to the latter question is affirmative, by providing a complete non-perturbative proof of the independence of the probability of excitation of atom B with regard to atom A.
- (Section 5.1) We have exploited again the experimental amenability of circuit QED to propose a realistic experiment to check the causal behavior of the probability of excitation, coming true a hitherto considered as “gedanken” experiment. The experiment, together with the theoretical clarification given above, would close a long-lasting controversy on the Fermi problem, confirming the causal behavior of Nature at this level and shedding light on the meaning and implications of the notion of causality.

Quantum simulations

Although circuit QED can be understood as a closed 1D universe and its physics is interesting by itself, it can also be understood as a quantum simulator for matter-radiation interactions. Besides, we have also introduced some results on quantum simulations of relativistic quantum mechanics with trapped ions.

- (Sections 6.1 and 6.2) We have introduced a new family of generalized hamiltonians, ‘Majorana Hamiltonians’ which do not follow the standard textbook definition of hermiticity but we have shown that induce a norm-conserving dynamics and can always be simulated with regular Hamiltonians. In particular, we have proposed a trapped ion quantum simulation of one conspicuous member of the family, namely the pseudo-hamiltonian appearing in the Majorana equation- the Relativistic Quantum Mechanics equation of a fermion with a Majorana mass term-. We have explored astounding properties of the Majorana Hamiltonians, as the possibility of measure initial global phases in the evolution of physical observables. Thus, this experiment would be useful to explore fundamental questions being at the edges of Quantum Mechanics and Quantum Field Theory. But the scope is more general and includes possible simulations of operations like time reversal, charge conjugation or partial transpose in the lab.
- (Section 6.3) We have introduced a method to use the current simulations of free relativistic Hamiltonians to simulate also Hamiltonians including

potentials, opening the way to more complex simulations of interacting many-body relativistic equations, in which the results of the first parts of this Thesis could be explored within different frameworks.

Bibliography

- [1] A. Einstein, B. Podolsky, and N. Rosen. Can Quantum-Mechanical Description of Physical Reality Be Considered Complete? *Phys. Rev.*, 47:777, 1935.
- [2] E. Schrödinger. Discussion of Probability Relations between Separated Systems. *Proc. Cambridge Phil. Soc.*, 31:555, 1935.
- [3] N. Bohr. Can quantum-mechanical description of physical reality be considered complete? *Phys. Rev.*, 48:696–702, Oct 1935.
- [4] J. S. Bell. On the Einstein Podolsky Rosen paradox. *Physics*, 1:195, 1954.
- [5] Alain Aspect, Philippe Grangier, and Gérard Roger. Experimental Realization of Einstein-Podolsky-Rosen-Bohm *Gedankenexperiment*: A New Violation of Bell’s Inequalities. *Phys. Rev. Lett.*, 49:91–94, Jul 1982.
- [6] M. Żukowski, A. Zeilinger, M. A. Horne, and A. K. Ekert. “Event-ready-detectors” Bell experiment via entanglement swapping. *Phys. Rev. Lett.*, 71:4287, 1993.
- [7] R. Ghosh and L. Mandel. Observation of nonclassical effects in the interference of two photons. *Phys. Rev. Lett.*, 59:1903–1905, Oct 1987.
- [8] S. J. Summers and R. F. Werner. The vacuum violates Bell’s inequalities. *Phys. Lett. A*, 110:257, 1985.
- [9] B. Reznik, A. Retzker, and J. Silman. Violating Bell’s inequalities in vacuum. *Phys. Rev. A*, 71:042104, 2005.
- [10] J. D. Franson. Generation of entanglement outside of the light cone. *J. Mod. Opt.*, 55:2117, 2008.
- [11] R. P. Feynman. *The theory of fundamental processes*. Westview Press, 1998.
- [12] A. Retzker, J. I. Cirac, and B. Reznik. Detecting Vacuum Entanglement in a Linear Ion Trap. *Phys. Rev. Lett.*, 94:050504, 2005.

- [13] G. Ghirardi, A. Rimini, and T. Weber. A general argument against superluminal transmission through the quantum mechanical measurement process. *Lettere Al Nuovo Cimento*, 27:293–298, 1980.
- [14] Ll. Masanes, A. Acín, and N. Gisin. General properties of nonsignaling theories. *Phys. Rev. A*, 73:012112, 2006.
- [15] E. Fermi. Quantum theory of radiation. *Rev. Mod. Phys.*, 4:87, 1932.
- [16] Gerhard C. Hegerfeldt. Causality problems for Fermi’s two-atom system. *Phys. Rev. Lett.*, 72(5):596–599, Jan 1994.
- [17] Detlev Buchholz and Jakob Yngvason. There Are No Causality Problems for Fermi’s Two-Atom System. *Phys. Rev. Lett.*, 73(5):613–616, Aug 1994.
- [18] Richard Feynman. Simulating physics with computers. *International Journal of Theoretical Physics*, 21:467–488, 1982.
- [19] L Lamata, J Casanova, R Gerritsma, C F Roos, J J García-Ripoll, and E Solano. Relativistic quantum mechanics with trapped ions. *New Journal of Physics*, 13(9):095003, 2011.
- [20] B. Thaller. *The Dirac Equation*. Springer-Verlag, 1992.
- [21] W. Greiner. *Relativistic Quantum Mechanics. Wave equations*. Springer, 2000.
- [22] R. Gerritsma, G. Kirchmair, F. Zähringer, E. Solano, R. Blatt, and C. F. Roos. Quantum simulation of the Dirac equation. *Nature*, 463:68–71, January 2010.
- [23] Ettore Majorana. Teoria simmetrica dell’elettrone e del positrone. *Il Nuovo Cimento*, 14:171–184, 1937.
- [24] Herbert Jehle. Two-component wave equations. *Phys. Rev.*, 75(10):1609, May 1949.
- [25] J. Serpe. Two-component wave equations. *Phys. Rev.*, 76(10):1538, Nov 1949.
- [26] C. Cohen-Tannoudji, J. Dupont-Roc, and G. Grynberg. *Photons and atoms : introduction to quantum electrodynamics*. Wiley Interscience, 1989.
- [27] D. P. Craig and T. Thirunamachandran. *Molecular Quantum Electrodynamics*. Dover Publications, 1998.
- [28] M. O. Scully and M. S. Zubairy. *Quantum Optics*. Cambridge University Press, 1997.
- [29] G. Compagno, R. Passante, and F. Persico. *Atom-Field Interactions and Dressed Atoms*. Cambridge University Press, September 1995.

- [30] B. Yurke and J. S. Denker. Quantum network theory. *Phys. Rev. A*, 29:1419–1437, March 1984.
- [31] M. H. Devoret. Quantum Fluctuations in Electrical Circuits. In S. Reynaud, E. Giacobino, & J. Zinn-Justin, editor, *Fluctuations Quantiques/Quantum Fluctuations*, page 351, 1997.
- [32] J. Q. You and F. Nori. Atomic physics and quantum optics using superconducting circuits. *Nature*, 474(7353):589–597, 06 2011.
- [33] J. Robert Johansson. Quantum mechanics in superconducting qubits and nanomechanical devices. PhD. Thesis.
- [34] Alexandre Blais, Ren-Shou Huang, Andreas Wallraff, S. M. Girvin, and R. J. Schoelkopf. Cavity quantum electrodynamics for superconducting electrical circuits: An architecture for quantum computation. *Phys. Rev. A*, 69(6):062320, Jun 2004.
- [35] A. Wallraff, D.I. Schuster, A. Blais, L. Frunzio, R.-S. Huang, J. Majer, S. Kumar, S. M. Girvin, and R. J. Schoelkopf. Strong coupling of a single photon to a superconducting qubit using circuit quantum electrodynamics. *Nature*, 431:162–167, 2004.
- [36] G. Romero, J. J. García-Ripoll, and E. Solano. Microwave Photon Detector in Circuit QED. *Physical Review Letters*, 102(17):173602, May 2009.
- [37] G. Romero, J. José García-Ripoll, and E. Solano. Photodetection of propagating quantum microwaves in circuit QED. *Physica Scripta Volume T*, 137(1):014004, December 2009.
- [38] S. Hill and W. K. Wootters. Entanglement of a Pair of Quantum Bits. *Phys. Rev. Lett.*, 78:5022, 1997.
- [39] G. Vidal and R. F. Werner. Computable measure of entanglement. *Phys. Rev. A*, 65(3):032314, 2002.
- [40] A. Miranowicz and A. Grudka. Ordering two-qubit states with concurrence and negativity. *Phys. Rev. A*, 70:032326, 2004.
- [41] M. Horodecki, P. Horodecki, and R. Horodecki. Mixed-State Entanglement and Distillation: Is there a “Bound” Entanglement in Nature? *Physical Review Letters*, 80:5239–5242, June 1998.
- [42] P. Horodecki. Separability criterion and inseparable mixed states with positive partial transposition. *Physics Letters A*, 232:333–339, February 1997.
- [43] S. J. Summers and R. F. Werner. Bell’s inequalities and quantum field theory. II. Bell’s inequalities are maximally violated in the vacuum. *J. Math. Phys.*, 28:2448, 1987.

- [44] M. B. Plenio, J. Eisert, J. Dreissig, and M. Cramer. Entropy, Entanglement, and Area: Analytical Results for Harmonic Lattice Systems. *Physical Review Letters*, 94(6):060503, 2005.
- [45] G. C. Hegferfeldt. Instantaneous Spreading and Einstein Causality in Quantum Theory. *Annalen Phys.*, 7:716, 1998.
- [46] E. A. Power and T. Thirunamachandran. Analysis of the causal behavior in energy transfer between atoms. *Phys. Rev. A*, 56:3395, 1997.
- [47] J. D. Franson and M. M. Donegan. Perturbation theory for quantum-mechanical observables. *Phys. Rev. A*, 65:052107, 2002.
- [48] C. Cabrillo, J. I. Cirac, P. García-Fernández, and P. Zoller. Creation of entangled states of distant atoms by interference. *Phys. Rev. A*, 59:001025, 1999.
- [49] L. Lamata, J. J. García-Ripoll, and J. I. Cirac. How Much Entanglement Can Be Generated between Two Atoms by Detecting Photons? *Phys. Rev. Lett.*, 98:010502, 2007.
- [50] P. W. Milonni, D. F. V. James, and H. Fearn. Photodetection and causality in quantum optics. *Phys. Rev. A*, 52(2):1525, 1995.
- [51] A. K. Biswas, G. Compagno, G. M. Palma, R. Passante, and F. Persico. Virtual photons and causality in the dynamics of a pair of two-level atoms. *Phys. Rev. A*, 42:4291, 1990.
- [52] C. H. Bennett, H. J. Bernstein, S. Popescu, and B. Schumacher. Concentrating partial entanglement by local operations. *Phys. Rev. A*, 53:2046, 1996.
- [53] D. P. Craig and T. Thirunamachandran. An analysis of models for resonant transfer of excitation using quantum electrodynamics. *Chem. Phys.*, 167:229, 1992.
- [54] H. Bateman. *Tables of Integral Transforms Vol. I*. McGraw-Hill, New York, 1954.
- [55] S. J. van Enk, J. I. Cirac, and P. Zoller. Ideal Quantum Communication over Noisy Channels: A Quantum Optical Implementation. *Phys. Rev. Lett.*, 78:4293, 1997.
- [56] X. L. Feng, Z. M. Zhang, X. D. Li, S. Q. Gong, and Z. Z. Xu. Entangling Distant Atoms by Interference of Polarized Photons. *Phys. Rev. Lett.*, 90:217902, 2003.
- [57] L. M. Duan and H. J. Kimble. Efficient Engineering of Multiatom Entanglement through Single-Photon Detections. *Phys. Rev. Lett.*, 90:253601, 2003.

- [58] C. Simon and W. T. M. Irvine. Robust Long-Distance Entanglement and a Loophole-Free Bell Test with Ions and Photons. *Phys. Rev. Lett.*, 91:110405, 2003.
- [59] D. L. Moehring, P. Maunz, S. Olmschenk, K. C. Younge, D. N. Matsukevich, L. M. Duan, and C. Monroe. Entanglement of single-atom quantum bits at a distance. *Nature*, 68:449, 2007.
- [60] S. Zippilli, G. A. Olivares-Rentería, G. Morigi, C. Schuck, F. Rhode, and J. Eschner. Entanglement of distant atoms by projective measurement: the role of detection efficiency. *New Journal of Physics*, 10:103003, 2008.
- [61] K. Mattle, H. Weinfurter, P. G. Kwiat, and A. Zeilinger. Dense Coding in Experimental Quantum Communication. *Phys. Rev. Lett.*, 76:4656, 1996.
- [62] Karol Życzkowski, Paweł Horodecki, Michał Horodecki, and Ryszard Horodecki. Dynamics of quantum entanglement. *Phys. Rev. A*, 65(1):012101, 2001.
- [63] L. Diósi. Progressive Decoherence and Total Environmental Disentanglement. *Lect. Notes Phys.*, 622:157, 2003.
- [64] T. Yu and J. H. Eberly. Finite-Time Disentanglement Via Spontaneous Emission. *Phys. Rev. Lett.*, 93:140404, 2004.
- [65] T. Yu and J. H. Eberly. Quantum Open System Theory: Bipartite Aspects. *Phys. Rev. Lett.*, 97:140403, 2006.
- [66] M Yönaç, Ting Yu, and J H Eberly. Pairwise concurrence dynamics: a four-qubit model. *J. Phys. B: At. Mol. Opt. Phys.*, 40:S45, 2007.
- [67] A. Jamróz. Local aspects of disentanglement induced by spontaneous emission. *J. Phys. A: Math. Gen.*, 39:7727, 2006.
- [68] Z. Ficek and R. Tanaś. Dark periods and revivals of entanglement in a two-qubit system. *Phys. Rev. A*, 74:024304, 2006.
- [69] B. Bellomo, R. Lo Franco, and G. Compagno. Entanglement dynamics of two independent qubits in environments with and without memory. *Phys. Rev. A*, 77:032342, 2008.
- [70] J. P. Paz and A. J. Roncaglia. Dynamics of the Entanglement between Two Oscillators in the Same Environment. *Phys. Rev. Lett.*, 100:220401, 2008.
- [71] C. E. López, G. Romero, F. Lastra, E. Solano, and J. C. Retamal. Sudden Birth versus Sudden Death of Entanglement in Multipartite Systems. *Phys. Rev. Lett.*, 101:080503, 2008.

- [72] S. Chan, M. D. Reid, and Z. Ficek. Entanglement evolution of two remote and non-identical Jaynes-Cummings atoms. *Journal of Physics B Atomic Molecular Physics*, 42(6):065507, March 2009.
- [73] J. H. Cole. Understanding entanglement sudden death through multipartite entanglement and quantum correlations. *Journal of Physics A Mathematical General*, 43(13):135301, April 2010.
- [74] M. P. Almeida, F. de Melo, M. Hor-Meyll, A. Salles, S. P. Walborn, P. H. Souto Ribeiro, and L. Davidovich. Environment-Induced Sudden Death of Entanglement. *Science*, 316:579, 2007.
- [75] Z. Ficek and R. Tanaś. Delayed sudden birth of entanglement. *Phys. Rev. A*, 77:054301, 2008.
- [76] R. H. Lehmburg. Radiation from an N-Atom System. I. General Formalism. *Phys. Rev. A*, 2:883, 1970.
- [77] G. S. Agarwal. Quantum Optics. *Springer Tracts Mod. Phys.*, 70:1, 1974.
- [78] F.-Q. Wang, Z.-M. Zhang, and R.-S. Liang. Decoherence of two qubits in non-Markovian reservoirs without the rotating-wave approximation. *Phys. Rev. A*, 78(6):062318, December 2008.
- [79] C. Cohen-Tannoudji, J. Dupont-Roc, and G. Grynberg. *Atom-photon interactions*. Wiley Interscience, New York, 1998.
- [80] P. W. Milonni and P. L. Knight. Retardation in the resonant interaction of two identical atoms. *Phys. Rev. A*, 10(4):1096, 1974.
- [81] He-Shan Song and Chang-shui Yu. Free entanglement measure of multiparticle quantum states. *Phys. Lett. A*, 330:377, 2004.
- [82] C. Sabín and G. García-Alcaine. A classification of entanglement in three-qubit systems. *Eur. Phys. J. D*, 48(3):435, 2008.
- [83] P. Facchi, G. Florio, and S. Pascazio. Probability-density-function characterization of multipartite entanglement. *Phys. Rev. A*, 74(4):042331, 2006.
- [84] Pranaw Rungta, V. Bužek, Carlton M. Caves, M. Hillery, and G. J. Milburn. Universal state inversion and concurrence in arbitrary dimensions. *Phys. Rev. A*, 64(4):042315, 2001.
- [85] I. Chiorescu, P. Bertet, K. Semba, Y. Nakamura, C. J. P. M. Harmans, and J. E. Mooij. Coherent dynamics of a flux qubit coupled to a harmonic oscillator. *Nature*, 431:159–162, September 2004.
- [86] J. M. Raimond, M. Brune, and S. Haroche. Manipulating quantum entanglement with atoms and photons in a cavity. *Rev. Mod. Phys.*, 73(3):565–582, Aug 2001.

- [87] H. Walther, B. T. H. Varcoe, B.-G. Englert, and T. Becker. Cavity quantum electrodynamics. *Reports on Progress in Physics*, 69:1325–1382, May 2006.
- [88] D. Leibfried, R. Blatt, C. Monroe, and D. Wineland. Quantum dynamics of single trapped ions. *Rev. Mod. Phys.*, 75(1):281–324, Mar 2003.
- [89] T. Niemczyk, F. Deppe, H. Huebl, E. P. Menzel, F. Hocke, M. J. Schwarz, J. J. Garcia-Ripoll, D. Zueco, T. Hümmer, E. Solano, A. Marx, and R. Gross. Circuit quantum electrodynamics in the ultrastrong-coupling regime. *Nature Physics*, 6:772–776, October 2010.
- [90] P. Forn-Díaz, J. Lisenfeld, D. Marcos, J. J. García-Ripoll, E. Solano, C. J. P. M. Harmans, and J. E. Mooij. Observation of the Bloch-Siegert Shift in a Qubit-Oscillator System in the Ultrastrong Coupling Regime. *Physical Review Letters*, 105(23):237001, December 2010.
- [91] E. K. Irish, J. Gea-Banacloche, I. Martin, and K. C. Schwab. Dynamics of a two-level system strongly coupled to a high-frequency quantum oscillator. *Phys. Rev. B*, 72(19):195410, Nov 2005.
- [92] E. K. Irish. Generalized rotating-wave approximation for arbitrarily large coupling. *Phys. Rev. Lett.*, 99(17):173601, Oct 2007.
- [93] S. Ashhab and Franco Nori. Qubit-oscillator systems in the ultrastrong-coupling regime and their potential for preparing nonclassical states. *Phys. Rev. A*, 81(4):042311, Apr 2010.
- [94] I. Lizuain, J. Casanova, J. J. García-Ripoll, J. G. Muga, and E. Solano. Zeno physics in ultrastrong-coupling circuit QED. *Phys. Rev. A*, 81(6):062131, Jun 2010.
- [95] Johannes Hausinger and Milena Grifoni. Qubit-oscillator system: An analytical treatment of the ultrastrong coupling regime. *Phys. Rev. A*, 82(6):062320, Dec 2010.
- [96] B. Peropadre, P. Forn-Díaz, E. Solano, and J. J. García-Ripoll. Switchable ultrastrong coupling in circuit QED. *Phys. Rev. Lett.*, 105(2):023601, Jul 2010.
- [97] J. Hausinger and M. Grifoni. Qubit-oscillator system under ultrastrong coupling and extreme driving. *Phys. Rev. A*, 83(3):030301, March 2011.
- [98] P. Facchi and S. Pascazio. Quantum zeno dynamics: mathematical and physical aspects. *Journal of Physics A: Mathematical and Theoretical*, 41(49):493001, 2008.
- [99] Andreas Kurcz, Antonio Capolupo, Almut Beige, Emilio Del Giudice, and Giuseppe Vitiello. Energy concentration in composite quantum systems. *Phys. Rev. A*, 81(6):063821, Jun 2010.

- [100] Tommaso Calarco and Roberto Onofrio. Optimal measurements of magnetic flux in superconducting circuits and macroscopic quantum mechanics. *Physics Letters A*, 198(4):279 – 285, 1995.
- [101] T. Picot, R. Schouten, C. J. P. M. Harmans, and J. E. Mooij. Quantum nondemolition measurement of a superconducting qubit in the weakly projective regime. *Phys. Rev. Lett.*, 105(4):040506, Jul 2010.
- [102] A. Lupascu, S. Saito, T. Picot, P. C. de Groot, C. J. P. M. Harmans, and J. E. Mooij. Quantum non-demolition measurement of a superconducting two-level system. *Nature Physics*, 3:119–125, February 2007.
- [103] T. Werlang, A. V. Dodonov, E. I. Duzzioni, and C. J. Villas-Bôas. Rabi model beyond the rotating-wave approximation: Generation of photons from vacuum through decoherence. *Phys. Rev. A*, 78(5):053805, Nov 2008.
- [104] A V Dodonov. How 'cold' can a markovian dissipative cavity QED system be? *Physica Scripta*, 82(3):038102, 2010.
- [105] D. Salart, A. Baas, C. Branciard, N. Gisin, and H. Zbinden. Testing spooky action at a distance. *Nature*, 454:861–864, 2008.
- [106] N. N. Bogolubov, A. A. Logunov, and I. T. Todorov. *Introduction to axiomatic quantum field theory*. University of California Press, Massachusetts, U.S.A., 1975.
- [107] John M. Martinis, Michel H. Devoret, and John Clarke. Energy-Level Quantization in the Zero-Voltage State of a Current-Biased Josephson Junction. *Phys. Rev. Lett.*, 55(15):1543–1546, Oct 1985.
- [108] V. Bouchiat, D. Vion, P. Joyez, D. Esteve, and M. H. Devoret. Quantum coherence with a single Cooper pair. *Phys. Scr*, T76:165–170, 1998.
- [109] J. E. Mooij, T. P. Orlando, L. Levitov, Lin Tian, Caspar H. van der Wal, and Seth Lloyd. Josephson Persistent-Current Qubit. *Science*, 285(5430):1036–1039, 1999.
- [110] Jens Koch, Terri M. Yu, Jay Gambetta, A. A. Houck, D. I. Schuster, J. Majer, Alexandre Blais, M. H. Devoret, S. M. Girvin, and R. J. Schoelkopf. Charge-insensitive qubit design derived from the Cooper pair box. *Phys. Rev. A*, 76(4):042319, Oct 2007.
- [111] Jr. A. A. Abdumalikov, O Astafiev, Y. Nakamura, Y. A. Pashkin, and J. Tsai. Vacuum Rabi splitting due to strong coupling of a flux qubit and a coplanar-waveguide resonator. *Phys. Rev. B*, 78(18):180502, 2008.
- [112] J. Bourassa, J. M. Gambetta, A. A. Abdumalikov, O. Astafiev, and Y. Nakamura. Ultrastrong coupling regime of cavity QED with phase-biased flux qubits. *Phys. Rev. A*, 80:032109, 2009.

- [113] G. Günter, A. A. Anappara, J. Hees, A. Sell, G. Biasiol, L. Sorba, S. De Liberato, C. Ciuti, A. Tredicucci, A. Leitenstorfer, and R. Huber. Sub-cycle switch-on of ultrastrong light-matter interaction. *Nature*, 458:178, 2009.
- [114] J. H. Plantenberg, P. C. de Groot, C. J. P. M. Harmans, and J. E. Mooij. Demonstration of controlled-NOT quantum gates on a pair of superconducting quantum bits. *Nature*, 447:836–839, June 2007.
- [115] R. C. Bialczak, M. Ansmann, M. Hofheinz, E. Lucero, M. Neeley, A. D. O’Connell, D. Sank, H. Wang, J. Wenner, M. Steffen, A. N. Cleland, and J. M. Martinis. Quantum process tomography of a universal entangling gate implemented with Josephson phase qubits. *Nature Physics*, 6:409–413, June 2010.
- [116] J. Yngvason. The role of type III factors in quantum field theory. *Reports on Mathematical Physics*, 55:135–147, February 2005.
- [117] J. E. Mooij, T. P. Orlando, L. Levitov, Lin Tian, Caspar H. van der Wal, and Seth Lloyd. Josephson Persistent-Current Qubit. *Science*, 285(5430):1036–1039, 1999.
- [118] Yuriy Makhlin, Gerd Schön, and Alexander Shnirman. Quantum-state engineering with Josephson-junction devices. *Rev. Mod. Phys.*, 73(2):357–400, May 2001.
- [119] C. Zener. Non-Adiabatic Crossing of Energy Levels. *Royal Society of London Proceedings Series A*, 137:696–702, September 1932.
- [120] J. R. Johansson, G. Johansson, C. M. Wilson, and F. Nori. Dynamical Casimir Effect in a Superconducting Coplanar Waveguide. *Physical Review Letters*, 103(14):147003, October 2009.
- [121] J. R. Johansson, G. Johansson, C. M. Wilson, and F. Nori. Dynamical Casimir effect in superconducting microwave circuits. *Phys. Rev. A*, 82(5):052509, November 2010.
- [122] T. Picot, R. Schouten, C. J. P. M. Harmans, and J. E. Mooij. Quantum nondemolition measurement of a superconducting qubit in the weakly projective regime. *Phys. Rev. Lett.*, 105(4):040506, Jul 2010.
- [123] F. Costa and F. Piazza. Modeling a particle detector in field theory. *New Journal of Physics*, 11(11):113006, November 2009.
- [124] F. Wilczek. Majorana returns. *Nature Physics*, 5:614–618, September 2009.
- [125] K. M. Case. Reformulation of the Majorana Theory of the Neutrino. *Phys. Rev.*, 107(1):307–316, Jul 1957.

- [126] Andreas Aste. A Direct Road to Majorana Fields. *Symmetry*, 2(4):1776–1809, 2010.
- [127] P. B. Pal. Dirac, Majorana, and Weyl fermions. *American Journal of Physics*, 79:485–498, May 2011.
- [128] A. Zee. *Quantum field theory in a nutshell*. Princeton University Press, New Jersey, 2003.
- [129] Eugene P. Wigner. Normal forms of antiunitary operators. *Journal of Mathematical Physics*, 1(5):409–413, 1960.
- [130] Matthew McKague, Michele Mosca, and Nicolas Gisin. Simulating quantum systems using real hilbert spaces. *Phys. Rev. Lett.*, 102(2):020505, Jan 2009.
- [131] Eugene P. Wigner. *Group theory and its application to the quantum mechanics of atomic spectra*. Academic Press, 1959.
- [132] W. K. Wootters. Entanglement Sharing in Real-Vector-Space Quantum Theory. *Foundations of Physics*, published online, July 2010.
- [133] J. Batle, A. R. Plastino, M. Casas, and A. Plastino. On the entanglement properties of two-rebits systems. *Physics Letters A*, 298:301–307, June 2002.
- [134] R. F. Streater and A. S. Wightman. *PCT, spin and statistics and all that*. Princeton University Press, 2000.
- [135] L. Lamata, J. León, T. Schätz, and E. Solano. Dirac Equation and Quantum Relativistic Effects in a Single Trapped Ion. *Physical Review Letters*, 98(25):253005, June 2007.
- [136] P. Lougovski, H. Walther, and E. Solano. Instantaneous measurement of field quadrature moments and entanglement. *European Physical Journal D*, 38:423–426, June 2006.
- [137] O. Klein. Die Reflexion von Elektronen an einem Potentialsprung nach der relativistischen Dynamik von Dirac. *Zeitschrift für Physik A Hadrons and Nuclei*, 53:157–165, 1929. 10.1007/BF01339716.
- [138] J. Casanova, J. J. García-Ripoll, R. Gerritsma, C. F. Roos, and E. Solano. Klein tunneling and Dirac potentials in trapped ions. *Phys.Rev. A*, 82(2):020101, August 2010.
- [139] R. Gerritsma, B. P. Lanyon, G. Kirchmair, F. Zähringer, C. Hempel, J. Casanova, J. J. García-Ripoll, E. Solano, R. Blatt, and C. F. Roos. Quantum Simulation of the Klein Paradox with Trapped Ions. *Physical Review Letters*, 106(6):060503, February 2011.

- [140] A. Bermudez and M. A. Martin-Delgado. Hyper-entanglement in a relativistic two-body system. *Journal of Physics A Mathematical General*, 41:5302, December 2008.
- [141] M. Moshinsky, G. Loyola, and C. Villegas. Anomalous basis for representations of the Poincaré group. *Journal of Mathematical Physics*, 32:373–381, February 1991.
- [142] K. Mølmer and A. Sørensen. Multiparticle Entanglement of Hot Trapped Ions. *Physical Review Letters*, 82:1835–1838, March 1999.
- [143] C. F. Roos. Ion trap quantum gates with amplitude-modulated laser beams. *New J. Phys.*, 10:013002, 2008.